Research

Evaluation of a Field Permeameter
to Measure Saturated
Hydraulic Conductivity of
Base/Subgrade Materials

**Minnesota Local
Road Research
Board**

1. Report No. MN/RC – 2001-19	2.	3. Recipients Accession No.	
4. Title and Subtitle EVALUATION OF A FIELD PERMEAMETER TO MEASURE SATURATED HYDRAULIC CONDUCTIVITY OF BASE/SUBGRADE MATERIALS		5. Report Date July 2001	
		6.	
7. Author(s) Timothy R. Clyne[1], Vaughan R. Voller[1], Bjorn Birgisson[2]		8. Performing Organization Report No.	
9. Performing Organization Name and Address [1]University of Minnesota, Department of Civil Engineering 500 Pillsbury Drive S.E., Minneapolis, MN 55455-0116 [2]University of Florida, Civil & Coastal Engineering Gainsville, FL 32611		10. Project/Task/Work Unit No.	
		11. Contract (C) or Grant (G) No. c) 74708 wo) 81	
12. Sponsoring Organization Name and Address Minnesota Department of Transportation 395 John Ireland Boulevard Mail Stop 330 St. Paul, Minnesota 55155		13. Type of Report and Period Covered Final Report 1999-2001	
		14. Sponsoring Agency Code	
15. Supplementary Notes			

16. Abstract (Limit: 200 words)

This report presents the results of a cooperative study on the field use of a permeameter, built by researchers at the Minnesota Department of Transportation (Mn/DOT) and the University of Minnesota, to estimate the saturated hydraulic conductivity of pavement base materials.

Field measurements using the permeameter were taken on various highway construction projects, and researchers measured the saturated hydraulic conductivity of samples in the laboratory. Researchers also reviewed theories for converting a field-measured flow rate into a saturated hydraulic conductivity estimate.

By numerical simulation and analysis of the field data, researchers determined an appropriate method for converting the Mn/DOT permeameter flow measurements into estimates of hydraulic conductivity. Variations between the field estimated and laboratory measured hydraulic conductivity are within one order of magnitude. Variations between the field estimate and numerical simulation, however, are much closer.

The study found the Mn/DOT permeameter can be used to obtain a reliable estimate of the base hydraulic conductivity provided that the base layer is at least 15 cm (six inches) deep. When the base is to thin, permeameter readings are restricted to early infiltration times.

17. Document Analysis/Descriptors Hydraulic Conductivity Permeability		18. Availability Statement No restrictions. Document available from: National Technical Information Services, Springfield, Virginia 22161	
19. Security Class (this report) Unclassified	20. Security Class (this page) Unclassified	21. No. of Pages 152	22. Price

EVALUATION OF FIELD PERMEAMETER TO MEASURE SATURATED HYDRAULIC CONDUCTIVITY OF BASE/SUBGRADE MATERIALS

Final Report

Prepared by:

Timothy R. Clyne[1]
Vaughan R. Voller[1]
Bjorn Birgisson[2]

[1]Department of Civil Engineering
University of Minnesota
500 Pillsbury Dr. S.E.
Minneapolis, MN 55455

[2]University of Florida
Civil & Coastal Engineering
Gainesville, FL 32611

July 2001

ACKNOWLEDGEMENTS

TABLE OF CONTENTS

APPENDIX A – MINNESOTA DEPARTMENT OF TRANSPORTATION PERMEAMETER USER'S MANUAL

APPENDIX B – RAW DATA FROM FIELD PERMEABILTY TESTS

APPENDIX C – SIEVE ANALYSIS DATA

LIST OF TABLES

LIST OF FIGURES

EXECUTIVE SUMMARY

In determining the performance of a given drainage material the value of saturated hydraulic conductivity, k_{sat}, along with information on the unsaturated characteristics of the material, is an important item of information. When water infiltrates into a base material under a constant head it is observed that over time the infiltration rate converges to a steady value. If the base layer is thick enough models of the infiltration process can be used to arrive at an equation that will convert the steady flow into an estimate of the saturated hydraulic conductivity. The Minnesota Department of Transportation (Mn/DOT) permeameter was designed to measure the in situ saturated hydraulic conductivity of a granular pavement base. Its use involves digging a cylindrical well hole (radius a) in the base and measuring the flow rate, Q (volume/time), of water into the soil. A constant head H is maintained by feeding the well from an annular tube reservoir incorporated in the permeameter. The flow rate is measured by observing the water drop, Δl, with time in the annular tube reservoir. An estimate of the steady flow is obtained by fitting the measured flow rates to an exponential decaying infiltration model. A literature search provided a number (8) of theoretical equations that can be used to convert the steady flow rate into a saturated hydraulic conductivity estimate. Each model had the basic form of $k_{sat} = C*Q$, where, C is a shape factor that describes the shape of the saturated bulb in the material. A key assumption in all of these models is that the base layer is thick, homogeneous and isotropic. Testing at 31 sites over two summers with the Mn/DOT permeameter indicated that the available models provided estimates that were qualitatively the same with quantitative differences attributed to the different shape factors used. Based on this observation, from the point of view of robustness and convenience, the so-called GP-L model that equates

$$k_{fs} = \frac{CQ}{2\pi H^2 \left[1 + \frac{C}{2}\left(\frac{a}{H}\right)^2\right]}$$

where the shape factor

$$C = \frac{D\left[\frac{H}{a}\right]^{2/3}}{2\pi H^2}$$

was chosen as the model for more extensive investigation. A comparison with laboratory measurements made on samples taken from each site indicated that the range of observed conductivities

Material	Field			Laboratory		
	low k, cm/s	high k, cm/s	range, cm/s	low k, cm/s	high k, cm/s	range, cm/s
Class 5	5.52E-06	8.08E-04	8.03E-04	2.80E-06	2.60E-04	2.57E-04
Class 6	2.90E-06	5.34E-05	5.05E-05	5.00E-06	2.23E-04	2.18E-04
Select Granular	4.27E-06	1.28E-03	1.28E-03	1.60E-06	2.10E-04	2.08E-04

could be well matched with the GP-L model when the factor D was set to a value of ~0.02. This was confirmed by a detailed analysis based around a direct simulation using the SEEP/W commercial saturated/unsaturated flow code. A one-to-one comparison between field estimated and the laboratory measured values, however, showed a poor correlation. This poor correlation can be attributed to (1) a mismatch between the laboratory and field conditions and/or (2) a thin base layer, which would render the theory relating flow to conductivity invalid. In contrast to the poor correlation seen between the field and laboratory, the correlation between the field values of saturated conductivity and those obtained in a direct numerical simulation using the SEEP/W code was significantly better. This result indicates that the when the assumption of a thick homogenous isotropic layer is valid the permeameter can be used to obtain a reasonable estimate of the base hydraulic conductivity. The key here is how thick? An analysis of an axisymmetric

limiting Green-Ampt solution showed that the permeameter should not be used when the base thickness below the well hole, s, is less than 5 cm (2 inches). This translates to a total base thickness of 15 cm assuming a borehole depth of 10 cm. Further the analysis showed that the maximum drop in the annular tube reservoir over which flow measurements should be taken is given by the relationship

$$\Delta l_{max} = 0.17s^2 + 2.8s$$

where the units of s and Δl_{max} are in cm.

Subject to a thick enough base layer the study concluded that the Mn/DOT permeameter can be used to obtain a reliable estimate of the base hydraulic conductivity.

CHAPTER 1

INTRODUCTION

Background

Drainage Design in Highway Pavements

Providing an adequate drainage system (in terms of material characteristics) is very important in the process of pavement design. Drainage systems on a highway should allow for the flow of water off the surface of the pavement. More importantly, drainage systems should remove infiltrated water from the base and subgrade layers. Inadequate drainage, and therefore excess moisture, will in time result in damage to the pavement structure. Until recently, the idea of drainage has not been given the attention it deserves in the pavement design process. However, more and more engineers are beginning to realize how important the concept of drainage is in pavement design.

If water is not drained from the pavement system, the granular base and subbase materials will increase in moisture content. As the materials become saturated, their physical properties change, compromising their stability and strength capabilities. Huang [1] notes that a common misconception is that good drainage is not required if the thickness design of a pavement is based on saturated conditions. This concept may have been accurate during the early days of pavement design. As the weight and number of axle loads increase, however, water may cause more damage to pavements, such as pumping and degradation of paving materials, other than the loss of shear strength. Figure 1.1 shows a cross-sectional view of a pavement system, with typical thicknesses of the layers noted.

1
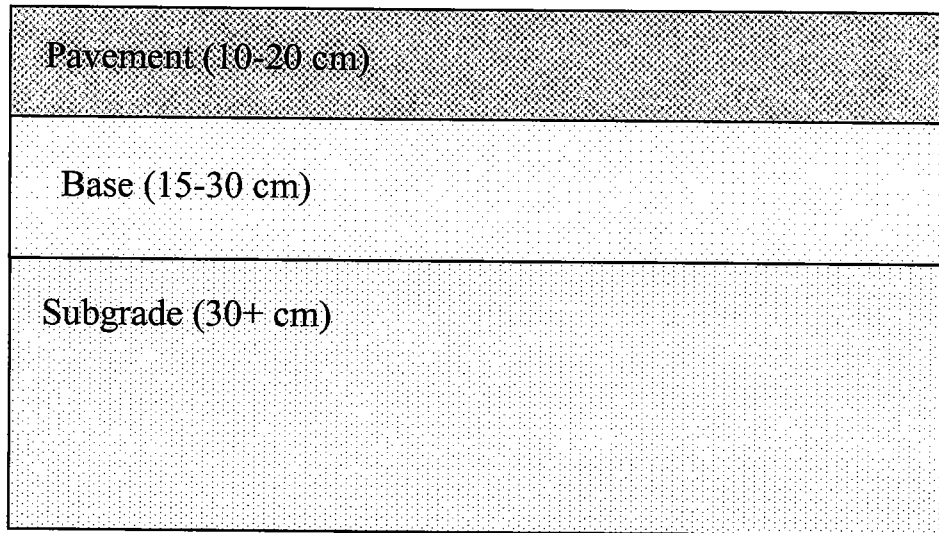
Figure 1.1 Pavement System Cross-Section

Inadequate drainage may ultimately result in poor pavement performance [1]. When excess water is entrapped in the pavement system, it can have a number of detrimental effects. It reduces the strength of unbound granular materials and subgrade soils. Excess water causes pumping in concrete pavements, which leads to faulting, cracking, and general shoulder deterioration. With the elevated hydrodynamic pressure generated by moving traffic, pumping of fines in the base layer of flexible pavements may also occur with the resulting loss of support. In northern climates high water table increases the potential for frost heave and contributes to the reduction of load-carrying capacity during the spring thaw period. Excess water also causes differential heaving over swelling soils. Finally, continuous contact with water causes stripping of the asphalt mixture and durability cracking of concrete [1].

Water Movement Through Pavement Systems

Water in the pavement system can exist in a variety of forms. These include water vapor, bound moisture, capillary moisture, and gravitational or free water [2]. The first two are considered negligible for this project. This research will concern itself mainly with draining gravitational free water out of the pavement system.

2

Water can enter the pavement system by two main sources: groundwater and infiltration. Groundwater is water existing in the natural ground in the zone of saturation below the water table. Infiltration is surface water that enters the pavement section by seeping through joints or cracks in the pavement surface, through voids in the pavement itself, or from ditches on the side of the road [2]. Once water enters the pavement system, it can cause or accelerate a number of pavement distresses. The quick and efficient removal of water out of a pavement system is desirable in order to reduce potential distresses. Perhaps the most straightforward way to remove water is to use a base material that allows water to freely drain. This type of material would be characterized by a high hydraulic conductivity, k (see [3] for a discussion on hydraulic conductivity). Note, however, that hydraulic conductivity is only one component of subsurface flow. Unsaturated flow components may also have an effect on subsurface drainage.

To avoid premature failure of pavement systems due to excess moisture, field investigations are conducted. These measurements are useful in characterizing the drainage properties of granular materials. An understanding of subsurface flow will lead to a good understanding of how water drains out of a pavement system. This knowledge of the in situ drainage characteristics of pavement base materials at an early stage of the road design process allows the pavement designer to avoid many design-related problems. The use of a device or process to measure the in situ drainability of base and subgrade materials during construction would indicate whether or not the granular layers are capable of removing infiltrated water from the pavement system at a rate adequate to prevent accelerated pavement deterioration. Table 1.1 shows typical hydraulic conductivity values for different types of soil [4]. The hydraulic conductivity of granular base materials should be similar to that of the gravels in Table 1.1.

Table 1.1 Typical Hydraulic Conductivity Values

Soil	k (m/s)
Clays	$< 10^{-9}$
Sandy Clays	$10^{-9} - 10^{-8}$
Peat	$10^{-9} - 10^{-7}$
Silt	$10^{-8} - 10^{-7}$
Very Fine Sands	$10^{-6} - 10^{-5}$
Fine Sands	$10^{-5} - 10^{-4}$
Coarse Sands	$10^{-4} - 10^{-3}$
Sand with Gravel	$10^{-3} - 10^{-2}$
Gravels	$> 10^{-2}$

Methods to Determine Hydraulic Conductivity of Base Materials

<u>Empirical Equations</u>

One way to determine the hydraulic conductivity of a granular base material is simply to use empirical equations that are based on basic physical properties taken from field measurements. These properties are then input into equations that approximate the hydraulic conductivity. The Federal Highway Administration released a document in 1980 entitled "Highway Subdrainage Design" [2] in which they describe the methods for designing drainage systems in highway pavements. In it, an empirical equation is developed to calculate the hydraulic conductivity of a soil based on basic physical properties [2]. The equation is:

$$k = \frac{\left(6.214 \times 10^5\right)\left(D_{10}^{1.478}\right)\left(1 - \frac{\gamma_d}{62.4G}\right)^{6.654}}{P_{.075}^{.0597}} \qquad (1.1)$$

where D_{10} is the effective grain size (mm), γ_d is the dry density (lb/ft^3), $P_{.075}$ is the percent passing the 0.075-mm sieve, and G is the specific gravity of the soil. The hydraulic conductivity is calculated in ft/d. To convert to cm/s, k should be multiplied by 0.000353.

Elsayed and Lindly [5] describe a number of empirical equations for the hydraulic conductivity. The Hazen formula for the hydraulic conductivity of a clean filter sand is:

$$k(cm/s) = C \cdot D_{10} \tag{1.2}$$

where D_{10} is the effective grain size in cm and C is a coefficient that varies from 90 to 120 with a value of 100 often used. Cedergren presented a simple chart, reproduced in Figure 1.2, which can be used to estimate the hydraulic conductivity [5]. Each curve in the chart has a specific gradation and an associated coefficient of permeability.
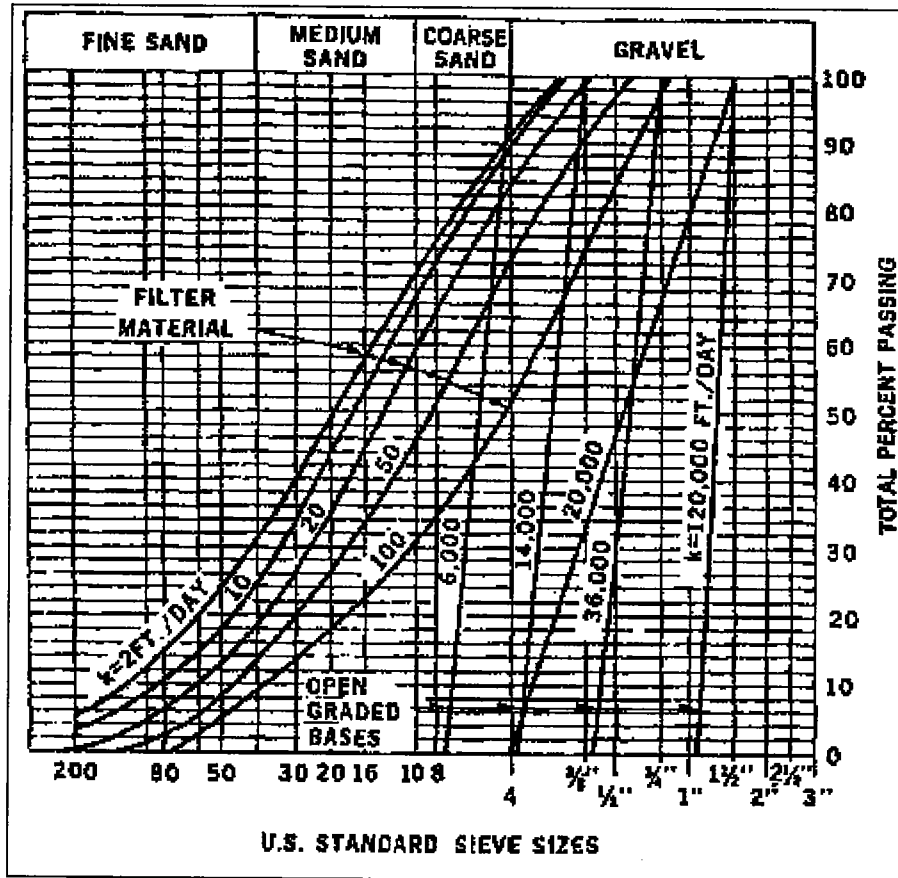
Figure 1.2 Cedergren Chart

In addition, Elsayed and Lindly [5] used a computerized statistical analysis program to conduct a multiple regression analysis. The equation they developed is based on the void ratio and percent by weight of aggregates that pass the 0.6-mm and 0.075-mm sieves. Jaynes and Tyler [6], Schuh and Sweeney [7], and Richardson [8], among others, also developed empirical

5

equations based on material properties. The porosity, effective grain size, bulk density, and gradation are certain characteristics that are used in these equations.

While empirical equations may be useful in characterizing the hydraulic conductivity of a material in some instances, they have some drawbacks. Most importantly, these equations were primarily developed using specific soil or aggregate types. Application of the empirical equations is not universal. The limitations of empirical equations make it desirable to use some sort of device to determine the in situ hydraulic conductivity of a material. The following section lists some of the approaches that have been used to measure the drainage characteristics of a material in the field.

Field Methods

Perhaps the most common test for determining the in situ hydraulic conductivity of a material is the percolation test. Elrick and Reynolds [9] describe it as a very simple test in that it consists of merely pouring water into a hole and measuring how fast it soaks into the soil. However, this test is empirical and not standardized. They also warn that the percolation rate is not only dependent on the hydraulic conductivity but also on many other factors. Additionally, they state that soils are highly variable with respect to their hydraulic properties. To overcome these problems, Elrick and Reynolds developed a new analysis of the percolation test based on three-dimensional, saturated-unsaturated flow theory.

Fernuik and Haug [10] studied various types of infiltrometers to determine the in situ hydraulic conductivity. The sealed single-ring infiltrometer is a device used to measure the rate of infiltration. The hydraulic conductivity can be determined if the head and depth of infiltration are known. The sealed double-ring infiltrometer is a similar device that enables measurement of hydraulic conductivity without piezometers or identification of the wetting front. The double

ring prevents lateral spreading of the permeant (water), and it can eliminate sources of error associated with soil suction and unsaturated hydraulic conductivity. The air-entry permeameter [10] is also similar to the single-ring infiltrometer, except the air-entry permeameter is equipped with a mercury manometer to measure the change in soil suction during infiltration. Infiltrometer measurements of hydraulic conductivity are often based on the assumption that the entire wetted zone is saturated. However, this fails to consider that the soil is not completely saturated near the wetting front and thus soil suction increases the hydraulic gradient.

Reynolds and Elrick [11] also discuss using a single-ring infiltrometer to determine in situ hydraulic conductivity. In addition, they describe using disc permeameters for measuring infiltration with a small head. In a separate study, they describe using tension infiltrometers [12]. They employ a simple method to determine the hydraulic conductivity from either disk or ring infiltrometers. Youngs [13] and Mohanty et al [14] also discuss using infiltrometers to measure in situ hydraulic conductivity. In addition, Mohanty et al describe using a velocity permeameter (falling-head permeameter) and the double-tube method in the field.

Scott et al [15] describe a Field Permeability Testing Device (FPTD) that was constructed at the University of Florida. This is a large and cumbersome device in which two water tanks, a coring machine, generator, Mariotte tank, flow system, control box, hydraulic system, and the probe are mounted on a trailer. This device can use either a constant head or falling head test to determine the hydraulic conductivity. Randolph et al [16] discuss a different FPTD that was modified from an earlier design by Moulton and Seals. This device uses an injection tube to develop saturated steady radial flow in the base, and two radial probes measure the electrical resistance that is translated into velocity. Either a differential manometer or a differential

7

pressure transducer measures the loss in head. This data is then used to calculate the hydraulic conductivity.

Another method that is used to determine the in situ hydraulic conductivity is the cone penetrometer method. Gribb et al [17] describe this device that injects water from a screen and measures pore water pressures at two locations in the soil. Flow data are analyzed via parameter optimization to estimate the hydraulic properties of the material. In saturated soil, the cone permeameter can be used as a simple piezometer for obtaining the hydraulic conductivity.

Constant-Head Permeameter

The most promising device for this study to determine the in situ hydraulic conductivity of a granular material is the constant-head permeameter. This method involves maintaining a constant head of water at the bottom of a cylindrical well hole and measuring the flow rate out of the permeameter and into the soil. One such apparatus is the Guelph permeameter, which was developed in the mid-1980's at the University of Guelph, Ontario, Canada. The permeameter is an in-hole constant-head permeameter that employs the Mariotte principle [18].

The Guelph permeameter, while being relatively simple and quick to operate, is focused on investigating agricultural soils. This study is concerned with much more coarse-grained materials that would be found in pavement base, select granular, and sandy subgrade layers. In addition, the Guelph permeameter was thought to lack the durability needed for repeated field use. This led to the design and assembly of the Minnesota Department of Transportation (Mn/DOT) permeameter as a joint effort between the University of Minnesota and the Minnesota Department of Transportation. The design closely follows that of the Guelph, with a few minor modifications. Refer to Appendix A for a full description of how to operate the Mn/DOT permeameter.

8

The operation of the Mn/DOT permeameter is governed by the Mariotte principle, a simple pressure balance inside the device (Figure 1.3). A constant head level in the well hole is established and maintained by regulating the level of the air tube in the center of the permeameter. As the water level in the permeameter falls, a vacuum is created in the air space above the water. The vacuum is relieved when air, which enters at the top of the air tube, bubbles out of the air inlet tip and rises to the surface of the reservoir. When the water level in the well drops below the elevation of the air inlet tip, air bubbles emerge from the tip and rise into the reservoir air space. The vacuum is then partially relieved and water from the permeameter refills the water in the well. The size and geometry of the openings in the air inlet tip are designed to control the size of air bubbles in order to prevent the well water level from fluctuating.

The permeameter is open to the atmosphere and thus is not a closed system. Therefore, at equilibrium the partial vacuum in the air space above the water in the permeameter plus the pressure due to the height of the water column is equal to the atmospheric pressure.
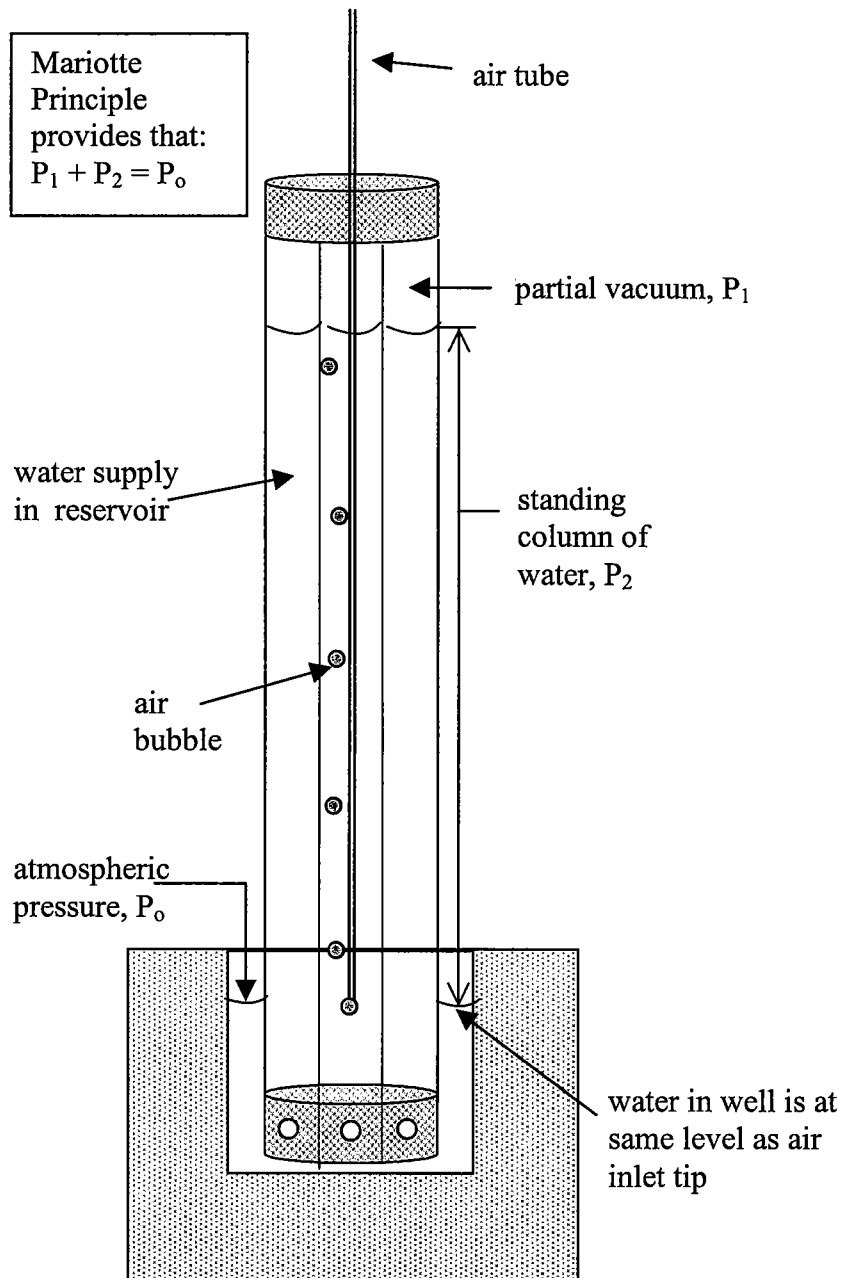
Figure 1.3 Mariotte Principle

Relationship to Previous Work

This project came about from a need for a simple device to measure the hydraulic

conductivity of in situ materials. Researchers and designers from the Minnesota Department of

Transportation (Mn/DOT) were looking for a way to quickly determine the saturated hydraulic

conductivity of base and subgrade materials. Their goal was to identify a device or method that

would be used by field or research personnel to ensure that base and subgrade materials are capable of removing water from pavement systems in order to prevent accelerated pavement deterioration. The device or method was to be durable and easy to use by field personnel.

Birgisson and Solseng [19] performed a comprehensive literature search to identify methods and devices for measuring in situ drainage characteristics of aggregate base and granular subgrade materials. Some of these methods and devices were briefly described above. The significant characteristics of these methods and devices were summarized. A more detailed evaluation and analysis was performed on the most promising methods and devices from the literature search. Ultimately, a new device was built that was closely modeled after the Guelph permeameter.

Objectives

The overriding goal of this research project was to test a simple device, the Mn/DOT permeameter, for its use in measuring the saturated hydraulic conductivity of granular base materials. To accomplish this main goal, the following objectives were considered:

- Evaluate the Mn/DOT permeameter for its ability to accurately measure the in situ saturated hydraulic conductivity of granular materials.
- Test various classes of granular base and subgrade material that are commonly used in Minnesota at the Minnesota Road Research Facility (Mn/ROAD) and at highway construction projects around the state.
- Perform laboratory saturated hydraulic conductivity tests on samples taken from field testing sites.
- Identify a systematic evaluation technique that can be used to obtain reliable field estimates of the hydraulic conductivity of granular materials using the Mn/DOT permeameter.

11

Companion Studies

In addition to the central goal of evaluating a simple device that is used to measure the saturated hydraulic conductivity of an in situ material, a number of companion studies have been conducted. The first of these companion studies consists of constructing a database for use with Microsoft Access. The objective of this project is to collect and store field permeability test data from around Minnesota. The database allows easy access to the data and the gradual addition of data to the database by Mn/DOT personnel during future testing and analysis. This database is fully reported elsewhere [20].

A second companion study involves performing laboratory hydraulic conductivity tests on the same granular materials that were tested in the field. While the testing conditions were likely dissimilar between the field and lab, laboratory tests are currently the standard method for measuring the saturated hydraulic conductivity of each constituent material in the pavement system. Laboratory hydraulic conductivity testing is further reported in Chapters 3 and 4 of this report.

A third and final companion study to the field permeability tests is numerical calibration work done with the SEEP/W program[1]. This work, performed at the University of Florida, uses the actual field conditions (geometry of the well hole) as input and employs an optimization method to solve for the hydraulic conductivity of the material. Results from this numerical study are found in Chapter 5 of this report.

---

[1] SEEP/W, Version 4.20. *GEO-SLOPE International Ltd.*, Calgary, 1998.

Scope

Laboratory and field test results were used to develop procedures for using the Mn/DOT permeameter. This involved developing both standard field techniques/protocols and data interpretation and analysis procedures. A number of theoretical equations that convert the field-measured flow rate into the saturated hydraulic conductivity were identified. These equations were evaluated by comparing the saturated hydraulic conductivity values in the field to (a) those measured in the laboratory and (b) those obtained with the numerical code SEEP/W.

Organization of Report

This report is arranged into six sections: Introduction, Literature Review, Research Methodology, Results and Discussion, Numerical Calibration, and Conclusions and Recommendations. The literature review will provide background information about the theory of saturated/unsaturated flow and different methods used to calculate hydraulic conductivity. Research methodology will discuss field testing procedures over two summers of data collection. The results of all laboratory and field tests will be analyzed and discussed. Numerical calibration will provide a summary of the procedure and results using computer code to model subsurface flow. Conclusions and recommendations present the findings and make recommendations for future research objectives. Literature sources used for background information are cited in the bibliography. The appendices present raw test data and a full user's manual for the Mn/DOT permeameter.

CHAPTER 2

METHODS TO CALCULATE HYDRAULIC CONDUCTIVITY

Introduction

The premise for this research is based on a simple concept. A field permeability test is conducted on an in situ base material as part of a pavement system. The purpose of the field test is to determine the steady flow rate of water out of a constant-head permeameter. By consideration of the nature of the flow of this water into the granular material, one can determine the representative saturated hydraulic conductivity of the base material in the pavement drainage system.

The key to obtaining a reliable estimate of the field-saturated hydraulic conductivity is that the equation that converts flow rate to hydraulic conductivity must capture the essential theoretical features of saturated/unsaturated flow in porous media. Equations of this form in the literature are presented in the context of ideal field conditions. These conditions assume that the material is homogeneous, isotropic, and infinite in all directions. Water is allowed to flow in two directions: vertical and horizontal. Later in this chapter, the development of a number of these equations is outlined. It is recognized, however, that field condidtions are far from ideal. In particular, the material is likely heterogeneous and anisotropic. Pavement base layers are often thin (around 15 cm), so the water from the well hole may also flow into the underlying layers. In addition, effects from the edge of the base layer must also be considered. A discussion of extending the ideal field conditions to actual field conditions is also found in this chapter.

Description of Flow from a Constant-Head Permeameter

Figure 2.1 shows a cross-section of a constant-head permeameter in ideal field conditions. Under these circumstances, the material is assumed to be homogeneous, isotropic, and semi-infinite. The operation of the permeameter creates a cylindrical well hole of radius a in the material that maintains a fixed head H. After a period of time, under the fixed head the flow rate from the permeameter will reach a steady value [21]. At this condition the cross-section under the permeameter shows two distinct regions: (1) a field-saturated "bulb" and (2) an unsaturated fringe region ahead of the bulb.
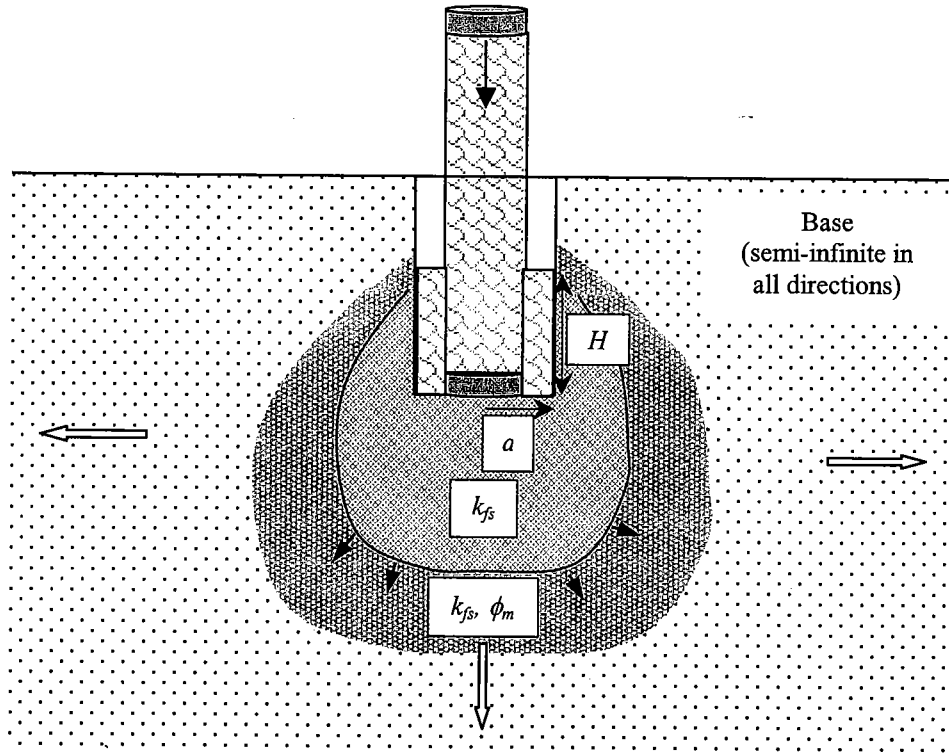
Figure 2.1 Saturated/Unsaturated Flow in Ideal Field Conditions

Saturated flow occurs when all voids in the soil are filled with water. The flow of water in the saturated region is controlled by Darcy's law [3]:

$$q = -k\nabla h \qquad\qquad (2.1)$$

16

In Equation 2.1, q is the volume flux of water (m^3/m^2s), h is the hydraulic head (m) (the sum of pressure and elevation heads), and k is the hydraulic conductivity (m/s). In homogeneous, isotropic soils k is constant and it accounts for the ability of a soil to conduct water under a unit hydraulic potential gradient. In field conditions due to entrapped air the value of the conductivity needs to be replaced by the field-saturated hydraulic conductivity, k_{fs}, a value that is also constant in the saturated region [18]. Based on Equation 2.1, in a saturated isotropic homogeneous medium, continuity of flow reduces to the Laplacian of pressure [4]:

$$\nabla^2 h = 0 \tag{2.2}$$

At the point in which air enters the soil pores, the transition to unsaturated flow occurs. This is shown by the lighter-colored region surrounding the saturated bulb in Figure 2.1. The head at a point in the unsaturated region is given by [22, 23]:

$$h = \psi + z \tag{2.3}$$

where ψ is the pressure head (m) and z is the elevation from a datum. In the unsaturated region the flow is controlled by a Richards equation [22]:

$$q = -k(\psi)\nabla h \tag{2.4}$$

This is similar in form to the Darcy equation (Equation 2.1), but in this case the hydraulic conductivity is not a constant but a function of ψ. In the unsaturated region there will be storage of moisture and the continuity of flow equation, obtained from Equation 2.4, is [22]:

$$\frac{\partial \theta}{\partial t} - \nabla \cdot k(\psi)\nabla h = 0 \tag{2.5}$$

Expanding the second term in Equation 2.5 using Equation 2.3 gives [22, 24]:

$$\frac{\partial \theta}{\partial t} - \nabla \cdot k(\psi)\nabla \psi - \frac{\partial k}{\partial z} = 0 \tag{2.6}$$

This is a commonly used form of Richards equation. Note that as a point approaches saturation

($\theta \rightarrow \theta_{sat}$), Equation 2.6 will reduce to the continuity of flow equation for saturated flow (see Equation 2.2). Hence Equation 2.6 can be used to describe the flow in both the saturated and unsaturated regions. The pressure head ψ will take negative values in the unsaturated region, positive values in the saturated region, and a zero value at the saturated/unsaturated transition.

In seeking a solution to the Richard's equation, it is convenient to linearize the divergence term by introducing the flux potential, ϕ, defined by the Kirchhoff transformation [23]:

$$\phi = \int_{\psi_i}^{\psi} k(\alpha) d\alpha \qquad (2.7)$$

where ψ_i is the initial or far-field pressure head. By the Leibniz rule, the use of Equation 2.7 results in the alternative form of the Richard's equation:

$$\frac{\partial \theta}{\partial t} - \nabla^2 \phi - \frac{\partial k}{\partial z} = 0 \qquad (2.8)$$

Reynolds et al [23] break down the flux potential in Equation 2.7 into two parts:

$$\phi = \int_{\psi_i}^{0} k(\alpha) d\alpha + \int_{0}^{\psi} k(\alpha) d\alpha = \phi_m + k_{fs} \cdot \psi \qquad (2.9)$$

They refer to ϕ_m as the matric flux potential. It is a measure of the capillary action of a unit volume of unsaturated soil. The higher the ϕ_m value, the stronger the capillary effect in the soil. As the soil approaches saturation, the matric flux potential approaches zero.

A number of factors can influence the hydraulic conductivity, $k(\psi)$, of a granular base material [8]. These include:

- Pore size distribution
- Pore continuity
- Pore shape
- Grain size distribution

- Amount of fine materials
- Particle shape
- Relative density
- Degree of saturation or moisture content
- Mineralogical composition
- Viscosity, unit weight, and chemical composition of water

Calculating Field-Saturated Hydraulic Conductivity from a Constant-Head Permeameter

The steady flow, Q, out of a cylindrical well of height H and radius a can be written as [23]:

$$Q = 2\pi H^2 \left[\frac{1}{C^*} + \frac{k_{fs}}{2} \left(\frac{a}{H} \right)^2 \right]$$ (2.10)

where C^* is a dimensionless parameter that depends on the nature of the flow in the saturated/unsaturated regions beyond the well. In physical terms, the C^* factor represents the integral of the pressure head gradients adjacent to the submerged surface of the well [23].

If Equation 2.10 is to be used to calculate k_{fs} from a constant-head permeameter flow rate, the parameter C^* needs to be determined. This requires the solution of the Richard's equation in the saturated/unsaturated domains.

Full analytical solutions of the Richard's equation in order to obtain C^* in Equation 2.10 are not available. Numerical solutions are not feasible. The practical alternative is to seek approximate solutions. A number of approximate methods to determine C^* and k_{fs} are presented in the following sections. These can be split into three classes: (1) those that can be derived from the general analysis of Reynolds and colleagues [23, 25], (2) those based on an analysis by Philip

19

[21], and (3) methods that simultaneously calculated both k_{fs} and ϕ_m [26, 27]. Figure 2.2 shows

the basic parameters that are input into these various theoretical equations.

A = area of permeameter
a = well radius
b = depth to ponded height
H = head
s = depth to impermeable layer

Permeameter

A

b   BASE

H

a

s

SUBGRADE
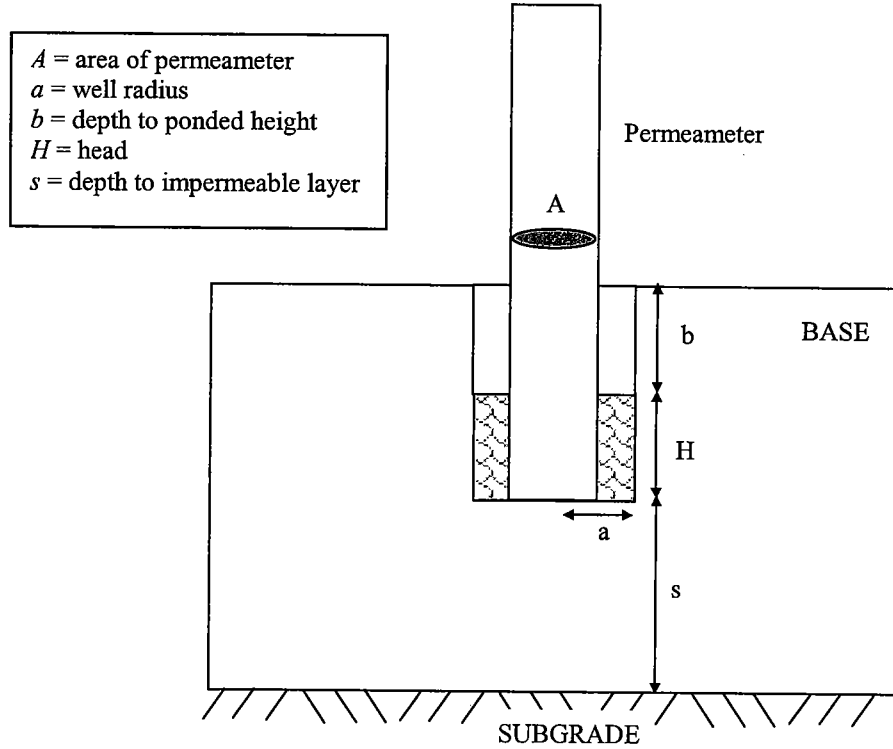
Figure 2.2 Equation Parameters

Reynolds et al Analysis

Reynolds et al [23] attempt a solution of the C factor by simplifying the Richard's

equation. They assume steady flow and neglect gravity effects in the material:

$$\nabla \cdot k(\psi)\nabla \psi = 0 \qquad (2.11)$$

From this simplified model, Reynolds and Elrick [25] obtain the following expression for steady

flow out of a well:

$$Q = \frac{2\pi H^2 k_{fs} + C\pi a^2 k_{fs} + 2\pi H \phi_m}{C} \qquad (2.12)$$

Note that the parameter C in Equation 2.12 is different than C^* in Equation 2.10. This is an

20

extension of the general equation for steady flow from a well (Equation 2.10) that explicitly accounts for the suction in the unsaturated region by the appearance of the matric flux potential, ϕ_m. Elrick and Reynolds [9] interpret Equation 2.12 as follows: the first term on the right side represents the "hydraulic push" of water into the material due to hydrostatic pressure, the second term is the "gravitational pull" of water through the base of the well, and the third term represents the "matric pull" of water out of the well hole due to capillary forces in the surrounding unsaturated region.

Reynolds et al [23] developed an approximate analytical expression for the C factor in Equation 2.12 based on a solution of Equation 2.11 that represents the well as a line source:

$$C = \frac{H^2 \left\{ \frac{(H-b)}{H} \sinh^{-1}\left[\frac{(H-b)}{a}\right] - \sqrt{\left(\frac{a}{H}\right)^2 + \left[\frac{(H-b)}{H}\right]^2} + \frac{a}{H} \right\}}{(H-b)^2} \qquad (2.13)$$

This C factor is dependent on the hydraulic head, H, radius of the well, a, and the depth to the ponded height, b (cm), describing the length of measurement at the well (see Figure 2.2). One important limitation concerning this C factor is that the hydraulic head, H, cannot be equal to the depth to the ponded height, b. If it is, Equation 2.13 is undefined. Amoozegar and Warrick [28] note that when $H \gg a$, Equation 2.13 simplifies to:

$$C = \ln\left[\left(\frac{H}{a}\right) + \sqrt{\left(\frac{H}{a}\right)^2 + 1}\right] - 1 \qquad (2.14)$$

Alternatively, Elrick and Reynolds [29] have created a plot of C vs. H/a (see Figure 2.3). The plot was produced for three different soil types (sand, structured loam and clay, and unstructured clay) [18], but only the curve for sand is reproduced below. This material is most similar to the gravel base materials encountered in this project.
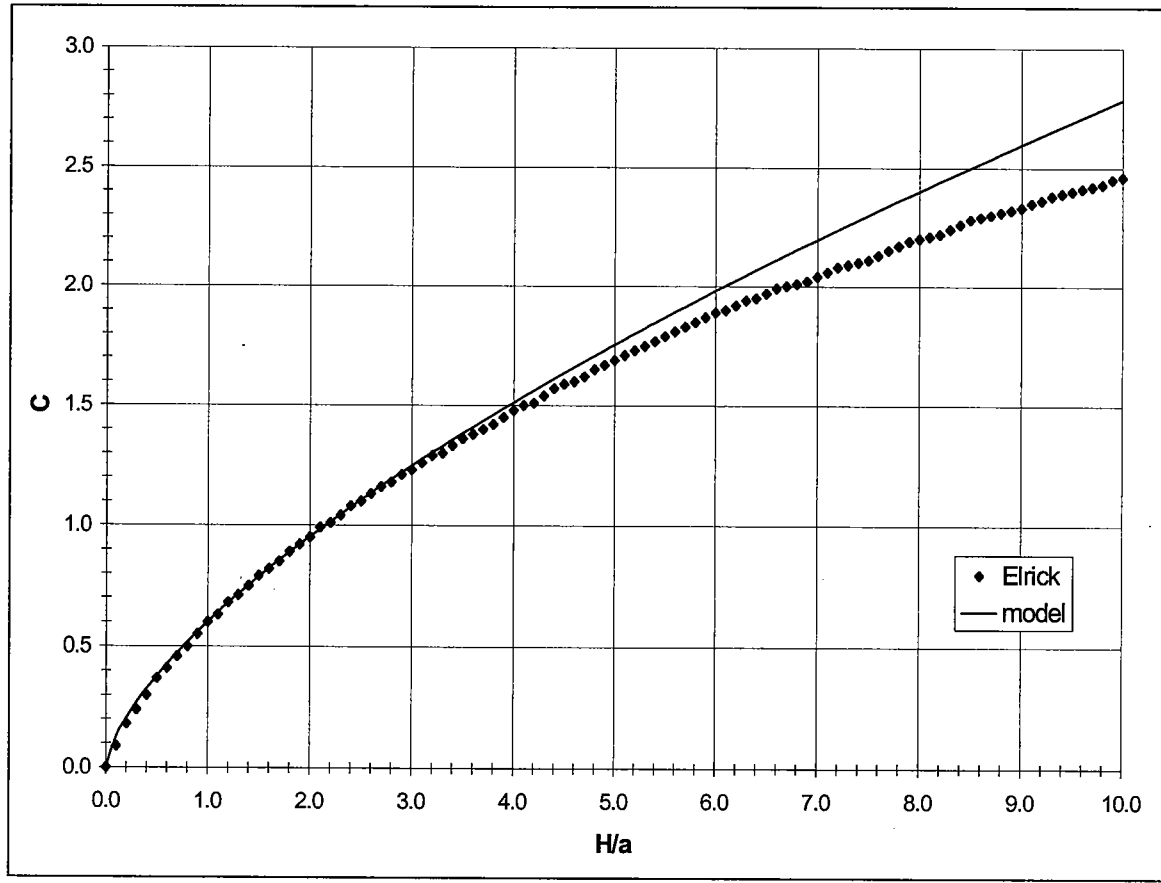
Figure 2.3 Chart for Determining *C* Factor
(After [18])

A simple analysis of this curve reveals that it follows a power law:

$$C = 0.6 * \left(\frac{H}{a}\right)^{2/3} \qquad (2.15)$$

For the range of H/a values that are encountered in this research ($H/a < 3$), the model from Equation 2.15 is virtually identical to the curve proposed by Elrick and Reynolds. The model does not fit the curve quite as well as the value of H/a increases.

22

Models Based on Reynolds et al Analysis

The simplest approach to solving for the hydraulic conductivity neglects the effects of gravity and unsaturated flow from the well [30]. The steady flow out of the well is obtained by neglecting the last two terms in Equation 2.12:

$$Q = \frac{2\pi H^2 k_{fs}}{C} \qquad (2.16)$$

Rearranging this equation to solve for the field-saturated hydraulic conductivity yields:

$$k_{fs} = \frac{CQ}{2\pi H^2} \qquad (2.17)$$

For this research, two models were used to determine the hydraulic conductivity from Equation 2.17. Elrick_a used Equation 2.13 to obtain the C factor, and Elrick_b used the C factor from Figure 2.3.

Elrick et al [30] describe the Glover analysis for determining the field-saturated hydraulic conductivity. This solution again attributes all of the flow out of the borehole to hydrostatic pressure. Glover was concerned with cases where the drainage layer thickness is finite. If the depth to the impermeable layer, s, is greater than $2H$, Glover uses the basic Elrick_a model given in Equation 2.17 with the C factor calculated as:

$$C = \sinh^{-1}\left(\frac{H}{a}\right) - \sqrt{\left(\frac{a}{H}\right)^2 + 1} + \frac{a}{H} \qquad (2.18)$$

When $s < 2H$, however, Glover uses a Richard's solution from Amoozegar and Warrick [28] that accounts for the finite drainage layer depth. In this case the following equation for field-saturated hydraulic conductivity is obtained:

$$k_{fs} = \frac{3Q \ln\left(\frac{H}{a}\right)}{\pi H(3H + 2s)} \qquad (2.19)$$

23

For the most part, pavement base layers are relatively thin. Most often, Equation 2.19 will be used to calculate the hydraulic conductivity in the Glover analysis rather than Equation 2.17. An important limitation of Equation 2.19 is that the pressure head must be larger than the radius of the well hole. The $\ln(H/a)$ term in the numerator is negative if $H/a \leq 1$.

Stephens and Neuman [31] calculate the hydraulic conductivity from Equation 2.17 but account for the effects of both saturated and unsaturated flow. The regression equation they developed uses a different shape coefficient C. This coefficient C depends on H, a, H/a, and curve-fitting parameters of the empirical water content-pressure head relationship [29]. In this way, they arrive at:

$$C = \sinh^{-1}\left(\frac{H}{a}\right) - 1 \qquad (2.20)$$

There is again a limitation on the H/a ratio. This ratio must be above about 1.175 so that $\sinh^{-1}(H/a)$ is greater than one.

Reynolds and Elrick [26] take the model proposed by Elrick et al [30] one step further, ignoring only the effect of unsaturated flow. They assume that the matric flux potential has no effect on driving unsaturated flow in the soil around the saturated bulb. They call this revised model the GP-L model, which it will be referred to in the remainder of this report. Leaving out the third term in Equation 2.12, the steady flow out of a well is:

$$Q = \frac{2\pi H^2 k_{fs} + C\pi a^2 k_{fs}}{C} \qquad (2.21)$$

Equation 2.21 can then be rearranged to solve for the hydraulic conductivity:

$$k_{fs} = \frac{CQ}{2\pi H^2\left[1 + \frac{C}{2}\left(\frac{a}{H}\right)^2\right]} \qquad (2.22)$$

from which the C factor is determined from Figure 2.3 or Equation 2.15.

Philip Analysis

The next section describes the approximate methods to solve for C and k_{fs} based on the Philip analysis. Philip [21] solves the steady-state Richard's equation, but unlike Reynolds and coworkers accounts for gravity flow:

$$\nabla \cdot k(\psi)\nabla \psi - \frac{\partial k}{\partial z} = 0 \qquad (2.23)$$

Philip Model

Philip [21] made a number of improvements involving the assumptions used to calculate field-saturated hydraulic conductivity. He developed an approximate analysis based on revised geometry and flow assumptions. The adjustments made in his approach include:

- Replace cylindrical water-filled length of borehole by half a spheroid
- Replace calculated saturated bulb by a spheroid
- Estimate total flow (due to gravity and capillarity) from a spheroid using results for absorptive (capillary) flow from the spheroid and total flow from the sphere
- Include both gravity and capillarity terms in equations
- Adopt a constant C factor for a fixed H

Under these conditions, Philip developed the following approximate solution for flow from the well hole:

$$\frac{Q}{k_{fs}a^2} = \sqrt{\left(\frac{H}{a}\right)^2 - 1}\left\{ \frac{4.117\left(\frac{H}{a}\right)\left[1 - \left(\frac{a}{H}\right)^2\right]}{\ln\left[\left(\frac{H}{a}\right) + \sqrt{\left(\frac{H}{a}\right)^2 - 1}\right] - \sqrt{1 - \left(\frac{a}{H}\right)^2}} + \frac{4.028 + 2.517\left(\frac{a}{H}\right)}{\frac{a\alpha}{2}\ln\left[\left(\frac{H}{a}\right) + \sqrt{\left(\frac{H}{a}\right)^2 - 1}\right]} \right\} \qquad (2.24)$$

The term α is known as the alpha parameter; like the matric flux potential, ϕ_m, it is a measure of the capillarity of the material ($\alpha = k_{fs}/\phi_m$). As the material approaches saturation, α approaches

25

infinity. Philip questions the use of the borehole permeameter in unsaturated soil as a means determining k_{fs}, especially when H is small and α is not independently measured. He also finds fault with the simultaneous equations approach (described in a later section) because of experimental error and the likelihood of spatial variation in soil properties. In his opinion, the concept of analyzing a saturated bulb surrounded by an unsaturated zone has a greater potential for assessing the hydraulic conductivity of a granular soil.

Wu et al Model

Wu et al [32] simplified the Philip model that used the lower half of a spheroid to describe the shape of water in the borehole. This solution again assumed a value for α consistent with the soil type under investigation. Their solution for field-saturated hydraulic conductivity is:

$$k_{fs} = \cfrac{\cfrac{Q}{\pi a^2 \sqrt{\left(\dfrac{H}{a}\right)^2 - 1}}}{\cfrac{(1.5)^{\frac{2}{3}}\left(\dfrac{H}{a}\right)\left[1 - \left(\dfrac{a}{H}\right)^2\right]}{\ln\left[\left(\dfrac{H}{a}\right) + \sqrt{\left(\dfrac{H}{a}\right)^2 - 1}\right] - \sqrt{1 - \left(\dfrac{a}{H}\right)^2}} + \cfrac{2(1.5)^{\frac{1}{3}}\left(0.56 + 0.35H^{-1}\right)}{\dfrac{\alpha}{2}\ln\left[\left(\dfrac{H}{a}\right) + \sqrt{\left(\dfrac{H}{a}\right)^2 - 1}\right]}} \qquad (2.25)$$

If the alpha parameter is assumed to be infinity at saturation, the second term in the denominator disappears. This leads to a simpler equation:

$$k_{fs} = \cfrac{\cfrac{Q}{\pi a^2 \sqrt{\left(\dfrac{H}{a}\right)^2 - 1}}}{\cfrac{(1.5)^{2/3}\left(\dfrac{H}{a}\right)\left[1 - \left(\dfrac{a}{H}\right)^2\right]}{\ln\left[\left(\dfrac{H}{a}\right) + \sqrt{\left(\dfrac{H}{a}\right)^2 - 1}\right] - \sqrt{1 - \left(\dfrac{a}{H}\right)^2}}} \qquad (2.26)$$

Heinen and Raats Model

Heinen and Raats [33] also developed an equivalent solution to the Philip model using the more advanced geometry assumptions. Again, this method requires an assumption of either ϕ_m or α. However, α is assumed to go to infinity thus simplifying the equation. The solution attempts to consider the saturated bulb as well as the surrounding unsaturated envelope in the soil. The hydraulic conductivity is calculated as:

$$k_{fs} = \cfrac{Q \cdot \left\{ \left(\dfrac{H}{a}\right)\ln\left[\left(\dfrac{H}{a}\right) + \sqrt{\left(\dfrac{H}{a}\right)^2 - 1}\right] - \sqrt{\left(\dfrac{H}{a}\right)^2 - 1} \right\}}{(1.5)^{2/3} \pi a^2 \left[\left(\dfrac{H}{a}\right)^2 - 1\right]^{3/2}} \qquad (2.27)$$

The limitation of Equations 2.25 – 2.27 is that the ratio H/a must be greater than one for the function to be defined. In granular base materials used in pavements the layers are often quite thin. Therefore it is sometimes difficult to achieve this $H/a > 1$ requirement.

Discussion of Single Equation Methods

The theoretical models that calculate the field-saturated hydraulic conductivity consider part or all of the Richards equation (Equation 2.6), describing steady flow out of a cylindrical well hole. The basic assumptions used in each model are shown in Figure 2.4 and Table 2.1.

27

The terms "hydraulic push," "gravitational pull," and "matric pull" are coined by Elrick and Reynolds [9].
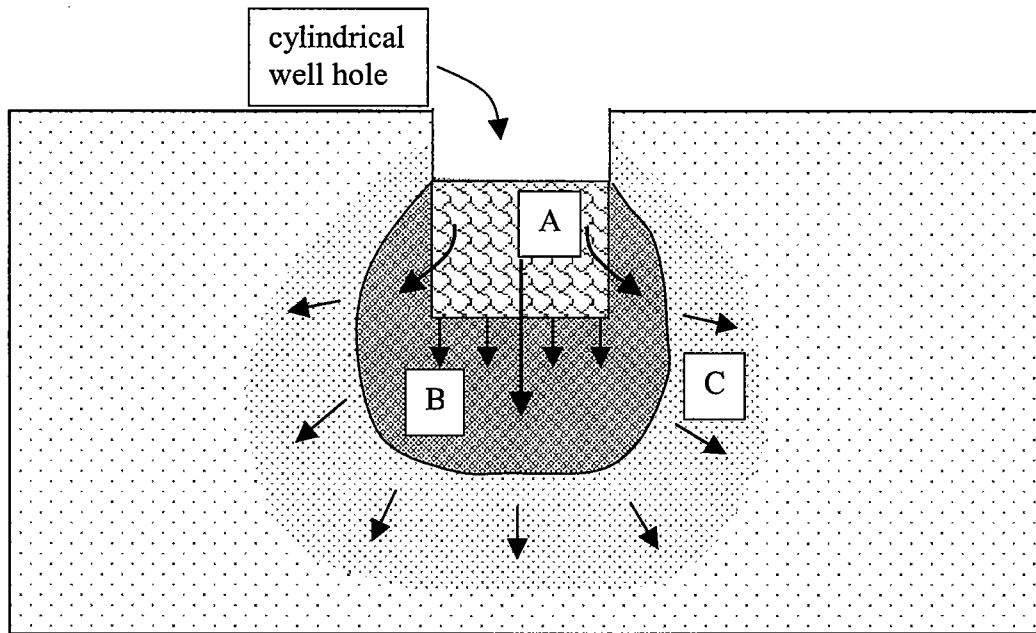
Figure 2.4 Steady Flow out of a Cylindrical Well Hole

Table 2.1 Flow Assumptions for Each Model

$Q \sim$	A hydraulic push due to hydrostatic pressure	B gravitational pull through the bottom of the well hole	C matric pull of water due to capillary forces in unsaturated soil	
Model				**Comments**
General Reynolds et al Analysis	x	x	x	solves $\nabla \cdot k(\psi)\nabla \psi = 0$
Elrick_a	x	—	—	neglect gravity, unsaturated flow
Elrick_b	x	—	—	neglect gravity, unsaturated flow
Glover	x	—	—	accounts for finite depth
Stephens	x	—	x	unsaturated flow included in C
GP-L	x	x	—	ignores only unsaturated flow
Simultaneous Equations Approach	x	x	x	solves Equation 2.12 twice for k_{fs} and ϕ_m
General Philip Analysis	x	x	x	solves $\nabla \cdot k(\psi)\nabla \psi - \dfrac{\partial k}{\partial z} = 0$
Heinen & Raats/ Wu et al	x	x	—	ignores only unsaturated flow

In essence, all of the above methods for calculating the hydraulic conductivity of material involve the steady flow rate multiplied by some shape factor, C^+. These can be written in the general form:

$$k_{fs} = C^+ Q \qquad (2.28)$$

The form of the shape factor is directly related to the simplifications used in each model (see Figure 2.4 and Table 2.1). Insight into how the form of C^+ changes between models can be obtained by plotting the C^+ for each of six one-equation models with the Elrick curve in Figure 2.3. To achive this, constant values of $H + b = 6$ inches, $s = 6$ inches and $a = 2$ inches are used and the value of $C^+/2\pi H^2$ is plotted against $0.5 < H/a < 2.5$ (the expected operating range of the Mn/DOT permeameter). For this H/a range, the five shape factors are plotted in Figure 2.5.
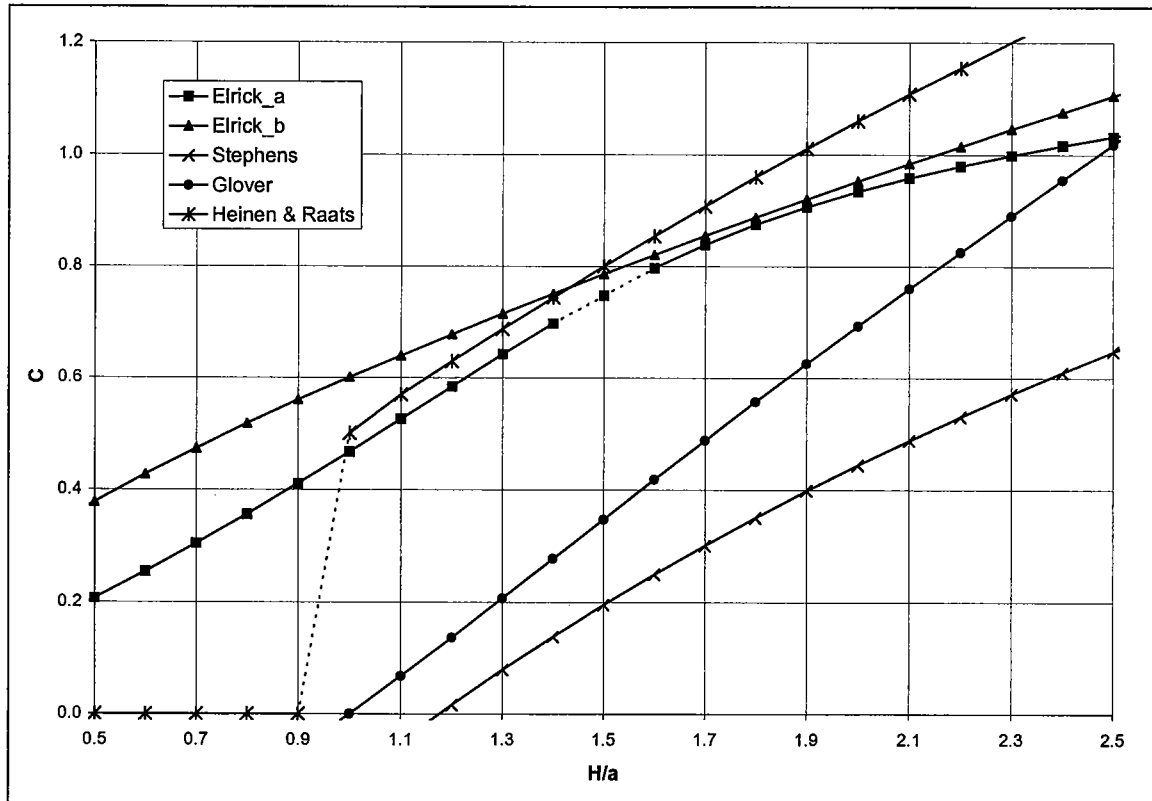
Figure 2.5 Shape Factor Comparison

There are some critical points to note:

1. The Elrick_a model that uses the C factor calculated in Equation 2.13 is singular at test points where $H = b$ (see dashed portion in Figure 2.5).

2. The calculation of the C factor in the Glover model and the models based on the Phillip model (Equation 2.24) is only valid if $H/a > 1$. Further, the calculation of the C factor in the Stephens model (Equations 2.17, 2.20) is only valid if $H/a > \sim 1.175$. At values below these limits a negative k_{fs} will result or the calculation will be invalid. As noted above in field measurements it is not always possible to achieve the $H/a > 1$ requirement.

3. The shift between the curves can be attributed to the different assumptions used in obtaining the approximate solutions of the Richards equation [34]. In particular note that (i) the lower level of the Glover model could be attributed to the fact that this model tries to account for a finite thickness in the drainage base, and (ii) the shift in the Heinen & Raats model is probably due to the assumption of spheroid as opposed to a cylindrical bulb.

4. For the most part, all of the curves have the same shape in the permeameter operating range, $0.5 < H/a < 2.5$, and all of the C curves in Figure 2.5 can be fitted with a fair degree of accuracy by adjusting the constant $D = 0.6$ in the power law fit to the Elrick C curve (see Equation 2.15).

Simultaneous Equations Approach

The hydraulic conductivity calculations in this section all involve ponding two or more heads in succession and measuring the corresponding steady flow rates out of the permeameter. They are used to simultaneously calculate the field-saturated hydraulic conductivity and the matric flux potential of the material.

<u>Guelph Model</u>

The Guelph model is a simultaneous equations approach that takes two successive ponded heights and the corresponding flow rates and calculates the hydraulic conductivity and matric flux potential. It involves writing the Richards equation (Equation 2.12) for steady flow twice for the two ponded heights, H_1 and H_2 [25]:

$$Q_1 = \frac{2\pi H_1^2 k_{fs} + C_1 \pi a^2 k_{fs} + 2\pi H_1 \phi_m}{C_1} \qquad (2.29a)$$

$$Q_2 = \frac{2\pi H_2^2 k_{fs} + C_2 \pi a^2 k_{fs} + 2\pi H_2 \phi_m}{C_2} \qquad (2.29b)$$

By solving Equations 2.29a and 2.29b simultaneously, the field-saturated hydraulic conductivity can be calculated as [23]:

$$k_{fs} = G_2 Q_2 - G_1 Q_1 \qquad (2.30)$$

where

$$Q_1 = A \cdot R_1 \qquad (2.31a)$$

$$Q_2 = A \cdot R_2 \qquad (2.31b)$$

$$G_2 = \frac{H_1 C_2}{\pi \{ 2H_1 H_2 (H_2 - H_1) + a^2 (H_1 C_2 - H_2 C_1) \}} \qquad (2.32)$$

and

$$G_1 = G_2 \frac{H_2 C_1}{H_1 C_2} \qquad (2.33)$$

The solution for matric flux potential is [26]:

$$\phi_m = J_1 Q_1 - J_2 Q_2 \qquad (2.34)$$

where

31

$$J_1 = \frac{\left(2H_2^2 + a^2 C_2\right)C_1}{2\pi\left[2H_1 H_2\left(H_2 - H_1\right) + a^2\left(H_1 C_2 - H_2 C_1\right)\right]} \quad (2.35)$$

and

$$J_2 = J_1 \frac{\left(2H_1^2 + a^2 C_1\right)C_2}{\left(2H_2^2 + a^2 C_2\right)C_1} \quad (2.36)$$

In the above equations, A (cm^2) is the cross-sectional area of the permeameter, R_1 and R_2 (cm/s) are the steady flow rates out of the permeameter, and C_1 and C_2 are dimensionless shape factors determined from Figure 2.3 [26].

This solution is based on the assumptions that the soil is homogeneous, isotropic, and free from large macropores or discontinuities. However, the Guelph approach often leads to negative values for k_{fs} or ϕ_m. Heinen and Raats [33] suggest that these negative values can be explained by the fact that most soils are not truly homogeneous, isotropic, or uniform. This observation leads to discharge ratios (Q_2/Q_1) that are either too large or too small. The ratio must fall within a certain range for the calculations to be meaningful. This assertion has been validated by numerical studies. Reynolds and Elrick [26] also support this notion and attribute negative calculations to a significant heterogeneity, such as a large macropore or layer boundary, encountered between the two H levels. When either k_{fs} or ϕ_m are found negative, both values should be discarded. Elrick et al [30] describe the main factors influencing the Q_2/Q_1 ratio as measurement errors or local small-scale variations of soil hydraulic properties. The errors that may affect Q_1 and Q_2 include non-attainment of "true" steady flow, errors because of air bubble size and reading errors, and entrapped air in soil during refilling of the permeameter.

Least-Squares Approach

Reynolds and Elrick [26] suggest that a persistent problem of negative values can often be solved by successive ponding of three or more H levels and using the least squares solution to

solve for the flow rate out of the well. This solution neglects the gravitational term in Equation 2.12 as follows [23]:

$$Q = \frac{\left(2\pi k_{fs}\right)H^2 + \left(2\pi\phi_m\right)H}{C}$$

(2.37)

The least squares solution for field-saturated hydraulic conductivity is [26]:

$$k_{fs} = \frac{\sum_{i=1}^{n}H_i^2\sum_{i=1}^{n}C_iQ_i\left(\frac{C_ia_i^2}{2}+H_i^2\right) - \sum_{i=1}^{n}H_iC_iQ_i\sum_{i=1}^{n}H_i\left(\frac{C_ia_i^2}{2}+H_i^2\right)}{2\pi\left\{\sum_{i=1}^{n}H_i^2\sum_{i=1}^{n}\left(\frac{C_ia_i^2}{2}+H_i^2\right)^2 - \left[\sum_{i=1}^{n}H_i\left(\frac{C_ia_i^2}{2}+H_i^2\right)\right]^2\right\}}$$

(2.38)

where n is the number of successive H levels. The least squares solution for matric flux potential is [26]:

$$\phi_m = \frac{\sum_{i=1}^{n}C_iQ_i\left(\frac{C_ia_i^2}{2}+H_i^2\right)\sum_{i=1}^{n}H_i\left(\frac{C_ia_i^2}{2}+H_i^2\right) - \sum_{i=1}^{n}H_iC_iQ_i\sum_{i=1}^{n}\left(\frac{C_ia_i^2}{2}+H_i^2\right)^2}{2\pi\left\{\left[\sum_{i=1}^{n}H_i\left(\frac{C_ia_i^2}{2}+H_i^2\right)\right]^2 - \sum_{i=1}^{n}H_i^2\sum_{i=1}^{n}\left(\frac{C_ia_i^2}{2}+H_i^2\right)^2\right\}}$$

(2.39)

This approach encounters a few problems. First, many of the base layers tested are only 15 cm thick. To pond three or more different heads in this thin of a layer is very difficult. There is often simply not enough room vertically to conduct the test. In addition, this approach calculates the matric flux potential at saturation, when it is assumed to be zero.

The hydraulic conductivity value obtained from the Richard's analysis effectively averages the vertical and horizontal k_{fs} values at a point measurement. This process assumes that the soil is homogeneous and isotropic. As previously mentioned, this is probably not the case. Therefore, it is suggested to replicate the test several times to assure the accuracy of the measurements. Heinen and Raats [33] also note that the wetted region of soil consists of a small

saturated zone around the well, surrounded by a much larger unsaturated envelope. They suggest that the solutions set forth by Reynolds and Elrick do not take both of these zones into account.

<u>Amoozegar Model</u>

Amoozegar [27] developed an equation similar to the Guelph approach presented by Reynolds and Elrick. The analysis consists of ponding two successive heads and measuring the corresponding flow rates. The field-saturated hydraulic conductivity is computed as:

$$k_{fs} = \left[\frac{C_2(a+2H_2)}{4\pi H_2^2(H_2-H_1)}\right]Q_2 - \left[\frac{C_1(a+2H_1)}{4\pi H_1^2(H_2-H_1)}\right]Q_1 \qquad (2.40)$$

where C is found from Equation 2.18.

The value calculated for k_{fs} represents the hydraulic conductivity over the distance ($H_2 - H_1$) at the bottom of the well hole. For homogeneous and isotropic materials, k_{fs} calculated by the Amoozegar solution is similar to k_{fs} obtained by the Guelph approach [27]. Like the Guelph approach, the Amoozegar approach often calculates a negative value for the hydraulic conductivity. It is not a very robust equation.

Summary of Equations

From the above description of theoretical models of flow, eight equations were selected for this research to investigate their usefulness in calculating the field-saturated hydraulic conductivity. These equations are reproduced in Table 2.2.

Table 2.2 Summary of Hydraulic Conductivity Equations

Model	Hydraulic Conductivity	Shape Factor C
Elrick_a	$k_{fs} = \dfrac{CQ}{2\pi H^2}$	Equation 2.13
Elrick_b	$k_{fs} = \dfrac{CQ}{2\pi H^2}$	Figure 2.3
Glover	$k_{fs} = \dfrac{3Q\ln\left(\dfrac{H}{a}\right)}{\pi H(3H + 2s)}$	--
Stephens	$k_{fs} = \dfrac{CQ}{2\pi H^2}$	Equation 2.20
GP-L	$k_{fs} = \dfrac{CQ}{2\pi H^2\left[1 + \dfrac{C}{2}\left(\dfrac{a}{H}\right)^2\right]}$	Figure 2.3
Heinen & Raats / Wu et al	$k_{fs} = \dfrac{Q\cdot\left\{\left(\dfrac{H}{a}\right)\ln\left[\left(\dfrac{H}{a}\right) + \sqrt{\left(\dfrac{H}{a}\right)^2 - 1}\right] - \sqrt{\left(\dfrac{H}{a}\right)^2 - 1}\right\}}{(1.5)^{2/3}\pi a^2\left[\left(\dfrac{H}{a}\right)^2 - 1\right]^{3/2}}$	--
Guelph	$K_{fs} = G_2 Q_2 - G_1 Q_1$	Equation 2.32, 2.33; Figure 2.3
Amoozegar	$k_{fs} = \left[\dfrac{C_2(a + 2H_2)}{4\pi H_2^2(H_2 - H_1)}\right]Q_2 - \left[\dfrac{C_1(a + 2H_1)}{4\pi H_1^2(H_2 - H_1)}\right]Q_1$	Equation 2.18

Flow in Actual Field Conditions

The equations in Table 2.2 provide a number of means by which field permeameter measurements of flow rate can be translated into approximate values for the field-saturated hydraulic conductivity. Use of these equations, however, explicitly assumes ideal field conditions, in particular a semi-infinite, isotropic, homogenous layer. It is realized that conditions in the field are often far from ideal. This project is concerned with pavement base materials, which are often composed of several different layers. If the base layer is too thin, water entering the pavement system through the well hole likely will also enter the subgrade

layer; this can be seen in Figure 2.6. This condition is not taken into account in any of the models presented in this chapter. The consequences of a thin layered system are investigated in detail in Chapter 5.
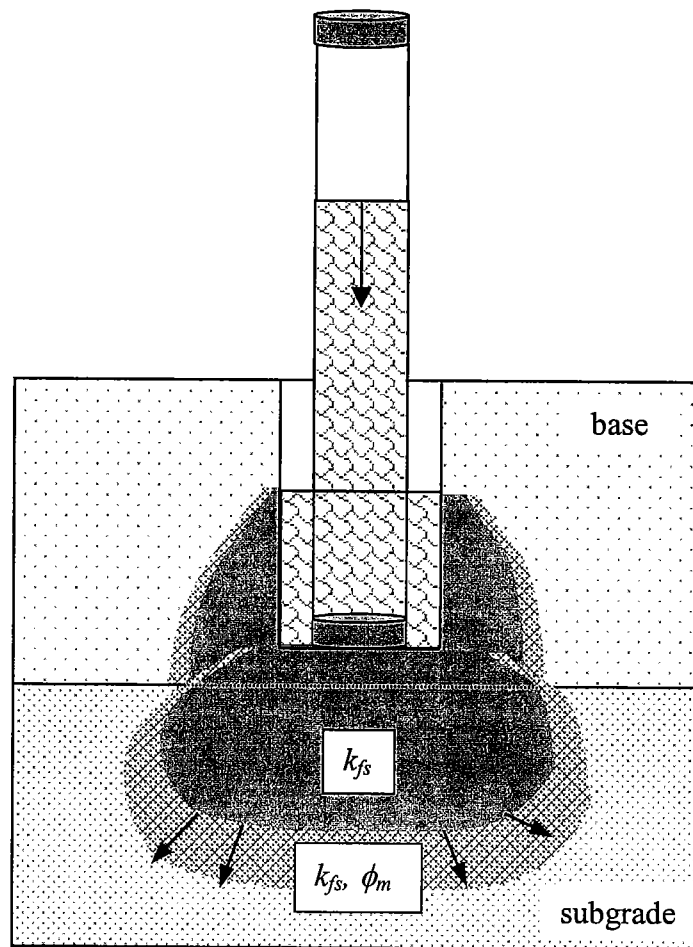
Figure 2.6 Saturated/Unsaturated Flow in Actual Field Conditions

Despite these concerns about using idealized equations in a field setting, it is worthwhile investigating the eight models presented in Table 2.2 for calculating the field-saturated hydraulic conductivity of granular base materials from a flow rate obtained by permeameter measurements. There are two ways in which to do this:

1. Collect field samples of the same material that was tested with the Mn/DOT permeameter and measure the laboratory saturated hydraulic conductivity value. The results of the laboratory tests will be compared to the results of the field tests in Chapters 3 and 4.

2. Use a numerical modeling procedure to determine the field-saturated hydraulic conductivity for each site and compare that value to the value obtained in the field. This will be described in Chapter 5.

CHAPTER 3

RESEARCH METHODOLOGY

Description of Base Materials

The focus of this research was to evaluate the Mn/DOT permeameter for its use in measuring the field-saturated hydraulic conductivity of pavement base materials. This was accomplished by visiting highway construction sites around the state of Minnesota and testing the saturated hydraulic conductivity of in situ base materials. Sites were chosen to represent the common materials used in highway construction in Minnesota. Pavement base layers are commonly constructed of Class 5 and/or Select Granular materials, although other materials are also used. Table 3.1 gives the gradation specifications for aggregate base materials used in Minnesota [35]. Mn/DOT also defines Select Granular material as any pit-run or crusher-run material that is so graded from coarse to fine that the ratio of the portion passing the 75-mm sieve divided by the portion passing the 25.0-mm sieve may not exceed 12 percent by mass (that is: 75 mm/25.0 mm ratio). The material shall not contain oversize salvaged bituminous particles or stone, rock, or concrete fragments in excess of the quantity or size permissible for placement as specified [36].

Table 3.1 Mn/DOT Aggregate Gradation [35]

Total Percent Passing Sieve Size		BASE AND SURFACING AGGREGATES						
English	Metric	Class 1	Class 2	Class 3	Class 4	Class 5	Class 6	Class 7 (a)(b)(c)
3"	75 mm	--	--	--	--	--	--	
2"	50 mm	--	--	100	100	--	--	
1.5"	37 mm	--	--	--	--	--	--	
1"	25 mm	--	--	--	--	100	100	
3/4"	19 mm	100	100	--	--	90-100	90-100	
3/8"	9.5 mm	65-90	65-90	--	--	50-90	50-85	
#4	4.75 mm	40-85	35-70	35-100	35-100	(A)35-80	35-70	
		--	--	--	--	(B)35-70	--	
#10	2.00 mm	25-70	25-45	20-100	20-100	(A)20-65	20-55	
		--	--	--	--	(B)20-55	--	
#40	0.425 mm	10-45	12-30	5-50	5-35	10-35	10-30	
#200	0.075 mm	8-15	5-13	5-10	4-10	3-10	(A)3-7	
		--	--	--	--	--	(B)4-8	

NOTES:
(A) Applies when the aggregate contains 60 percent or less of crushed quarry rock.
(B) Applies when the aggregate contains more than 60 percent crushed quarry rock.

(a) Refer to Section 3138.2B.
(b) Class 7 shall meet the gradation requirements for Class 5 when it is being substituted for Classes 1, 3, 4 and 5.
(c) Class 7 shall meet the gradation requirements for Class 6 when it is being substituted for Class 6.

In addition to testing gravel base materials around Minnesota, field testing was also done at Mn/DOT's MnROAD site. MnROAD was chosen for field testing because of strict control during construction and because of the many different class materials located on one project. Table 3.2 shows the more restrictive gradation requirements for MnROAD base materials [37].

Table 3.2 MnROAD Aggregate Gradation [37]

Sieve Size		Total Percent Passing			
English	Metric	Class 3 Sp.	Class 4 Sp.	Class 5 Sp.	Class 6 Sp.
1 1/2"	37.5 mm	--	100	--	--
1"	25.0 mm	--	95-100	100	100
3/4"	19.0 mm	--	90-100	90-100	85-100
1/2"	12.5 mm	100	--	--	--
3/8"	9.5 mm	95-100	80-95	70-85	50-70
#4	4.75 mm	85-100	70-85	55-70	30-50
#10	2.00 mm	65-90	55-70	35-55	15-30
#40	0.425 mm	30-50	15-30	15-30	5-15
#200	0.075 mm	8-15	5-10	3-8	0-5

NOTE: Both Class 3 Sp. and Class 4 Sp. meet Mn/DOT specifications
for "Granular Borrow" and "Select Granular Borrow"

Using the Mn/DOT Permeameter in the Field

Chapter 2 described saturated/unsaturated flow in the granular material during a field

permeability test. This section will briefly describe how to conduct the test. A hand auger is

used to dig a hole in the base material. The hole is roughly 10 cm in diameter and must go to

mid-depth of the base layer, or at least 15 cm deep. The Mn/DOT permeameter is then placed in

the well hole and supported upright. The air tube of the permeameter is lifted, allowing water to

flow into the granular material. The water flows out of the permeameter under a constant head,

and the flow rate is measured at regular time intervals. After a period of time, the flow rate will

reach a steady value. This steady flow rate is then used in the calculations for field-saturated

hydraulic conductivity. A more detailed procedure for carrying out field permeability tests is

explicitly laid out in the "Minnesota Department of Transportation Permeameter User's

Manual," which is attached as Appendix A.

Field Testing

Initial Field Testing – Summer 1999

Initial field testing was performed with the Mn/DOT permeameter during the summer of 1999. Hydraulic conductivity data was collected at twelve construction sites around the state. Table 3.3 summarizes the twelve sites. In addition to these construction sites, field testing was performed at the MnROAD site. Table 3.4 summarizes the test locations at MnROAD.

Table 3.3 1999 Testing Locations

Location	Material
Dakota Co. Rd. 26 Eagan	Class 5
US 169 Mille Lacs	Class 6
US 12 Cokato	Class 5
Blue Earth Co. Rd. 90 Mankato	Class 3
Blue Earth Co. Rd. 90 Mankato	Class 5
US 169 Onamia	Class 6
TH 25 Monticello	Class 6
TH 73 Kettle River	Class 6
I 35W Richfield	Class 5
TH 7 Silver Lake	Class 5
TH 371 Brainerd	Class 6
TH 371 Brainerd	Select Granular

Table 3.4 1999 MnROAD Locations

Location	Material
Cell 32	Class 1
Cell 33	Class 6
Cell 34	Class 5
Cell 35	Class 1
Test pad	Class 5

Detailed Field Testing – Summer 2000

The field testing procedure during this phase was very similar to the one used during initial field testing. However, one major concern was whether or not the flow rate out of the permeameter ever reached a steady value. Care was taken to ensure that the flow rate had indeed reached a steady value before each test was completed. This was usually accomplished by carrying out each test for 15-20 minutes. At times when the flow rate was very slow out of the

42

permeameter, the test took over one hour to complete. In these cases, the time intervals at which readings were taken were extended. This was an indication that the material had a very low hydraulic conductivity. At other times when the flow rate was very fast, the time interval used to measure the rate was significantly shortened. These cases indicated that the base material had a high hydraulic conductivity value.

Nineteen construction sites were tested during this phase. The Mn/DOT permeameter was again used to collect hydraulic conductivity data. Table 3.5 summarizes the testing locations. Fewer hydraulic conductivity tests were conducted at each site, but the focus was on performing the tests correctly and carefully.

Table 3.5 2000 Testing Locations

Location	Material
MnROAD Cell 32	Class 1-c
MnROAD Cell 52	Class 4
I 35W Richfield	Class 5
Olmsted Co. Rd. 117	Class 5
TH 371 Brainerd	Class 5
TH 5 Eden Prairie	Class 5
US 10 Hastings	Class 5
US 169 Jordan	Class 5
Olmsted Co. Rd. 104	Class 5 Modified
US 10 Hastings	Class 6
TH 14 Mankato	Class 7
TH 22 St. Peter	Class 7
I 94 Minneapolis	Sand
TH 371 Brainerd	Sand
TH 14 Mankato	Select Granular
TH 22 St. Peter	Select Granular
TH 610 Brooklyn Center	Select Granular
US 12 Cokato	Select Granular
US 212 Eden Prairie	Select Granular

Raw Data

The raw data collected from the field permeability tests is presented in Appendix B. The data collected at each site include:

- Location, material, and date of test
- Cross-sectional area of permeameter, A
- Radius of well, a
- Two successive head measurements, H_1 and H_2
- Depth to impermeable layer, s
- Depths to ponded heights, b_1 and b_2
- Flow rates R_1 and R_2 with each time stamp (R = change in height / change in time)

Additional Field Testing

In addition to the field hydraulic conductivity tests, in situ density and moisture tests were to be performed at each site. Testing was performed in accordance with ASTM D 1556 – 90, *"Standard Test Method for Density and Unit Weight of Soil in Place by the Sand-Cone Method."* A six-inch sand cone was used for the density testing. The original intent was to conduct in situ density and moisture tests at each site. However, these measurements were collected at only four locations during the summer of 1999. During the second phase of testing, in situ density and moisture tests were conducted at all nineteen sites.

Collection of Samples for Laboratory Testing

Besides performing hydraulic conductivity, density, and moisture tests in the field, samples of each material were also taken for further laboratory testing. The samples were taken directly out of the in place base material using a shovel. These samples were used in various laboratory tests, including:

- Flexible wall permeability
- Sieve analysis
- Specific gravity
- Modified Proctor

All of the samples taken during the summers of 1999 and 2000 have been tested in this fashion. This laboratory testing was done by Soil Engineering Testing, Inc. in Bloomington, Minnesota. Sieve analysis data for each material is collected in Appendix C. The results from the flexible wall permeability tests are shown in Table 3.6. These results will be used as a point of comparison in the next chapter.

Table 3.6 Flexible Wall Permeability Results

Location	Material	k_1, cm/s	k_2, cm/s	k_3, cm/s	k_{ave}, cm/s
Blue Earth Co. Rd. 90	Class 3	6.7E-05	1.1E-04	3.1E-05	6.93E-05
Blue Earth Co. Rd. 90	Class 5	2.0E-04	2.9E-04	2.9E-04	2.60E-04
Dakota Co. Rd. 26	Class 5	1.1E-04	7.4E-05	5.7E-05	8.03E-05
I 35W Richfield	Class 5	4.2E-05	1.0E-05	2.2E-05	2.47E-05
TH 25 Monticello	Class 6	2.3E-04	1.5E-04	1.4E-04	1.73E-04
TH 371 Brainerd	Class 6	2.9E-04	1.3E-04	1.2E-04	1.80E-04
TH 371 Brainerd	Select Granular	1.7E-04	1.3E-04	2.3E-04	1.77E-04
TH 7 Silver Lake	Class 5	1.4E-05	1.0E-05	7.6E-06	1.05E-05
TH 73 Kettle River	Class 6	2.9E-06	6.1E-06	6.0E-06	5.00E-06
US 12 Cokato	Class 5	3.1E-05	2.6E-05	1.2E-05	2.30E-05
US 169 Mille Lacs	Class 6	9.6E-05	7.6E-05	5.3E-05	7.50E-05
US 169 Onamia	Class 6	1.8E-04	2.7E-04	2.2E-04	2.23E-04
I 35W Richfield	Class 5	7.6E-05			
I 94 Minneapolis	Sand	3.5E-05			
MnROAD Cell 32	Class 1-c	1.3E-04			
MnROAD Cell 52	Class 4	1.9E-06			
Olmsted Co. Rd. 104	Class 5 Mod	9.1E-06			
Olmsted Co. Rd. 117	Class 5	1.4E-04			
TH 14 Mankato	Class 7	2.8E-06			
TH 14 Mankato	Select Granular	4.4E-05			
TH 22 St. Peter	Class 7	1.4E-04			
TH 22 St. Peter	Select Granular	3.7E-05			
TH 371 Brainerd	Class 5	2.5E-04			
TH 371 Brainerd	Sand 2	2.1E-04			
TH 5 Eden Prairie	Class 5	5.4E-05			
TH 610 Brooklyn Center	Select Granular	1.7E-04			
US 10 Hastings	Class 5	4.4E-05			
US 10 Hastings	Class 6	2.9E-05			
US 12 Cokato	Select Granular	1.6E-06			
US 169 Jordan	Class 5	2.2E-04			
US 212 Eden Prairie	Select Granular	1.0E-04			

The bulk of the material tested in the laboratory fell into one of three classes of material: Class 5, Class 6, and Select Granular. Considering the different grain size distribution

45

specifications given in Table 3.1, these materials all fell within a similar range of laboratory hydraulic conductivity values. Table 3.7 gives the maximum and minimum values of saturated hydraulic conductivity for each material as well as the range. This data is also presented in Figure 3.1, which plots the range of hydraulic conducitivities on a logarithmic scale.

Table 3.7 Range of Laboratory Hydraulic Conductivity Values

Material	low k, cm/s	high k, cm/s	range, cm/s
Class 5	2.80E-06	2.60E-04	2.57E-04
Class 6	5.00E-06	2.23E-04	2.18E-04
Select Granular	1.60E-06	2.10E-04	2.08E-04
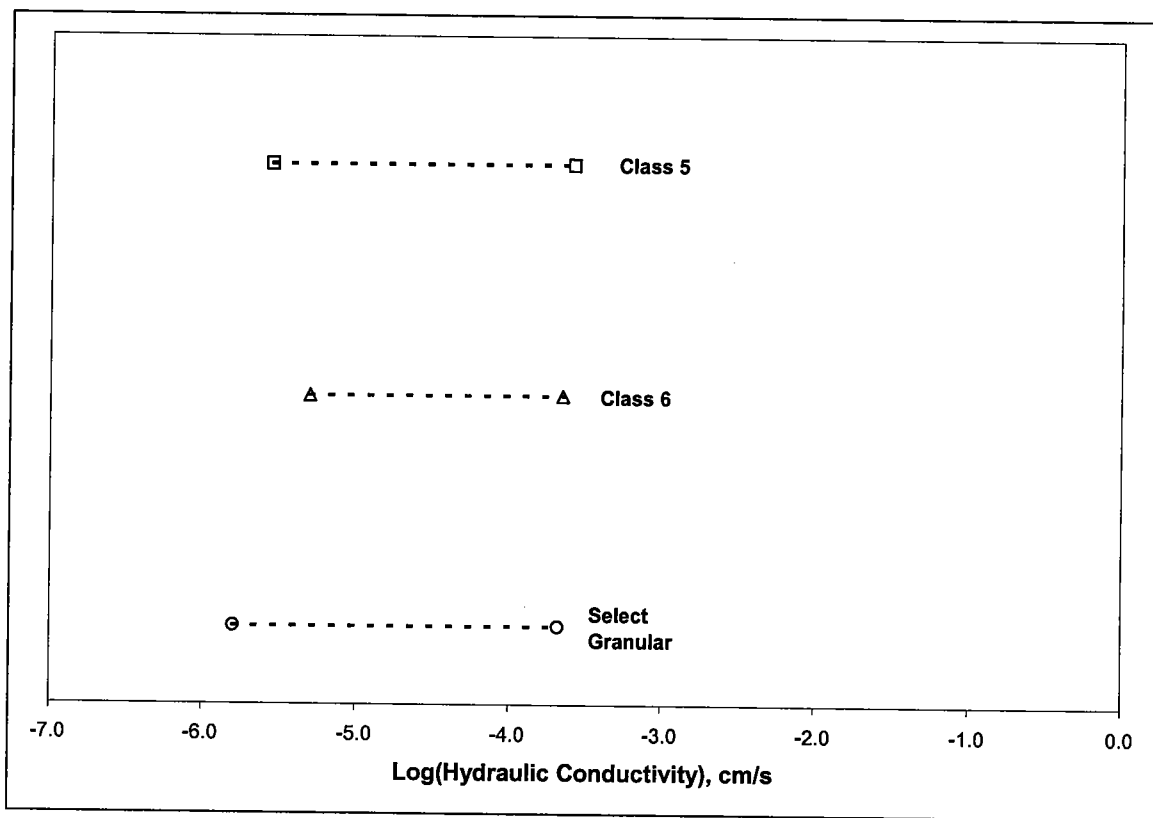
Figure 3.1 Laboratory Hydraulic Conductivity Ranges

The 12 sites investigated in 1999 had flexible wall permeability tests performed on three samples at identical moisture and density conditions (namely, optimum moisture content). It should be noted that these conditions were not necessarily the same as the density and moisture conditions tested in the field. The values reported at the top of Table 3.6 are the average of these

46

three values. For the materials tested in 2000, only one sample was tested per location. These testing locations are shown at the bottom of Table 3.6 These laboratory tests were performed at the same moisture and density conditions as in the field. A plot is shown in Figure 3.2, in which the individual k_{sat} measurements are plotted against the average k_{sat} value for each site in 1999. This plot suggests that the laboratory hydraulic conductivity test is quite consistent, showing only a small amount of spread in the data. A majority of the saturated hydraulic conductivity values measured in the laboratory for each site fell within a factor of two. This is deemed sufficient to use these values to compare with values calculated in the field.
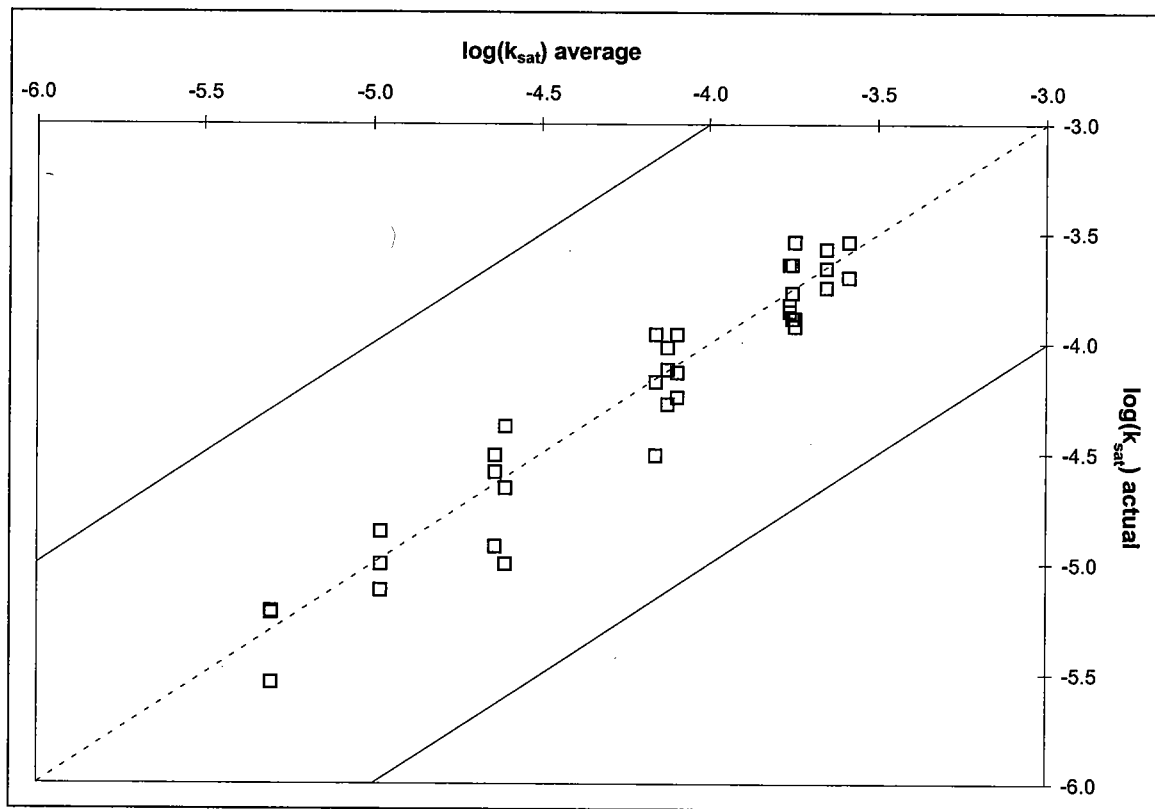
Figure 3.2 Laboratory Hydraulic Conductivity Variability

CHAPTER 4

RESULTS AND DISCUSSION

Introduction

The objective of this chapter is to investigate the feasibility of obtaining saturated hydraulic conductivity values from field measurements of volume flow rate using the models outlined in Chapter 2. This chapter will include the following steps:

1. Outline a means of obtaining a systematic value of flow rate from field measurements.

2. Compare the relative performance of each of the models in calculating the hydraulic conductivity of granular base materials.

3. Compare the hydraulic conductivity values obtained with the Mn/DOT permeameter to those measured in the laboratory.

4. Consider simple adjustments to equations that may improve their performance in terms of comparison with laboratory data.

Calculation of the Steady Flow Rate

The equations (see Table 2.2) used to convert the flow rates measured in the field into a hydraulic conductivity are all based on the assumption that steady flow is reached. It is important to obtain, in a systematic way, an accurate estimate of the steady flow rate from the field data. An estimate of the steady volume flow rate, Q (cm^3/s), from the field observed flow rate was obtained with the following steps:

1. The raw field data of flow rate R (cm/min), one for each individual test, was recorded. These values are listed in Appendix B.

2. The flow rate into the base was assumed to follow the Horton equation [38, 39]:

49

$$R = R_{steady} + B \cdot e^{-C \cdot t}$$

<div align="right">(4.1)</div>

where t is the time (minutes) and R_{steady}, B, and C are constants. Note in Equation 4.1 that as time goes to infinity, the transient term vanishes and the steady flow rate, R_{steady}, is achieved. Note a Philip's model for infiltration rate [38], $R = B * t^{-\frac{1}{2}} + R_{steady}$, can be used in place of equation 4.1.

3. Values for B, C, and in particular R_{steady}, for a given test at a given site, were obtained by minimizing the sum of squares of the differences between the field measurement of $R(t)$ and that given by Equation 4.1; the Solver routine in Excel[1] was used.

4. The field estimate of the volume flow rate Q was then obtained by multiplying R_{steady} by the permeameter area, A.

During field tests, anywhere from 2 to 12 measurements of the steady flow rates were made at each particular site. Figure 4.1 plots the individual Q values (cm³/s) vs. the average Q for each site on a log scale. This plot shows that the steady flow rates calculated with the above procedure are consistent and repeatable; all of the Q values at each site fell well within one order of magnitude, closer to a factor of two.

---

[1] *From Excel 2000 Help: Microsoft Excel Solver uses the Generalized Reduced Gradient (GRG2) nonlinear optimization code developed by Leon Lasdon, University of Texas at Austin, and Allan Waren, Cleveland State University.*
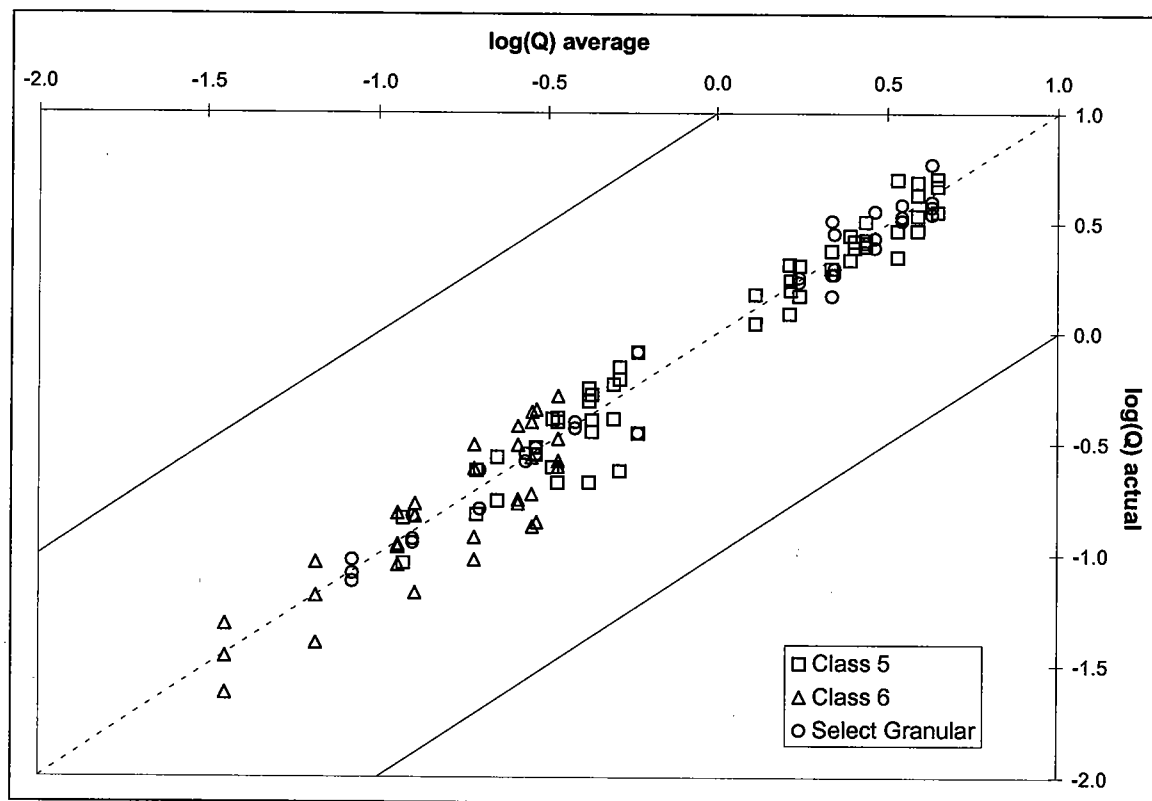
Figure 4.1 Steady Flow Rates in the Field

Comparison of the Hydraulic Conductivity Models

The steady volume flow rates obtained from the field measurements can be used to calculate the hydraulic conductivity. This is achieved by using each one of the eight models listed in Table 2.2. The required field inputs for these calculations, the radius of the well hole, head depths, depth to ponded heights, depth to an underlying impermeable layer, and the annular area of the permeameter, can be found or calculated with the raw data in Appendix B.

Table 4.1 lists the computed hydraulic conductivities using each of the models in Table 2.2 for each of the test sites. The values in Table 4.1 are obtained by averaging over all the specific tests performed at a site. A presentation of the data in Table 4.1 is made by making a line plot of the log(k_{fs}), Figure 4.2.

51

Table 4.1 Average Hydraulic Conductivity Values

Location	Material	Laplace	Elrick_a	Elrick_b	Wu, et al	Glover	Stephens	Guelph	Amoozegar	Lab
Blue Earth Co. Rd. 90	Class 3	2.23E-04	2.31E-04	2.64E-04	2.65E-04	1.20E-04	4.85E-05	1.92E-04	--	6.93E-05
Blue Earth Co. Rd. 90	Class 5	6.81E-03	7.15E-03	8.23E-03	8.00E-03	3.03E-03	8.91E-04	1.58E-03	--	2.60E-04
Dakota Co. Rd. 26	Class 5	9.39E-04	8.93E-04	1.16E-03	8.44E-04	3.68E-04	2.29E-05	--	--	8.03E-05
I 35W Richfield (1999)	Class 5	9.41E-03	9.86E-03	1.38E-02	5.88E-03	--	--	--	--	2.47E-05
TH 25 Monticello	Class 6	4.68E-04	4.73E-04	5.67E-04	5.49E-04	1.99E-04	5.73E-05	6.69E-05	--	1.73E-04
TH 371 Brainerd	Class 6	3.36E-04	3.54E-04	3.96E-04	5.17E-04	3.62E-04	8.67E-05	6.68E-04	2.05E-04	1.35E-04
TH 371 Brainerd	Select Granular	3.23E-04	3.27E-04	4.05E-04	3.02E-04	7.99E-05	--	2.02E-04	--	1.33E-04
TH 7 Silver Lake	Class 5	3.15E-03	3.27E-03	3.86E-03	3.44E-03	2.16E-03	2.15E-04	3.58E-04	--	7.90E-06
TH 73 Kettle River	Class 6	6.00E-04	6.10E-04	7.45E-04	4.80E-04	3.14E-04	--	--	--	5.00E-06
US 12 Cokato	Class 5	4.25E-03	4.40E-03	5.12E-03	5.00E-03	1.86E-03	6.14E-04	1.60E-03	--	2.30E-05
US 169 Mille Lacs	Class 6	1.36E-04	9.09E-05	1.61E-04	2.10E-04	8.24E-05	3.09E-05	2.64E-04	7.71E-05	7.50E-05
US 169 Onamia	Class 6	3.44E-04	3.62E-04	4.04E-04	4.14E-04	2.09E-04	9.55E-05	4.60E-04	4.84E-05	2.26E-04
I 35W Richfield (2000)	Class 5	1.48E-03	1.67E-03	2.29E-03	--	--	--	1.87E-03	--	7.60E-05
I 94 Minneapolis	Sand	4.33E-04	4.43E-04	5.26E-04	5.06E-04	4.23E-05	4.30E-05	--	--	3.50E-05
MnROAD Cell 32	Class 1-c	1.28E-04	1.33E-04	1.53E-04	1.99E-04	8.64E-05	2.13E-05	2.58E-04	7.58E-05	1.30E-04
MnROAD Cell 52	Class 4	3.27E-04	3.49E-04	3.93E-04	3.80E-04	2.72E-04	5.48E-05	9.12E-04	4.29E-04	1.90E-06
Olmsted Co. Rd. 104	Class 5 Mod	3.87E-04	--	5.33E-04	--	--	--	--	--	9.10E-06
Olmsted Co. Rd. 117	Class 5	8.23E-04	6.67E-04	1.11E-03	--	--	--	--	--	1.40E-04
TH 14 Mankato	Class 7	2.03E-03	1.84E-03	3.33E-03	--	--	--	2.27E-03	--	2.80E-06
TH 14 Mankato	Select Granular	1.07E-03	1.13E-03	1.28E-03	1.27E-03	5.39E-04	2.13E-04	1.01E-03	--	4.40E-05
TH 22 St. Peter	Class 7	2.97E-04	3.25E-04	3.50E-04	5.64E-04	1.78E-04	7.91E-05	9.19E-04	4.22E-04	1.40E-04
TH 22 St. Peter	Select Granular	6.40E-04	6.68E-04	7.87E-04	6.22E-04	1.63E-04	3.05E-05	1.25E-04	--	3.70E-05
TH 371 Brainerd	Class 5	8.32E-04	8.46E-04	1.04E-03	5.54E-04	1.91E-04	--	--	--	2.50E-04
TH 371 Brainerd	Sand 2	1.54E-02	1.37E-02	2.22E-02	1.14E-02	--	--	--	--	2.10E-04
TH 5 Eden Prairie	Class 5	4.26E-04	4.42E-04	5.27E-04	3.67E-04	1.20E-04	5.50E-06	--	--	5.40E-05
TH 610 Brooklyn Center	Select Granular	1.93E-04	1.92E-04	2.32E-04	2.27E-04	8.59E-05	2.53E-05	2.55E-05	--	1.70E-04
US 10 Hastings	Class 5	1.19E-02	1.21E-02	1.80E-02	--	--	--	9.47E-03	--	4.40E-05
US 10 Hastings	Class 6	8.03E-04	8.47E-04	1.01E-03	7.31E-04	1.90E-04	--	--	--	2.90E-05
US 12 Cokato	Select Granular	5.04E-03	4.82E-03	6.20E-03	4.76E-03	8.31E-04	1.97E-04	5.75E-04	--	1.60E-06
US 169 Jordan	Class 5	4.88E-03	5.18E-03	6.63E-03	6.97E-03	--	--	4.02E-03	--	2.20E-04
US 212 Eden Prairie	Select Granular	7.86E-03	7.50E-03	1.10E-02	7.43E-03	--	--	--	--	1.00E-04
MnROAD Cell 32	Class 1	1.39E-04	1.48E-04	1.73E-04	1.77E-04	3.77E-05	--	1.58E-04	--	--
TH 371 Brainerd	Sand	1.11E-03	8.86E-04	1.36E-03	1.16E-03	1.02E-04	7.17E-05	--	--	--
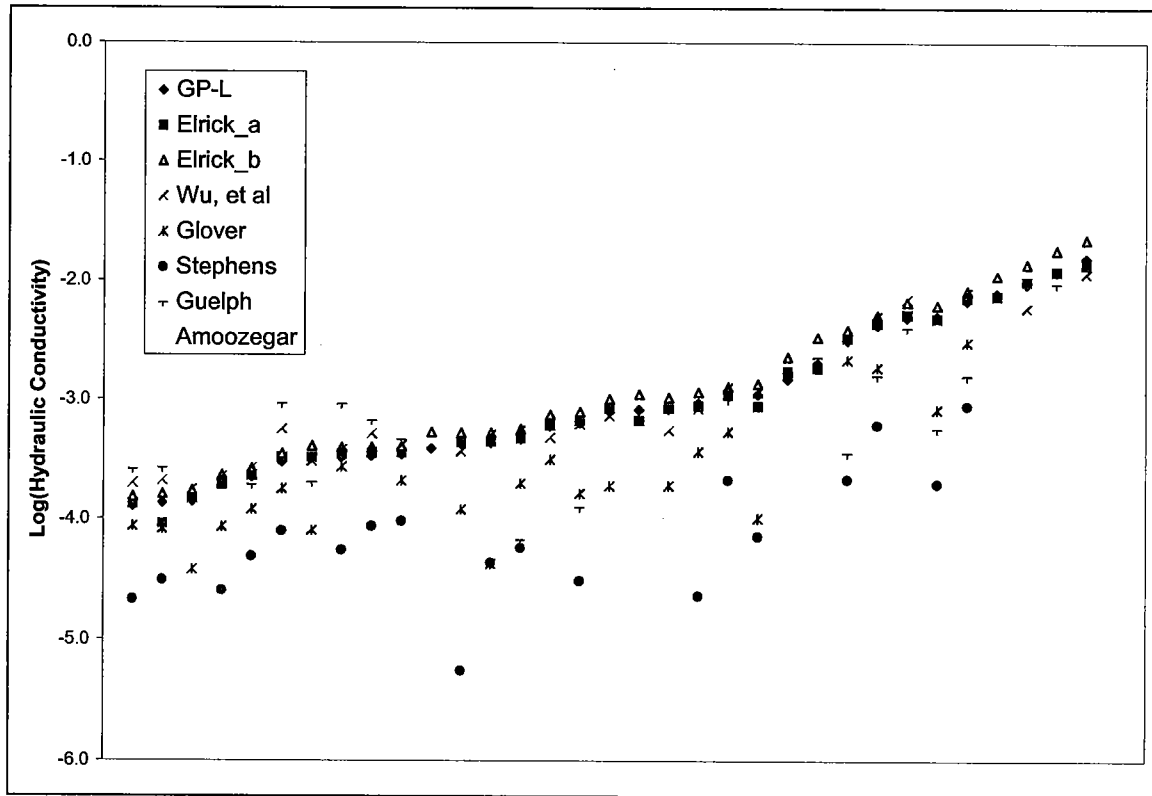
Figure 4.2 Log(k_{fs}) for Each Model

For the most part hydraulic conductivity values calculated with the various models listed

in Table 2.2 are qualitatively similar. Some points, however, require discussion:

1. The first 6 columns of values in Table 4.1 are hydraulic conductivity estimates obtained

   with the one-equation models. The variation in these estimates can be attributed to the

   different shape factors used (see discussion in Chapter 2 and Figure 2.5).

2. In some cases (indicated by a dash in Table 4.1) specific one-equation models were

   unable to calculate a value or provided a negative value. In such cases, as fully explained

   in Chapter 2, the negative values *do not* indicate that conditions in the drain are outside of

   the assumptions of the model. They simply indicate that the head and borehole radius

   dimensions for that particular test combined to be a mathematically impossible

   calculation. The only one-equation models that will always give a positive reading,

regardless of the borehole configuration, are the Elrick_b and GP-L; one-equation methods that use the C factor curve which can be approximated by

$$C = D\left(\frac{H}{a}\right)^{2/3}$$

(4.2)

where the constant $D = 0.6$.

3. The simultaneous equation approaches in Table 4.1, Guelph and Amoozegar, quite often calculate negative values. As discussed in Chapter 2 these methods are very sensitive to non-uniformities and heterogeneities in the base (e.g., a layer boundary) [26, 33]. When compared with the ideal homogeneous base case, these conditions will lead to small differences in the flow rate. Such flow rate differences would not be expected to have a significant impact on the one-equation models but are magnified in the simultaneous equation models by the use of the ratio (Q_2/Q_1). Due to the relatively shallow depth and layering in pavement systems, it is reasonable to expect that the ability of the simultaneous equation models to predict physically reasonable values of k_{fs} will be limited.

In the next section predictions obtained with the various models tested above will be compared with the laboratory measurements of hydraulic conductivity presented in Chapter 3. In some cases, the GP-L model will be chosen as a specific test model to provide a better focus on the performance of the field models. This choice is made on noting that the GP-L model

- is simple to use, only requiring one head and one flow rate,
- will always predict positive values, and the shape factor can be obtained from a simple equation (see Equation 4.2),

- the shape factor can be readily adjusted, by simply changing the constant D, in Equation 4.2, and

- the flexibility in adjusting the shape factor will mean that features in a pavement drainage system, not explicitly included in the original GP-L analysis, could be accounted for by adjusting the D constant in Equation 4.2.

Comparison with Laboratory Data

Figures 4.3a and 4.3b are log-log scatter plots comparing the laboratory measurements of hydraulic conductivity (Table 3.6) to those estimated by using field measurements of the flow rate Q in each of the models listed in Table 2.2. In these plots the dashed line represents the perfect correlation and the solid lines demark a difference of plus or minus one order of magnitude. The scatter plots show that although the calculated values of hydraulic conductivity from each of the models are qualitatively the same, correlation with the laboratory measurements is weak.

There are a number of reasons why, in a one to one comparison, field estimates will not correlate to the laboratory measurements. In particular:

1. Due to sample disturbance field conditions, e.g., density, moisture and particle orientation, may not be consistent with those in the laboratory.

2. The models outlined in Chapter 2 do not specifically account for conditions such as layering (thin layers of different base materials) and unsaturated flow conditions; situations that will exist in the field.

3. The shape factors used in the existing models are not suitable for use with pavement base materials.

In Chapter 5 the effects of layering and unsaturated flow are investigated via the use of numerical modeling. In this chapter we investigate, by using the GP-L model, if the correlation between the field estimated and laboratory conductivity measurements can be improved by a simple adjustment of the shape factor parameter D in Equation 4.2. The value of D is chosen by comparing the range of predictions obtained with the GP-L model to the laboratory observed range (see Figure 3.1). In this way it is noted that a value of $D = 0.02$ in Equation 4.2 provides a reasonable agreement between the model calculated and laboratory measured hydraulic conductivity ranges for Class 5, Class 6 and Select Granular (Figure 4.4). Justification for this somewhat ad-hoc adjustment of D is made in Chapter 5 where a more rigorous adjustment of the shape factor, based on inverse numerical modeling, arrives at essentially the same value.
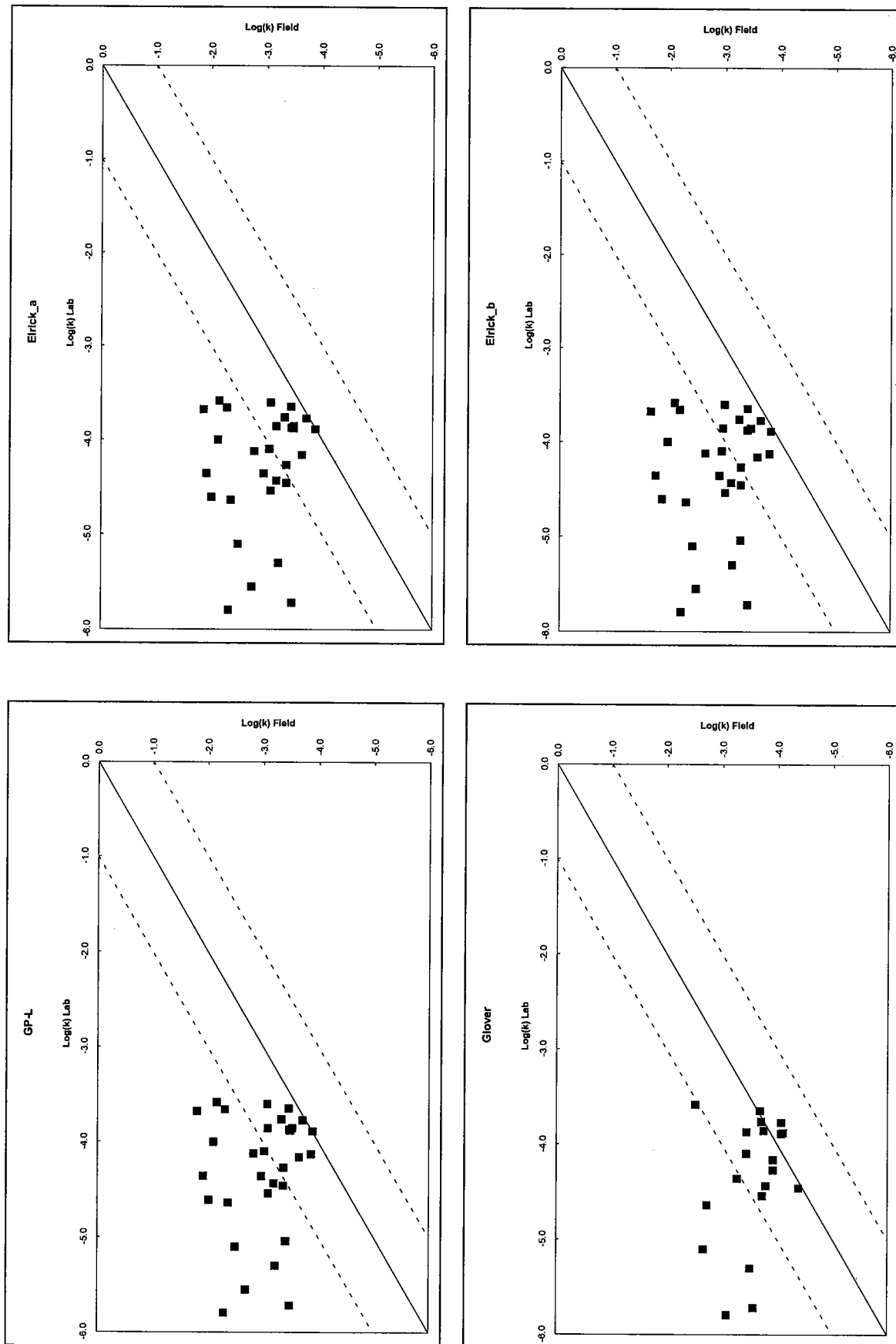
Figure 4.3a Field vs. Laboratory Hydraulic Conductivity

57
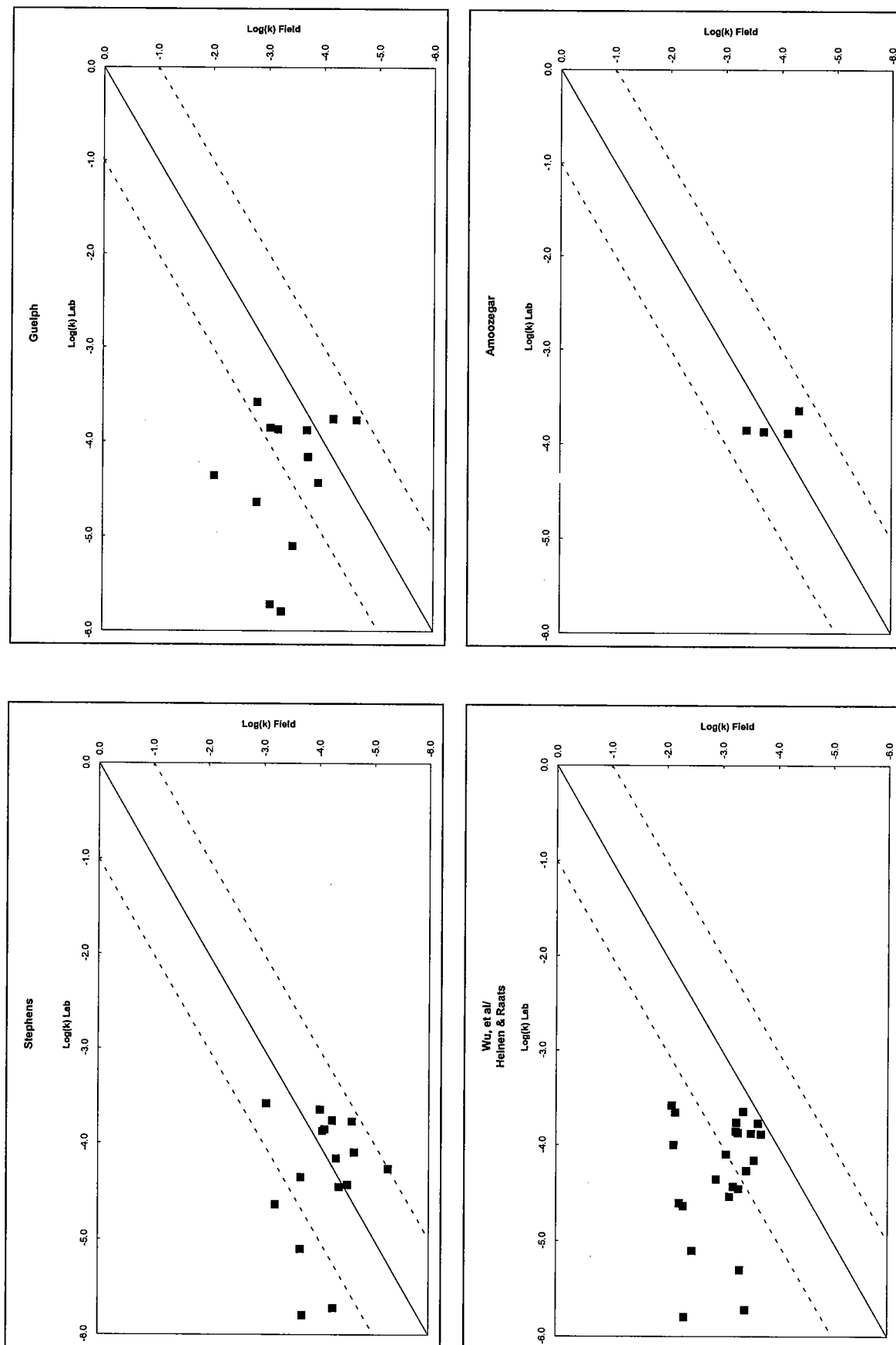
Figure 4.3b Field vs. Laboratory Hydraulic Conductivity

58
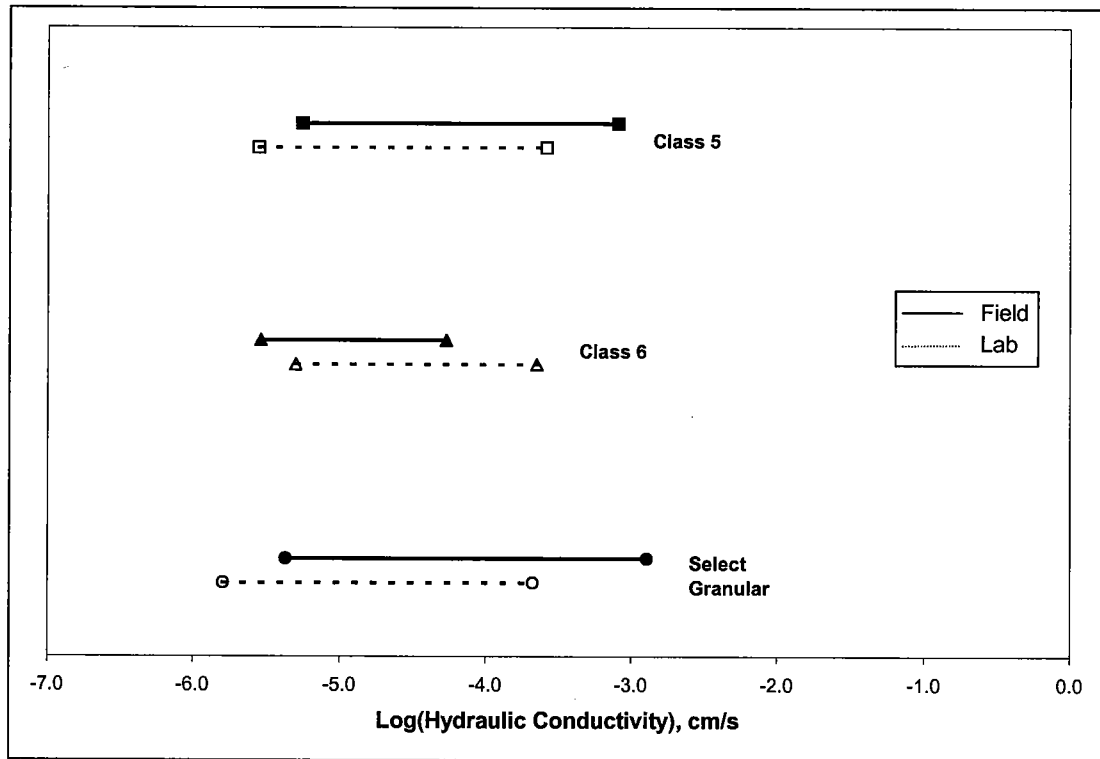
Figure 4.4 Field and Laboratory Hydraulic Conductivity Ranges

A Monte Carlo Simulation

Although, with reference to Figures 4.3a and 4.3b, the overall performance (when compared with laboratory measurements) of the adjusted GP-L model is reasonable, the one to one correlation between the field calculated and laboratory hydraulic conductivities, as shown in the scatter plot in Figure 4.5, is still poor. This observation is confirmed by the following Monte Carlo simulation. The concept involved here is to investigate if an intelligent guess for the field hydraulic conductivity will provide the same level of correlation with the laboratory measurements.
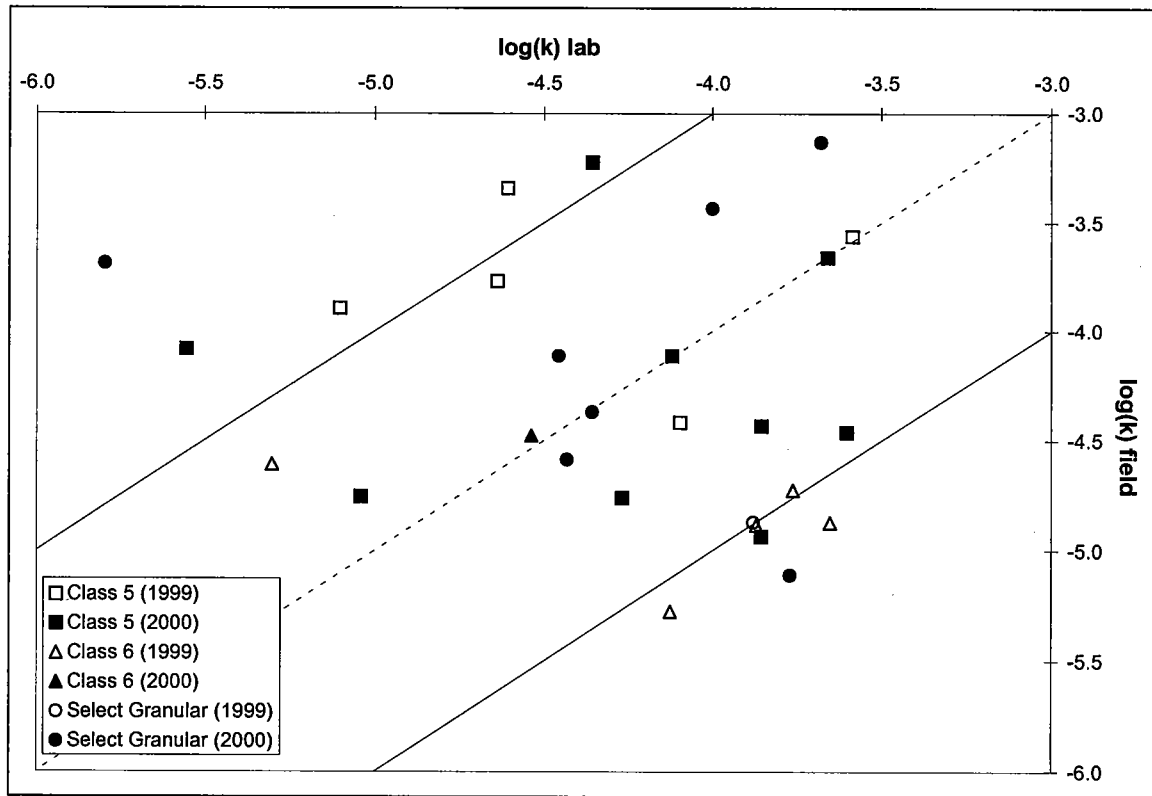
Figure 4.5 Field vs. Laboratory Hydraulic Conductivity (GP-L model w/ *D* = 0.02)

A single realization of the Monte Carlo simulation involves a random selection of a complete set of "field-measured" hydraulic conductivity values, k_{fs}, from a lognormal distribution (Figure 4.6) with a mean and standard deviation matching those found in the real field measurements.
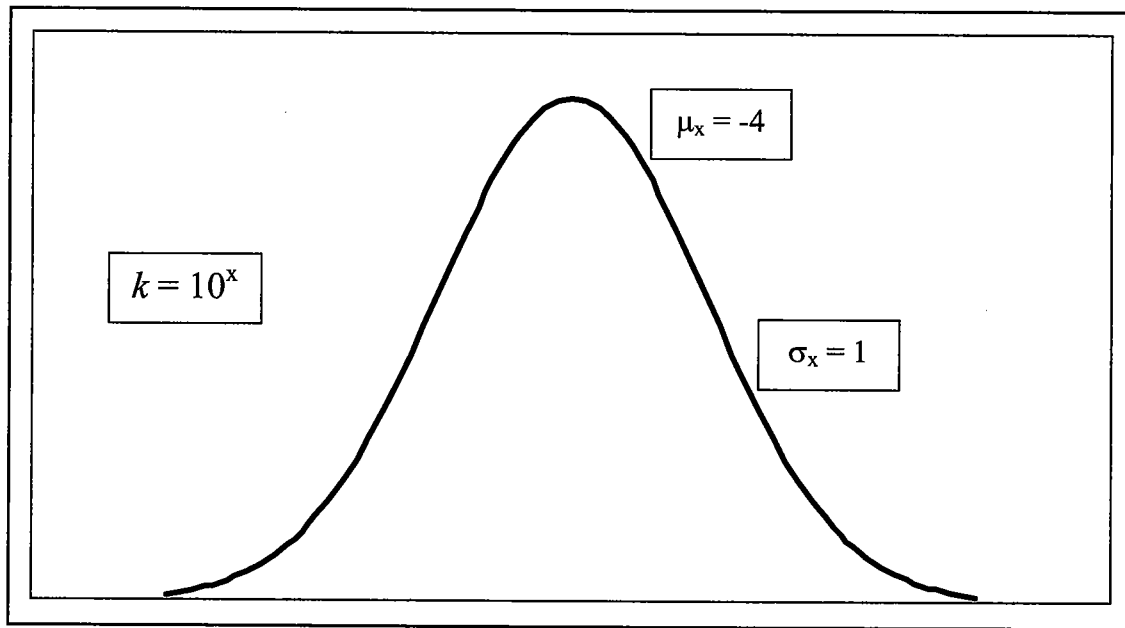
Figure 4.6 Normal Distribution

Figure 4.7 shows three realizations of this Monte Carlo simulation along with the actual k_{fs} values reproduced from Figure 4.5. The reader is challenged to determine which plot shows the actual values calculated in the field using the corrected GP-L model. (The lower-right picture contains the actual values.) Although not conclusive in a rigorous statistical sense, this result strongly indicates that a correlation between field values of saturated hydraulic conductivity in the granular base of a pavement system, calculated from a measured Q with the available models (e.g., GP-L) cannot be correlated with laboratory measurements.
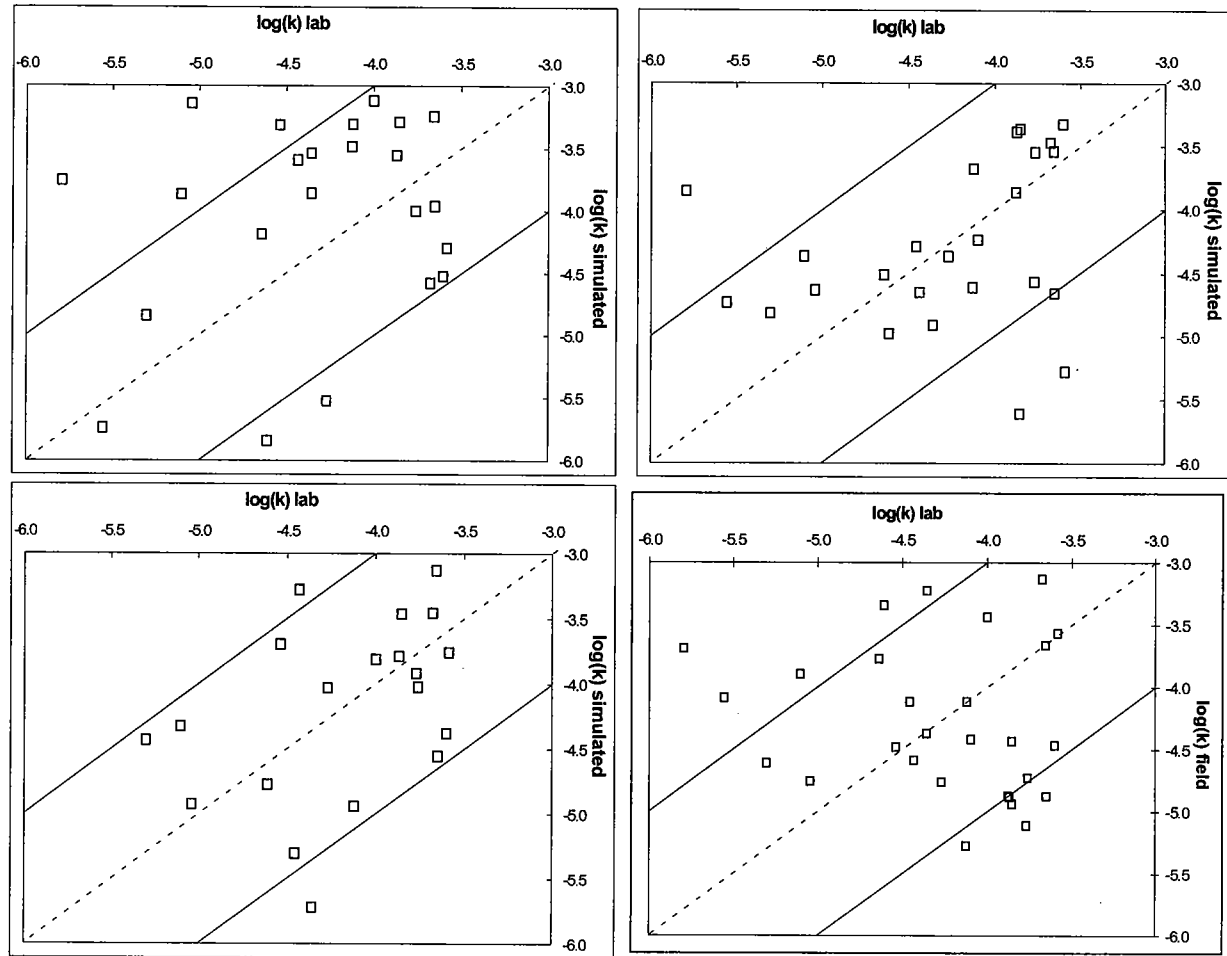
Figure 4.7 Monte Carlo Realizations

Summary and Discussion

1. The Mn/DOT permeameter serves as a reliable device for measuring the steady flow rate of water into a base material. This measurement of Q is consistent and reproducible (see Figure 4.1).

2. When non-negative finite values are obtained, all the proposed models for converting the field measured flow rate Q into a hydraulic conductivity estimate perform at close to the same level. The trends are similar and differences in values can be attributed to the nature of the shape factor used, see Figure 2.5.

3. In this work the GP-L single equation model is used for testing simply because it is the most robust. In particular, it will always provide a positive value and its use is not subject to constraints on the test geometry.

4. An adjustment of the shape factor used in the GP-L model results in hydraulic conductivity value ranges, for a given base material types, in reasonable agreement with the value ranges obtained in the laboratory, see Figure 4.4.

5. A Monte Carlo analysis, however, indicates that a one to one correlation between laboratory and field measurements of hydraulic conductivity cannot be achieved. The lack of correlation could be due to (1) a mismatch between the field and laboratory conditions and or (2) the effects of layering and the unsaturated flow characteristics.

CHAPTER 5

NUMERICAL CALIBRATION AND ANALYSIS

Overview

The objective of this chapter is to report on a comparison between of the permeameter and a direct numerical simulation conducted by Bjorn Birgisson at the University of Florida [40]. This comparison indicates that saturated hydraulic conductivity predictions obtained with the permeameter will be accurate under the assumption of an isotropic, homogeneous base. The chapter concludes with an analysis aimed at identifying how to obtain reliable field estimates from the permeameter in the case where the base layer is thin.

Comparison with Numerical Simulation

Background

The key task of the work in Florida was to, independent of the studies of the field data conducted at the University of Minnesota, develop a calibration for the conversion of field measured flow rates into saturated hydraulic conductivity. In essence the task was to find a shape factor, $C(H,a)$, see Figure 2.5, that could be used with the various theoretical equations (see Table 2.2) used in the calculation of k_{fs} from field measurements. The method to arrive at this calibration was to use the code SEEP/W, a commercial finite element code for the calculation of unsaturated/saturated groundwater flow. The concept was to set up an axisymmetric run of the code that would simulate the influx of water into a semi-infinite isotropic homogeneous region from a well (bore) hole subject to a constant head. Both the saturated bulb and unsaturated regions were considered in the analysis. The well hole and head conditions were chosen to match those used in the field trials of the permeameter. In the first

instance the lowest field head, H_1, was applied and the model run until a steady state was achieved. Immediately following this the second field head, H_2, was applied and run to steady state. In this way the model with the second head started with the initial condition set up with the first head, a situation that simulated the actual field testing mechanism. In the SEEP/W setup appropriate models were used to represent the water content and hydraulic conductivity vs. soil suction. In the hydraulic conductivity model, over repeated runs of the simulation, the researchers adjusted the saturated conductivity k_{fs} in the conductivity model until the SEEP/W predicted flow rate from the well, at steady state, matched the flow rate measured at the field site.

A cross section of 10 field sites were chosen from the 31 total sites investigated. These sites listed in Table 5.1 involved 31 separate measurements with the permeameter.

Table 5.1 Locations and Materials Used in this Study

Location	Material	Testing Date
I 35W Richfield	Class 6	09/01/99
TH 25 Monticello	Class 6	08/18/99
Blue Earth Co. Rd. 90	Class 5	07/27/99
US 169 Mille Lacs	Class 6	07/21/99
US 169 Onamia	Class 6	08/11/99
US12 Cokato	Class 5 w/ conc.	07/25/99
MnROAD Test Pad	Class 3 sp	10/04/99
MnROAD Cell 52	Class 4 sp	06/21/00
MnROAD Cell 34	Class 5 sp	07/15/99
MnROAD Cell 33	Class 6 sp	07/16/99

Flow Rate Predictions

Results that compare the field measured flow rates with the SEEP/W predicted flow rates are summarized in Table 3 of Task Report 1.4 [40] and plotted as a log-log scatter of $Q_{seep/w}$ vs. Q_{field} in Figure 5.1 below.
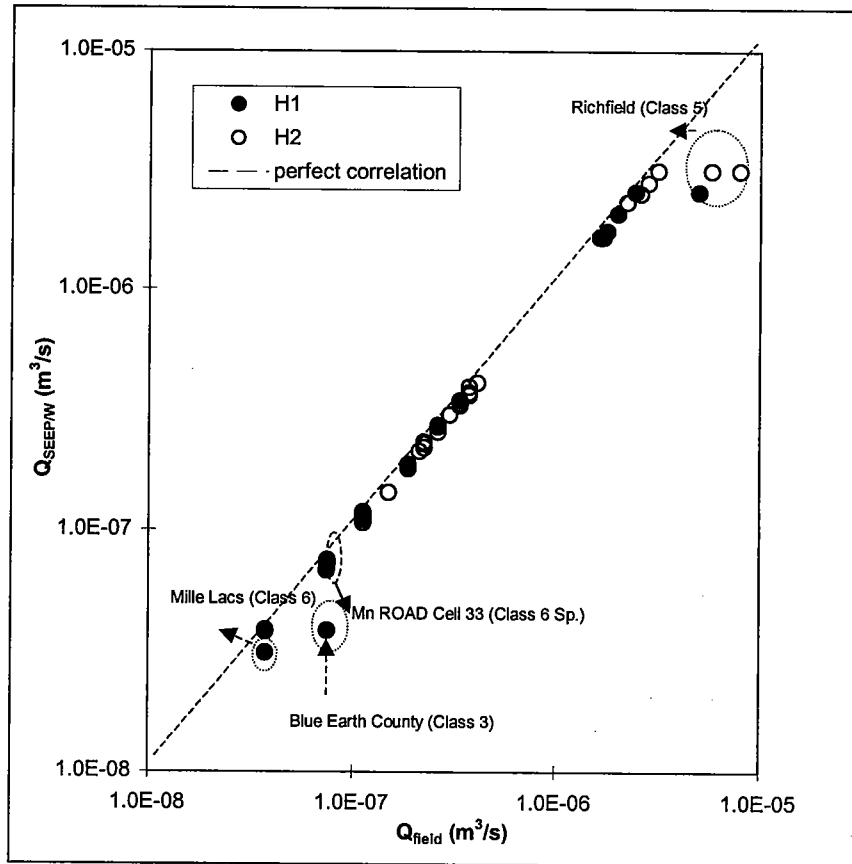
Figure 5.1 Scatter plot of Q_{field} vs. $Q_{SEEP/W}$ in m^3/s

For the most part the SEEP/W program was able to match the field flow rates. This indicates a high degree of self-consistency in the field measured Q's. In particular they indicate that the Excel curve fitting method for obtaining the flow rate from the field water height measurements (see Chapter 4) is robust and valid.

Hydraulic Conductivity Measurements

In addition to predicting the steady flow rate for a given head the SEEP/W model also predicted a value for the saturated hydraulic conductivity. For each site the values obtained from SEEP/W were averaged and compared with the corresponding laboratory values. The resulting scatter plot for the ten sites chosen for the numerical study are shown in Figure 28 in Task

Report 1.4 [40]. The scatter is of the same order and nature as the scatter observed in similar comparisons made in Chapter 4 (e.g., see Figure 4.8).

Calibration

The models presented in Chapter 2 (see Table 2.2) to convert a field measured flow rate into a hydraulic conductivity need, for the most part, three inputs: (1) a head, H, (2) a hole radius, a, and (3) a shape factor C. A major aim of the Florida research was to use the SEEP/W model to arrive at a suitable equation for the shape factor C, which will be a function of the ratio H/a. In brief, the following steps were used:

1. For each of the 31 SEEP/W runs averaged values of $k_{SEEP/W}$ were calculated (note there were slight difference in the k obtained with H_1 and H_2).

2. These k values were used in the SEEP/W model with five different values for the ratio H/a (0.5,1,0,1,5,2.0, 2.5), and the resulting steady values of $Q_{SEEP/W}$ were recorded.

3. For a selection of the models, listed in Table 2.2, the shape factor value C was adjusted, for each choice of H and a and predicted flow rate, until agreement was achieved with the k input into the SEEP/W simulation.

4. The resulting values of C were plotted against (H/a) and fit by a quadratic.

A number of C factor curves were obtained in this way, one for each model and material type (Class 5, Class 6 etc.). A detailed statistical analysis indicated that the shape factors obtained with the GP-L (Equation 2.22) provided the most consistent fit to the data. However, it is well worth noting that when the appropriate C factor was used the Guelph simultaneous equation approach also gave reasonable values. This is a significant finding. The field study (see Chapter 4) indicated that when the Guelph recommended shape factor was used the simultaneous equations would give non-physical negative predictions for the conductivity.

The overall C shape factor for use with the GP-L model, obtained by averaging across all of the materials types, resulting from the Florida numerical calibration is

$$C = 0.0046\left[\frac{H}{a}\right]^2 + 0.0318\left[\frac{H}{a}\right] - 0.0087 \tag{5.1}$$

This model holds in the range $0.5 < H/a < 2.5$. In this range the shape factor proposed by Elrick can be modeled as

$$C = 0.6\left[\frac{H}{a}\right]^{2/3} \tag{5.2}$$

and the model proposed in the analysis of the field data in Chapter 4 is

$$C = D\left[\frac{H}{a}\right]^{2/3} \tag{5.3}$$

where $D \sim 0.02$.

The Florida C, Equation 5.1, has been used to calculate hydraulic conductivities with the GP-L model using the entire set of field data presented in Chapter 4. Results in the form of a log-log scatter comparison with the laboratory measurements are shown in Figure 5.2.
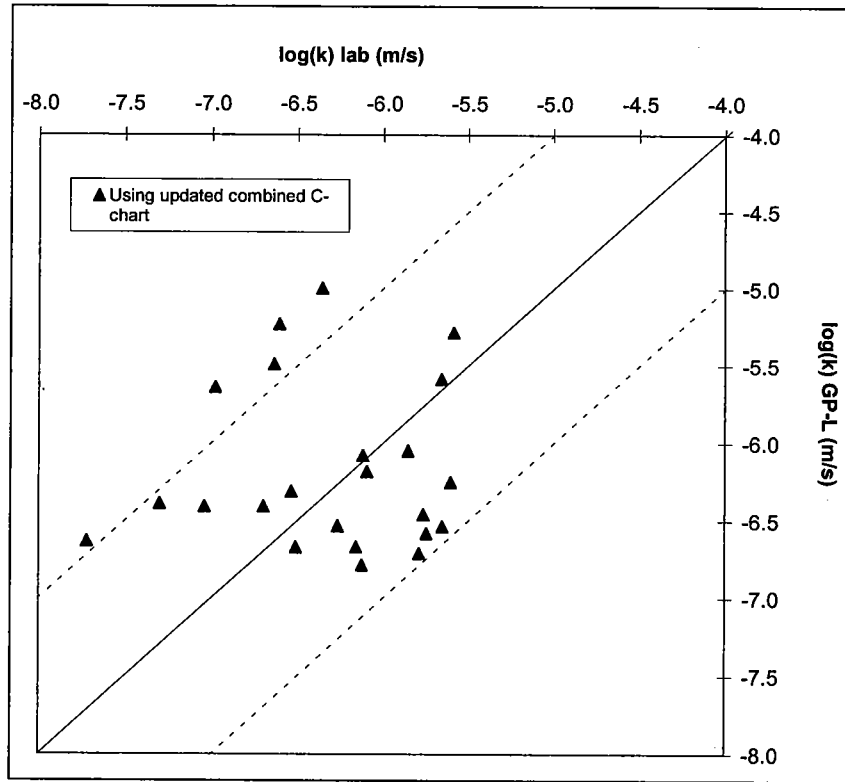
Figure 5.2 Comparison of the Measured and Predicted Conductivities for Classes 3, 4, 5, and 6 Materials using GP-L

Compared with the similar scatter plot presented in Chapter 4, Figure 4.4, there is a marginal improvement. For the most part predictions between the field and the laboratory measurements agree within one order of magnitude. This level of prediction may be adequate for some practical cases. Note, however, that, consistent with the finding in Chapter 4, the correlation between k values obtained in the field and the laboratory is still poor.

Comparisons of Numerical and Field Calibrations

The C shape factor resulting from the numerical calibration, Equation 5.1, is different than the one used in the field analysis in Chapter 4, Equation 5.3. It is worth examining the difference in performance between these two shape factors. This can be done by comparing the conductivity values predicted when the field C and the numerical C are used in the GP-L model. Figure 5.3 shows a log-log scatter plot of the k values predicted with the field shape factor

against the *k* values predicted with the numerical shape factor. Two values of the constant *D* in

Equation 5.3 are used. The results indicate close if not perfect agreement. This confirms that the

ad-hoc adjustment of the *D* constant in the Elrick curve, proposed in discussing the field data in

Chapter 4, is valid.
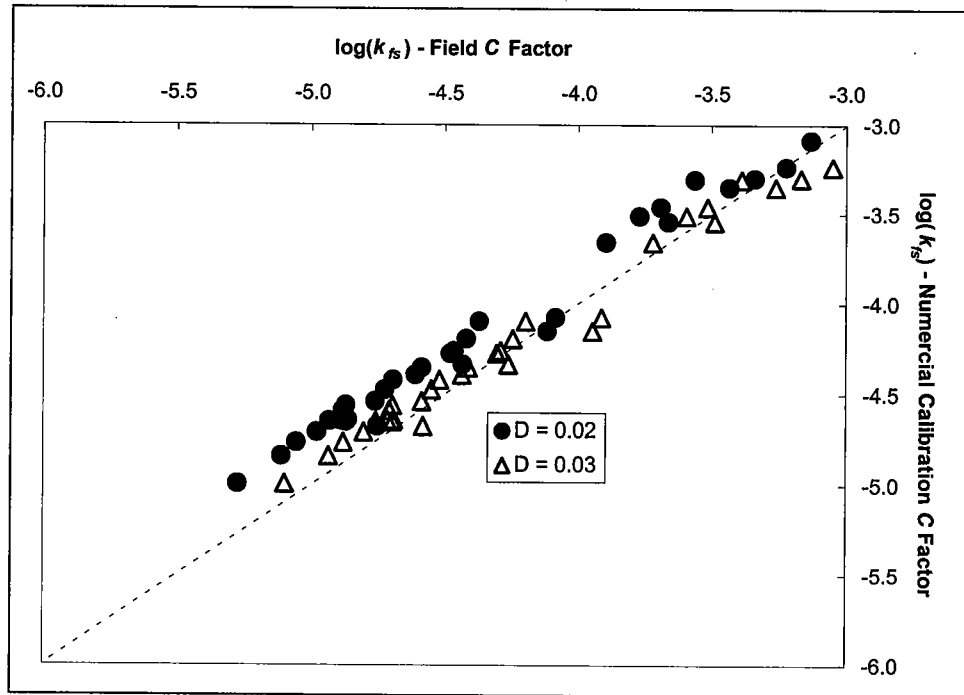
Figure 5.3 Comparison of the Performances of the Field and Numerical Shape Factors

Comparison of Field and Simulation Predictions for Hydraulic Conductivity

Hydraulic conductivity predictions obtained with the GP-L model are compared with the

values from the numerical simulation in a log-log scatter plot in Figure 5.4. In this prediction the

GP-L equation used the numerical shape factor, Equation 5.1, and the $Q_{SEEP/W}$ value for its input

flow rate.

71
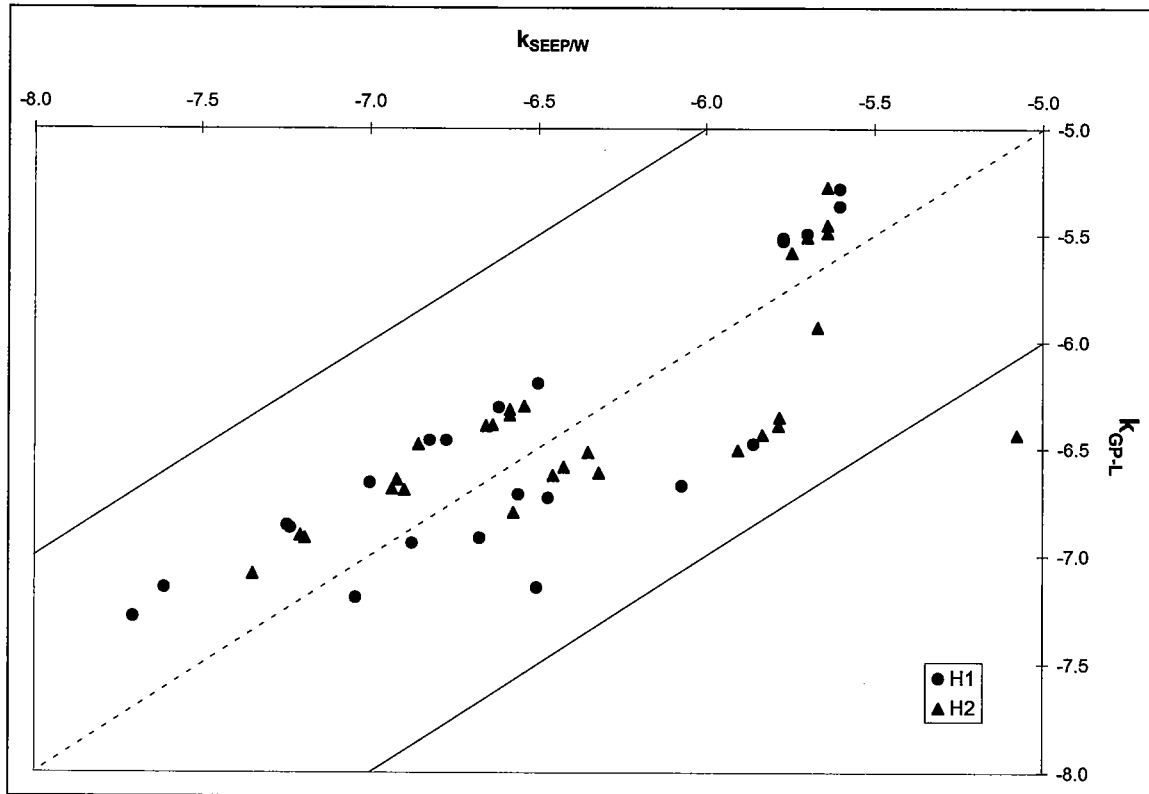
Figure 5.4 Comparison of Hydraulic Conductivities between GP-L and SEEP/W

This plot indicates that there is some spread but also clearly shows a strong correlation between the GP-L model and the SEEP/W simulation. This indicates that the operation of the permeameter to obtain field estimates of the hydraulic conductivity of the base material is valid if the base is deep enough such that the assumption of a single homogenous isotropic base is reasonable.

Estimate of Layer Depth for a Valid Permeameter Analysis

The above analysis shows that the proposed operation of the permeameter for predicting hydraulic conductivity will work well under the assumption of a thick homogeneous isotropic base layer. As noted previously in this report, however, the pavement base layer could be relatively thin (it is not unheard of to have a layer < 15 cm in extent). The case of water infiltration into layered soils has been extensively studied in the literature. Two important

72

effects as the wetted bulb moves across the interface between the two layers relevant to this work, are:

1. A change in the geometry of the wetted bulb, schematically shown in Figure 2.6.

2. A "kink" in the infiltration rate, see Figure 5.5 [38].
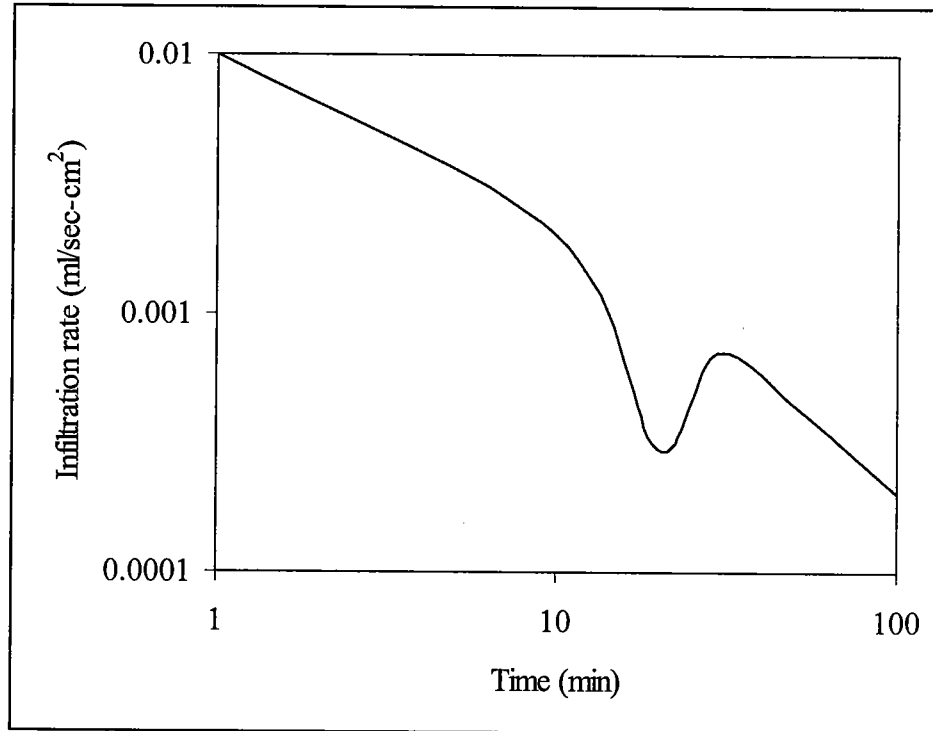
Figure 5.5 Schematic of Infiltration into a Clay over Sand Layer – Based on Figure 4.9 in Jury [38]

The essential feature of the permeameter is to equate the saturated hydraulic conductivity to the steady infiltration rate. The method for estimating a steady infiltration rate with the permeameter, as outlined in detail in Chapter 4 of this report, is to relate the observed water level drop, Δl, in the permeameter to the infiltration rate into the pavement. The data obtained in this way is fit to the Horton infiltration model (Equation 4.1) and an estimate of the steady infiltration rate obtained by looking at the limit of large time. In view of the nature of infiltration in layered systems, if a given pavement layer is thin, there will be a maximum water level drop, Δl_{max}, in the permeameter over which a reliable estimate of the infiltration rate for use in a fitting of the

73

Horton equation can be obtained. Readings taken from the permeameter after the total water level drop has exceeded Δl_{max} may be subject to the effects of layering noted above.

The object of this section is to obtain a conservative relationship between the maximum permeameter reading length Δl_{max} and s, the depth of the base layer below the well. This is achieved with the following infiltration analysis aimed at predicting the growth and shape of the wetted bulb. An axisymmetric cylindrical fixed head well of height $H = 10$ cm and radius $a = 5$ cm is used to model the field use of the permeameter. The Green-Ampt infiltration model [38] is assumed. In this model, often used to gain insight into infiltration processes, a sharp front exists between the saturated and initial moisture regions and a constant hydraulic conductivity is taken. The sharp wetted front is at the air-entry. If this value is set at a negative pressure head then the Green-Ampt solution is expected to provide a close approximation the actual shape taken by the saturated bulb and unsaturated fringe [38]. The governing equations for this Green-Ampt model are

$$\frac{\partial^2 h}{\partial x^2} + \frac{\partial^2 h}{\partial y^2} + \frac{\partial^2 h}{\partial z^2} \quad (x, y, z) \in \Omega_{sat} \tag{5.4}$$

where h is the head and Ω_{sat} is the saturated region. On the internal well surface a fixed pressure head $h = 0$ is applied. On the sharply defined saturated surface defined by the function $f(x,y,z,t) = 0$, $h = -z$ and the flow balance condition

$$-\frac{k}{\Delta \phi} \nabla h \cdot n = v_n \tag{5.5}$$

holds, where n is the outward pointing unit normal on the saturated front, v_n is the speed of the front in this direction, and $\Delta \phi$ is the difference between the saturated and residual moisture contents. Note in this formulation the air entry has been assumed to be at $h = 0$; it will be shown

below that this limit choice provides an lower bound of the maxim permeameter reading length, Δl_{max}.

The above equations are solved using a deforming control volume finite element code based on earlier work [41]. This code employs a deforming grid of a fixed number of nodes and elements that fits into and expands with the saturated bulb. Results in Figure 5.6 show the formation of the saturated bulb at four time snapshots. A dimensionless time parameter, $\tau = kt/\Delta\phi$ is used. Also shown are the corresponding volumes for the saturated bulb. Two observations are made:

1. The limit case of a hemispherical well and no gravity, a case where an analytical solution can be readily found, has been used to validate the code. In this limit case the volume and shape of the bulb predicted by the code agree within 1% to the analytical values.

2. As previously noted the specification of a negative as opposed to a zero air entry pressure would result in a more realistic simulation of the wetted bulb. Such a simulation, however, will also allow for more lateral expansion of the bulb in the x-y plane, and although, at a given point in time the predicted bulb will have a greater value, its penetration below the well base will be less than the simulation where a zero air entry pressure is used. Hence use of the simulation based on a zero air entry pressure head provides an upper bound on the predicted penetration, p, below the well.
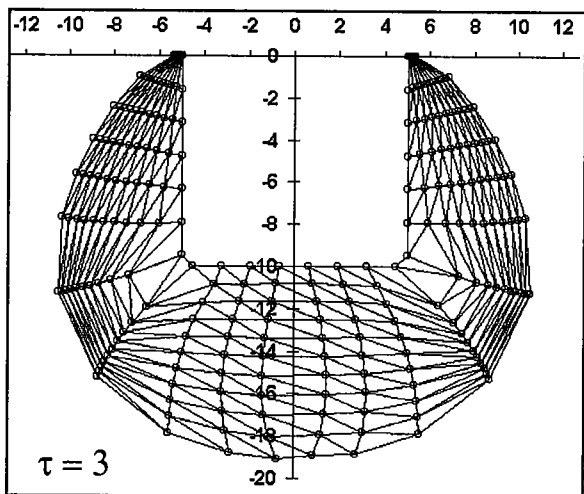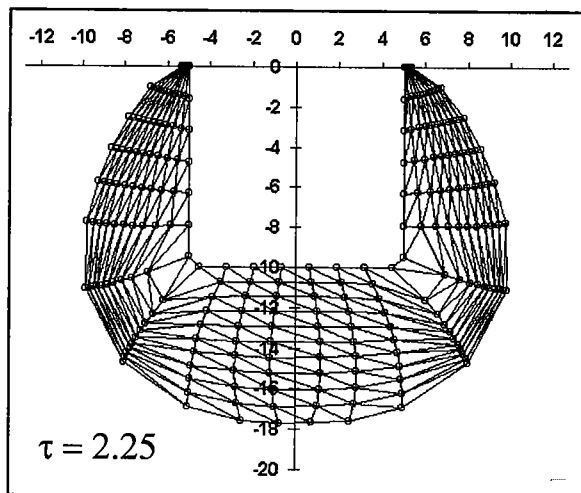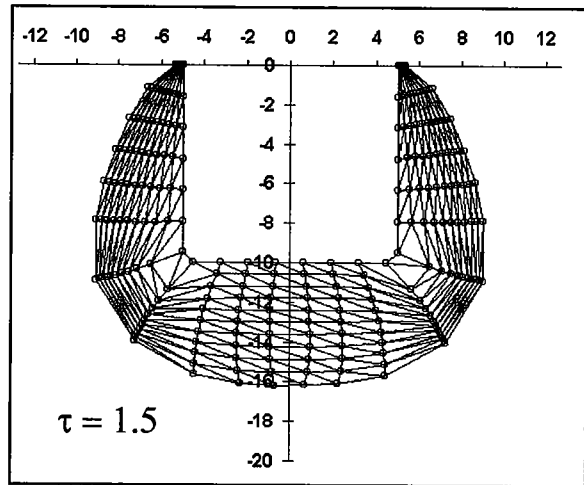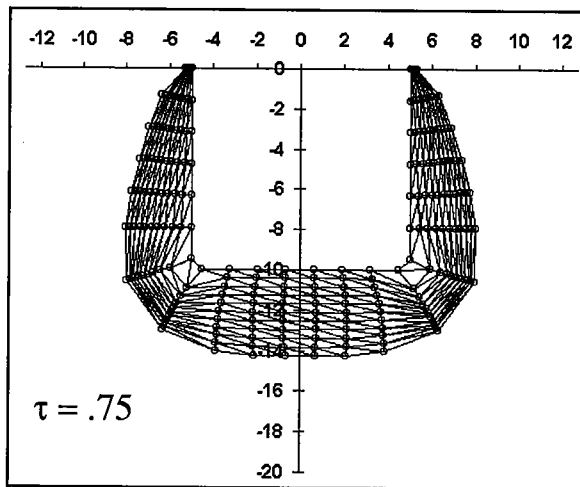
Figure 5.6 Saturated Bulb for Axisymmetric Green Ampt Solution
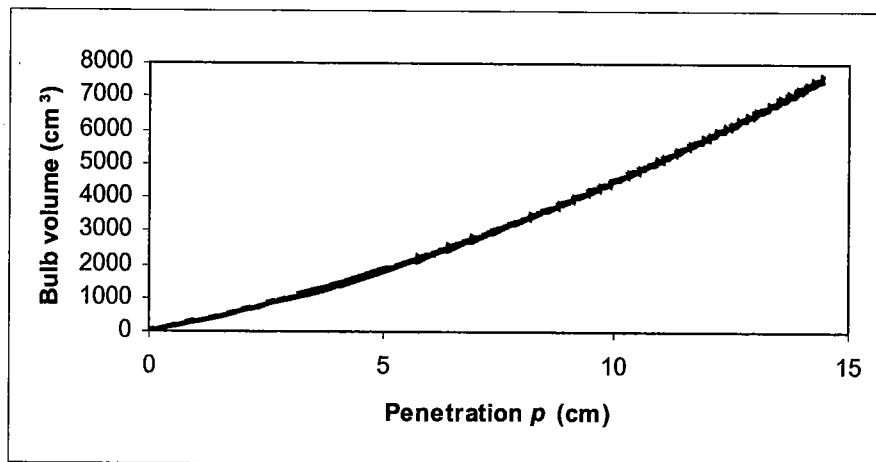
Figure 5.7 Penetration Below Well vs. Volume of Bulb

76

Figure 5.7 plots the penetration below the well against the corresponding bulb volume V_b, predicted with the zero air entry Green-Ampt model. The relationship shown in Figure 5.7 is indistinguishable from the curve fit

$$V_b = 17p^2 + 280p \qquad (5.6)$$

also shown in Figure 5.7. On noting that the cross sectional area for flow in the permeameter tube is 22.4 cm^2 and setting $\Delta\phi$ to the relatively small value of 0.224, Equation 5.6 can be modified to equate the drop in the tube Δl to the penetration below the well:

$$\Delta l = 0.17p^2 + 2.8p \qquad (5.7)$$

Hence, for a pavement base layer with a clearance s (cm) below the well hole, the maximum tube drop over which measurements matching those that would be seen in a single homogenous layer can be taken as:

$$\Delta l_{max} = 0.17s^2 + 2.8s \qquad (5.8)$$

For the case of a pavement depth of $s = 5$ cm below the bore hole, $\Delta l_{max} \sim 20$cm. When the saturated conductivity is high ($\sim 10^{-3}$ cm/s) this drop will be covered in around 4 minutes. Although remedial measures such as reducing the applied head form 10 cm to 5 cm may help, this situation is pushing the limits of the permeameter operation and use of the permeameter when $s < 5$ cm (2 inches) is not recommended. In less taxing situations, e.g., $s = 10$ cm and $k = 10^{-4}$ cm/s the maximum reading length becomes 45 cm and the time taken to drop this distance is ~ 100 minutes, which is well within the operating capabilities of the permeameter. As values of the hydraulic conductivity become smaller the infiltration times will become longer. For example if $k = 10^{-5}$ cm/s, roughly 400 minutes will be required for the water level to drop 20 cm. This value is at the lower limit of the permeameter operation.

Summary.

This chapter has provided two important findings:

1. A comparison with a direct numerical simulation has shown that the field use of the permeameter to predict the hydraulic conductivity of the base is sound if the base is thick enough.

2. An analysis of the Green-Ampt [38] infiltration model has arrived at an operation equation that relates the length of tube in the permeameter over which a reliable infiltration measurement can be taken to the depth of base below the well hole.

CHAPTER 6

CONCLUSIONS AND RECOMMENDATIONS

Overview

The purpose of this project was to investigate the possible uses of the fixed head Mn/DOT permeameter in measuring the saturated hydraulic conductivity of pavement base materials used in Minnesota. Tasks in the project involved:

1. Development of a procedure to obtain reliable steady flow estimates from field measurements of infiltration.

2. Field testing of the Mn/DOT permeameter.

3. Preparation of a handbook for field use of the permeameter.

4. Demonstration of the field application of the permeameter for members of Mn/DOT drainage committee.

5. Laboratory measurements of saturated hydraulic conductivities of granular base samples removed from the field during the permeameter well construction.

6. Formatting of a database that can be used to collect saturated hydraulic conductivity values of granular base materials used in Minnesota.

7. Identification and investigation of existing theoretical relationships that can be used to translate field measured steady flow rates into estimates of the field-saturated hydraulic conductivity of the base material.

8. Studies aimed at establishing a suitable shape factor for use in the existing theoretical relationships when applied to field measurements obtained with the Mn/DOT permeameter.

9. Numerical and analytical analyses to identify the conditions under which reliable estimates of hydraulic conductivity could be obtained with the Mn/DOT permeameter.

Results

1. Extensive field testing of the Mn/DOT permeameter was conducted over two construction seasons (1999 and 2000). Thirty-one sites were tested; each test included multiple uses of the permeameter. A procedure was developed to analyze the field data; in particular a non-linear curve fitting procedure was used in order to obtain consistent and reliable estimates of the steady flow rate from the field data. Measured steady flow rates, Q, ranged from 3.8×10^{-8} to 5.9×10^{-6} m^3/s. Results indicate that the variability in the permeameter use and field conditions can predict Q's in this range to within a factor of two (Figure 4.1).

2. Analysis of the 1999 laboratory hydraulic conductivity data shows that scatter due to variability in the laboratory testing is limited to a factor of two (Figure 3.2). The ranges of conductivities measured in this study are given in Table 3.7.

3. A comprehensive review of the literature resulted in the identification of eight possible models that could be used to relate the steady flow rate from a constant head permeameter to values of the field-saturated hydraulic conductivity (see summary in Table 2.2). Analysis in Chapter 4 showed that predictions obtained with the various models were qualitatively the same with quantitative differences attributed to the different shape factors used.

4. A study of the field data indicated that when the GP-L model

$$k_{fs} = \frac{CQ}{2\pi H^2 \left[1 + \frac{C}{2} \left(\frac{a}{H} \right)^2 \right]}$$ (6.1)

where the shape factor is given by

$$C = D \left[\frac{H}{a} \right]^{2/3}$$ (6.2)

($D \sim 0.02$) is used with the flow rate from the permeameter, field estimates of the saturated hydraulic conductivity provide a good match to the range of conductivities measured in the laboratory (see Figure 4.4). A numerical study based on the SEEP/W commercial code refined the field study and showed that the optimum shape factor for use in the GP-L model is

$$C = 0.0046 \left[\frac{H}{a} \right]^2 + 0.0318 \left[\frac{H}{a} \right] - 0.0087$$ (6.3)

Predictions obtained with this value are very close to those obtained when Equation 6.2 (with $D = 0.02$) is used.

5. One-to-one comparisons between the field estimated and laboratory measured hydraulic conductivities showed a poor correlation, with differences of up to one order of magnitude. The poor correlation was confirmed with a Monte Carlo analysis (see Figure 4.7). The poor correlation can be attributed to (1) a mismatch in conditions between the laboratory and field and/or (2) a thin base layer, which would render the theory relating steady infiltration to conductivity invalid.

6. In contrast to the poor correlation seen between the field and laboratory, the correlation between the field values of saturated conductivity and those obtained in a direct numerical simulation using the SEEP/W code was significantly better (see Figure 5.4).

81

Typically differences between the simulation and the field were within a factor of 2. This result indicates that when the assumption of a thick homogenous isotropic layer is valid the permeameter can be used to obtain a reasonable estimate of the base hydraulic conductivity.

7. An analysis of an axisymmetric limiting Green-Ampt solution showed that the permeameter should not be used when the base thickness below the well hole, s, is less than 5 cm (two inches). This translates to a total base thickness of 15 cm assuming a borehole depth of 10 cm. Further the analysis showed that the maximum drop in the annular tube reservoir over which flow measurements should be taken is given by the relationship

$$\Delta l_{\max} = 0.17s^2 + 2.8s \qquad (6.4)$$

Conclusions

The Mn/DOT permeameter can be used to estimate the saturated hydraulic conductivity in a homogeneous and isotropic base of a pavement system provided the conditions in Table 6.1 hold.

Table 6.1 Conditions Necessary for Using Mn/DOT Permeameter

1	The permeameter is used in a manner consistent with the guidelines set out in the operation manual (Appendix A).
2	The values obtained do not fall outside the operating range of the permeameter, which, to avoid excessively fast or slow flow rate into the base, are $$10^{-5} \text{ cm/s} \leq k_{sat} \leq 10^{-3} \text{ cm/s}.$$
3	A factor of two accuracy in the measure of the saturated hydraulic conductivity is sufficient for the task at hand. Note the estimate of the accuracy is based on the comparisons of permeameter measurements with those obtained with the SEEP/W numerical model (see Figure 5.4).
4	To avoid the effect of layering on the results, the thickness T of the base layer is larger than $$T > D + 5 \text{ cm (2 inches)}$$ where D is the depth of the borehole, dug for the operation of the permeameter (~ 10 cm).
5	In cases where the base layer meets this restriction but still may be thin, the reading of the permeameter should be governed by Equation 6.3 above.
6	The assumption of a homogeneous and isotropic base layer is reasonable.

Recommendations

1. In cases where the base layer is heterogeneous and anisotropic, or the base layer is thin, values obtained with the permeameter should not be interpreted as a point measure of saturated conductivity.   In heterogeneous and thin-layered systems the infiltration is controlled by many interacting coupled phenomena [38, 39].

2. When the conditions in Table 6.1 are met, the permeameter could be used in construction inspection, in the sense that if an acceptable range of hydraulic conductivity was given as a specification for a given base, the permeameter could be used to check for compliance of this specification.

3. When the conditions in Table 6.1 hold, the permeameter could be used in drainage design, provided there is a mechanism in place to use the single point measure of the hydraulic conductivity, along with other measures of the base characteristics, in a model of drainage performance. This last point is of critical importance. A full drainage system will involve many layers, which during a typical drainage event, will operate in the

unsaturated state. In analyzing drainage performance, obtaining a value of the saturated hydraulic conductivity of the base is a useful item of information but only one among many needed parameters, e.g., characteristic moisture curves [22], for the base materials that will also be required. Continuing research needs to be directed at developing methods to measure all of the base characteristics required for use in comprehensive drainage design models.

BIBLIOGRAPHY

1. Huang, Y. H., *Pavement Analysis and Design*, Prentice-Hall, Inc., Englewood Cliffs, NJ, 1993.

2. Moulton, L. K., "Highway Subdrainage Design," U. S. Department of Transportation, Federal Highway Administration, Report No. FHWA-TS-80-224, August 1980.

3. Das, B. M., *Principles of Geotechnical Engineering, Third Edition*, PWS Publishing Company, Boston, MA, 1994.

4. Strack, Otto D. L., *Groundwater Mechanics*, Strack Consulting Inc., North Oaks, Minnesota, 1999.

5. Elsayed, A. S. and J. K Lindly, "Estimating permeability of untreated roadway bases," *Transportation Research Record 1519*, Transportation Research Board, 1996, pp. 11-18.

6. Jaynes, D. B., and E. J. Tyler, "Using soil physical properties to estimate hydraulic conductivity," *Soil Science*, October 1984, pp. 298-305.

7. Schuh, W.M., and M. D. Sweeny, "Particle-size distribution method for estimating unsaturated hydraulic conductivity of sandy soils," *Soil Science*, November 1986, pp. 247-254.

8. Richardson, D. N., "Drainability characteristics of granular pavement base material," *Journal of Transportation Engineering*, September-October 1997, pp. 385-392.

9. Elrick, D. E., and W. D. Reynolds, "An analysis of the percolation test based on three-dimensional saturated-unsaturated flow from a cylindrical test hole," *Soil Science*, November 1986, pp. 308-321.

10. Fernuik, N., and M. Haug, "Evaluation of in situ permeability testing methods," *Journal of Geotechnical Engineering*, February 1990, pp. 297-311.

11. Reynolds, W. D., and D. E. Elrick, "Ponded infiltration from a single ring: I. Analysis of steady flow," *Soil Science Society of America Journal*, September-October 1990, pp. 1233-1241.

12. Reynolds, W. D., and D. E. Elrick, "Determination of hydraulic conductivity using a tension infiltrometer," *Soil Science Society of America Journal*, May-June 1991, pp. 633-639.

13. Youngs, E. G., "Estimating hydraulic conductivity values from ring infiltrometer measurements," *Journal of Soil Science*, December 1987, pp. 623-632.

14. Mohanty, B. P., Kanwar, R. S., and C. J. Everts, "Comparison of saturated hydraulic conductivity measurement methods for a glacial-till soil," *Soil Science Society of America Journal*, May-June 1994, pp.672-677.

15. Scott, N., Bloomquist, D., Armaghani, J., and A. Malpartida, "Development of field permeability testing device for concrete pavement support layers," PREPRINT, Transportation Research Board, 77th Annual Meeting, 1998.

16. Randolph, B. W., Steinhauser, E. P., Heydinger, A. G., and J. D. Gupta, "In situ test for hydraulic conductivity of drainable bases," *Transportation Research Record 1519*, Transportation Research Board, 1996, pp. 36-40.

17. Gribb, M. M., Simunek, J., and M. F. Leonard, "Development of cone penetrometer method to determine soil hydraulic properties," *Journal of Geotechnical and Geoenvironmental Engineering*, September 1998, pp. 820-829.

18. Guelph Permeameter 2800K1 Operating Instructions, Soilmoisture Equipment Corp. Santa Barbara, CA, 1986, pp. 1-28.

19. Birgisson, B., and P. B. Solseng, "An Evaluation of Methods/Devices for Measuring In-Situ Drainage Characteristics of Aggregate Base and Granular Subgrade Materials, Phase I," Barr Engineering Company, Minneapolis, MN, December 1996.

20. Ramasundaram, S., and B. Birgisson, "Minnesota Permeability Database: A User's Manual," Department of Civil and Coastal Engineering, University of Florida, April 2000.

21. Philip, J. R., "Approximate analysis of the borehole permeameter in unsaturated soil," *Water Resources Research*, July 1985, pp. 1025-1033.

22. Hillel, D., *Environmental Soil Physics*, Academic Press, New York, 1998.

23.   Reynolds, W. D., D. E. Elrick, and B. E. Clothier, "The constant head well permeameter: Effect of unsaturated flow," *Soil Science*, February 1985, pp. 172-180.

24.   Celia, M. A., Bouloutas, E. T., and R. L. Zarba, "A General Mass-Conservative Numerical Solution for the Unsaturated Flow Equation," *Water Resources Research*, July 1990, pp. 1483-1496.

25.   Reynolds, W. D., and D. E. Elrick, "In situ measurement of field-saturated hydraulic conductivity, sorptivity, and the α-parameter using the Guelph permeameter," *Soil Science*, October 1985, pp. 292-302.

26.   Reynolds, W. D., and D. E. Elrick, "A method for simultaneous in situ measurement in the vadose zone of field-saturated hydraulic conductivity, sorptivity and the conductivity-pressure head relationship," *Ground Water Monitoring Review*, Winter 1986, pp. 84-95.

27.   Amoozegar, A., "Comparison of the Glover solution with the simultaneous-equations approach for measuring hydraulic conductivity," *Soil Science Society of America Journal*, September-October 1989, pp. 1362-1367.

28.   Amoozegar, A., and A. W. Warrick, "Hydraulic conductivity of saturated soils: Field methods," *In* Methods of soil analysis, pt. 1. Physical and mineralogical methods, 2nd Ed. A. Klute (ed.). American Society of Agronomy, Madison, Wisconsin, 1986, pp. 735-770.

29.   Elrick, D. E., and W. D. Reynolds, "Methods for analyzing constant-head well permeameter data," *Soil Science Society of America Journal*, January-February 1992, pp. 320-323.

30.   Elrick, D. E., W. D. Reynolds, and K. A. Tan, "Hydraulic conductivity measurements in the unsaturated zone using improved well analyses," Ground *Water Monitoring Review*, Summer 1989, pp. 184-193.

31.   Stephens, D. B., and S. P. Neuman, "Vadose zone permeability tests: Summary," *Journal of the Hydraulics Division*, May 1982, pp. 623-639.

32.   Wu, L., J. B. Swan, J. L. Nieber, and R. R. Allmaras, "Soil-macropore and layer influences on saturated hydraulic conductivity measured with borehole permeameters," *Soil Science Society of America Journal*, July-August 1993, pp. 917-923.

33. Heinen, M., and P. A. C. Raats, "Evaluation of two models describing the steady discharge from a constant head well permeameter into unsaturated soil," *Soil Science*, July 1990, pp. 401-412.

34. Chapuis, R. P., "Shape factors for permeability tests in boreholes and piezometers," *Ground Water*, September-October 1989, pp. 647-654.

35. Minnesota Department of Transportation, Engineering Services Division, "Technical Memorandum No. 99-08-MRR-04, Attachment #4" March 1, 1999.

36. Minnesota Department of Transportation, "Specifications for Construction, Spec # 3149," Metric Edition, 1995.

37. Ovik, Jill M., "Characterizing Seasonal Variations in Pavement Material Properties for Use in a Mechanistic-Empirical Design Procedure," M.S. Thesis, University of Minnesota, Minneapolis, June 1998.

38. Jury, W.A., Gardner, W.R., and Gardner, W.H., *Soil Physics, 5th Edition*, John Wiley and Sons, New York, 1991.

39. Horton R. E., "Analysis of runoff plot experiments with varying infiltration capacity," Trans. Am. Geophs. Union, Part IV, 1939, pp. 693-694.

40. Birgisson, B., Task 1.4 Report, "Numerical Calibration," *Field Measurement of Granular Base Drainage Characteristics*, Department of Civil and Coastal Engineering, University of Florida, February 2001.

41. Voller, V. R., Peng, S., and Chen, Y. F., "Numerical solution of transient free surface problems in porous media," Int. J. Num Meth. Eng., 39, 1996, pp. 2889-2906.

APPENDIX A

MINNESOTA DEPARTMENT OF TRANSPORTATION

PERMEAMETER USER'S MANUAL

Introduction

The Mn/DOT permeameter is a constant-head device that operates on the Mariotte principle [18]. It provides a relatively quick and simple method for determining field-saturated hydraulic conductivity of an in situ granular base material. It is a rugged and versatile device that is meant to be used on coarse-grained soils. More specifically, it is useful for testing gravel base materials for highway pavements.

Using the Mn/DOT permeameter, measurements on in situ materials can be made and results calculated in about an hour by following the standard procedure and calculations that are detailed in this instruction manual. The permeameter can be stored in a simple custom-made PVC case to protect it during transportation. Component parts are made of strong acrylic tubes and nylon caps to withstand rugged field use and assure long-lasting performance.

Description of Parts

Reservoir Assembly

The Mn/DOT permeameter is constructed from simple parts that can be bought at a local hardware store or plastic supply store. The tubes are made of strong acrylic tubing and the end caps are made of nylon. The air valve is a simple brass coupling with a steel knob. The permeameter was built using English measurements but converted to the S.I. system for easy use. See Figure A.1 for a schematic drawing of the permeameter.
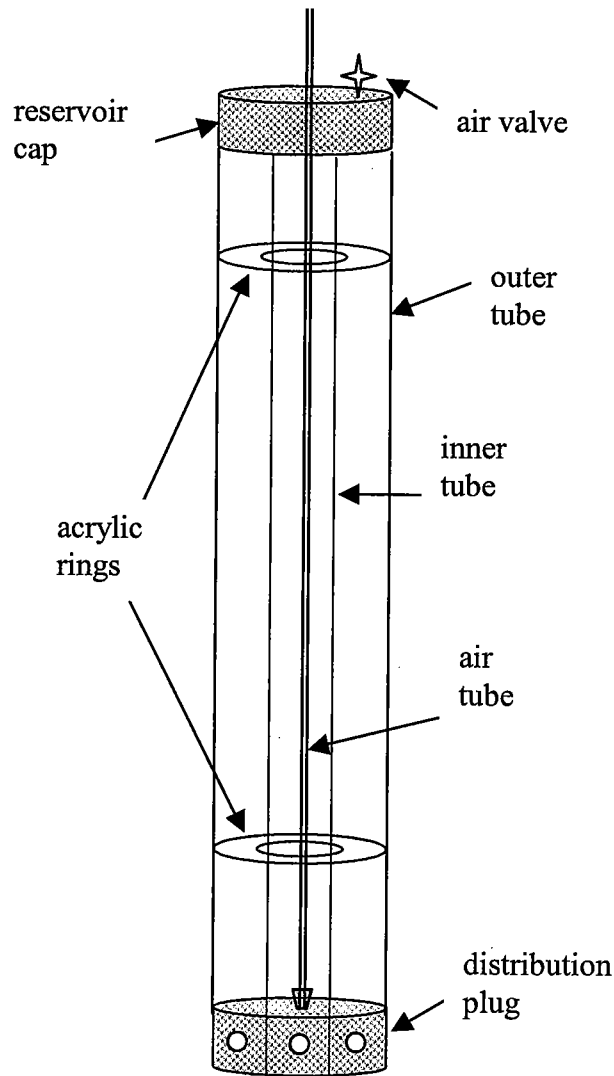
Figure A.1 Mn/DOT Permeameter

Labels in figure: reservoir cap, air valve, outer tube, inner tube, acrylic rings, air tube, distribution plug

Outer Tube

The outer tube of the permeameter is made of 6.35 mm (0.25 in) thick acrylic tubing. The outer diameter of the tube is 63.5 mm (2.5 in) and the length is 1.71 m (67 in). The outer tube acts as a reservoir for the water contained inside the permeameter.

Inner Tube

The inner tube of the permeameter is made of 6.35 mm (0.25 in) thick acrylic tubing. The outer diameter is 31.75 mm (1.25 in) and the length is 1.68 m (66 in). Two acrylic rings near the top and bottom of the permeameter assist in centering the inner tube inside of the outer

tube. The rings fit loosely and have no effect on the flow of water out of the permeameter and into the soil. To aid in measuring the flow rate out of the permeameter, a Mylar ruler[1] is taped on the inner tube. This allows the researcher to read the drop in water height inside the permeameter.

Air Tube

The air tube is made of acrylic tubing 1.59 mm (0.06 in) thick. The outer diameter is 9.53 mm (0.38 in) and the length is 1.84 m (72 in). An air inlet tip is located at the bottom of the air tube. This tip will fit snugly inside of the distribution plug when filling the reservoir with water.

Distribution Plug

The distribution plug allows water to flow out of the permeameter and into the soil (Figure A.2). It is a nylon cap cut to fit the outer tube. The hole in the center fits snugly with the air inlet tip. From this hole originates a series of water distribution holes 6.35 mm (0.25 in) in diameter. These passageways carry water from the permeameter reservoir out to the soil. They are distributed every 15° around the plug and staggered vertically. The two grooves cut in the plug are for holding O-rings in place. The O-rings seal the permeameter and prevent unwanted air from entering or exiting the reservoir.

---

[1] *Oregon Rule Company P.O. Box 5072 Oregon City, Oregon 97405*
(503) 657-8330 FAX (503) 655-8040 www.oregonruleco.com
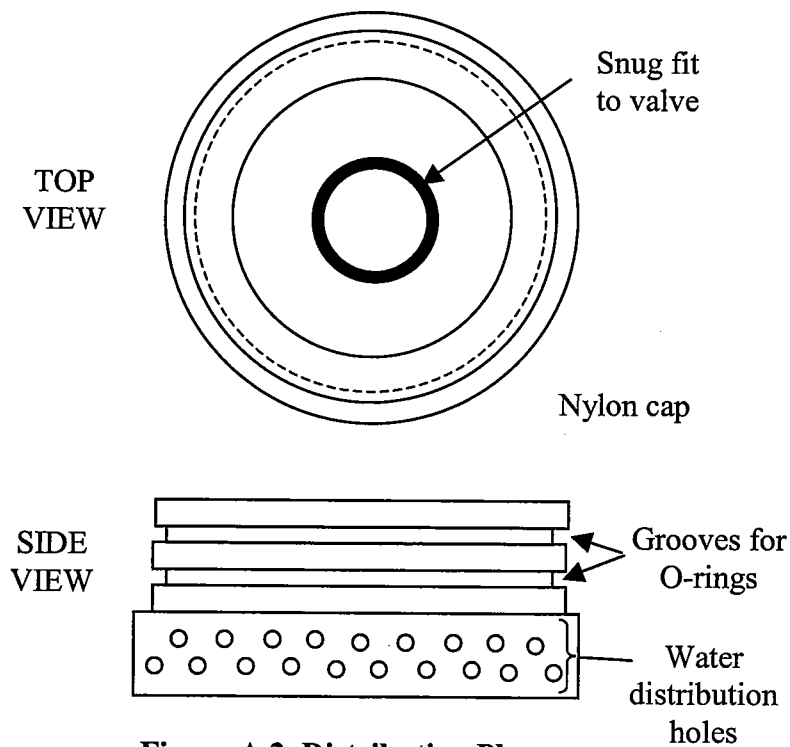
Figure A.2 Distribution Plug

TOP VIEW

Snug fit to valve

Nylon cap

SIDE VIEW

Grooves for O-rings

Water distribution holes

Top Plug

The top plug, made of nylon, attaches to the top of the outer tube. It has a hole in the middle for the air tube to slide up and down when setting the head level in the auger hole. The air valve consists of a brass coupling along with a steel rod for opening and closing the valve. An O-ring fits inside the groove cut in the top plug to seal the permeameter so that air cannot leak in or out.

Auxiliary Tools

To conduct field hydraulic conductivity testing, a number of tools should accompany the permeameter. These include:

- Hand auger for boring a hole in the soil
- Stiff brush to remove any smear layer created on the walls of the auger hole during the boring process
- Well screen to prevent collapse of the granular material into the hole

- Proper stand to hold the permeameter upright
- Container capable of holding 20 L of water
- Stopwatch and tape measure

Procedures for Field Use

There are a number of steps that must be completed before actually carrying out the field permeability test. It is necessary to evaluate the site and the granular material being tested, prepare the auger hole, fill the reservoir with water, and situate the permeameter in the auger hole.

Site and Material Evaluation

Evaluate the site being tested and select the area that is representative of the entire site. Preliminary information that should be noted in this evaluation are the date and time, station (exact location of test), offset from centerline, apparent longitudinal and cross slopes, water table depth, height of embankment, evidence of a positive drainage system, the last precipitation event and intensity, current weather conditions, visual description of the material, and a geological description of the granular material. In addition, the permeameter that is used for each test should be noted. If samples are taken for additional laboratory testing, the sample size should be recorded. It is also essential to measure and record the density and moisture content of the in situ material. This should be done in accordance with ASTM D 1556 – 90, "*Standard Test Method for Density and Unit Weight of Soil in Place by the Sand-Cone Method.*"

Well Preparation

The soil auger is used to bore out a hole in the granular material (Figure A.3). Auger the well hole by rotating the handle clockwise while applying a steady downward pressure on the handle. When the bucket is full, lift the auger out of the hole and invert it so that the collected sample slips out of the open end of the bucket. When augering, be careful to keep the shaft of the auger vertical to avoid excessive enlargement of the well hole. In a gravel soil, this may be difficult. The well hole should be augered to either mid-depth of the base layer or 150 mm (6 in), whichever is greater. Care should be taken not to auger into the underlying layer. It may be necessary to auger an exploratory hole to determine the actual thickness of each layer before the test is performed. Clean the debris from the bottom of the well hole to remove loose particles.

TEE-HANDLE

QUICK
CONNECTOR
(Standard Construction Only)

AUGER BUCKET
HEAD

EXTENSION
ROD
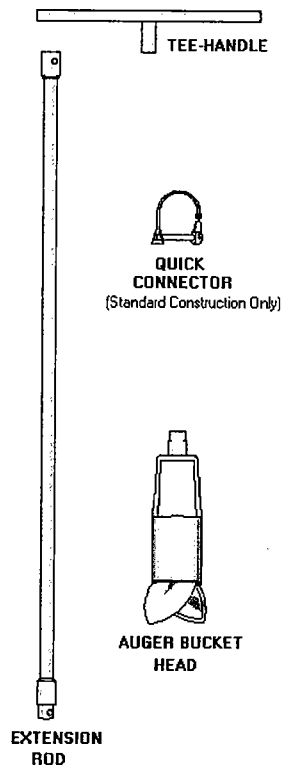
Figure A.3 Hand Auger

In moist granular materials, and especially those containing many fine particles, a smear layer may be created during the process of boring the hole. This will close up pores on the face of the hole and impede the natural flow of water out of the well and into the surrounding material. In order to obtain reliable results from the test, this smear layer must be removed. The stiff brush is used for this purpose. Use the brush to gently roughen the surface and scour the smear layer in the well. Do not brush the hole more than a few times, since each operation removes a thin layer of material from the hole. Repeated brushing may enlarge the hole beyond practical limits to carry out accurate testing.

Use a tape measure to measure the depth and diameter of the auger hole. Record these values on the data sheet.

Permeameter Setup

The Mn/DOT permeameter should be carried to the field in its durable PVC pipe case. This will protect it from cracks, chips, and breaks during routine transport. The setup of the permeameter includes filling it with water and inserting the device into the well hole.

Step 1

Set up the stand that will hold the permeameter in place. In the past, Mn/DOT has used a breakaway four-legged stand for temporary road signs. This has proved to be an adequate system to hold the permeameter upright. Extend the four legs of the brace and make sure it sits evenly on the ground.

Step 2

Place the well screen in the borehole (Figure A.4). The screen should rest firmly on the bottom of the auger hole and stand upright. It should reach above the level that the water will pond in the hole. The purpose of the screen is to prevent wet soil from collapsing the hole during

A-7

testing. It is made of a durable 0.3-mm (No. 50) mesh that allows water to pass freely through while holding the base material in place.
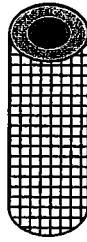
Figure A.4 Well Screen

Step 3

Place the permeameter inside of the screen in the well hole. The permeameter should stand upright and rest on the bottom of the hole. Bring the stand next to the permeameter so that the device can be held upright. Brace the permeameter in place by wrapping a bungee cord around the permeameter and the stand. The wrap should be sufficiently tight to hold the permeameter upright and should not obstruct the view of the ruler inside the permeameter. Leave enough room so that measurements can be made all the way to the bottom of the permeameter. The permeameter need not be plumbed perfectly; simply "eyeballing" it will do.

Step 4

The permeameter must be filled with water prior to testing. Open the air valve on the reservoir cap of the permeameter by turning it counterclockwise. Pull the reservoir cap up from the reservoir and slide it up along the air tube. This step can be difficult if the cap sticks inside the reservoir. A gentle twisting action while pulling the cap up should allow it to be removed. The air inlet tip should remain snugly seated at the bottom of the reservoir. Pour water into the permeameter, being careful not to spill any into the well hole. Normal tap water is sufficient for running the test. Fill the reservoir all the way to the top of the permeameter. Place the reservoir cap back on the permeameter by sliding it down the air tube. Push it evenly down inside the

reservoir until the cap is seated firmly. Water will squirt out of the air valve, effectively removing all of the air from inside the permeameter. Close the air valve by turning it clockwise.

Conducting a Hydraulic Conductivity Test

Make sure that enough water is available to carry out as many hydraulic conductivity tests as needed. Once the permeameter has been set up in the prepared well hole and filled with water, the following standard procedure should be used for making measurements.

Step 1 – Establish 5 cm Well Head Height (H_1)

Slowly raise the air inlet tip by gently twisting and pulling the air tube. Raising the air tube too quickly can cause turbulence and erosion in the well, which could temporarily overfill the well or cause all of the fines to clog up the pores. Raise the air tube until a ponded height of 5 cm (2 in) is established. Seat the tape measure on the reservoir cap to determine the proper height.

Step 2 – Measure Permeameter Outflow, First Ponded Height

The flow of water from the permeameter into the soil is indicated by the rate of fall of water in the reservoir. Read the water level in the reservoir using the scale taped on the inner reservoir tube. Start the stopwatch and record the water level on the data sheet. Readings should be made at regular time intervals. An interval of one minute is suggested, but any interval that allows a distinctive drop in water level (0.2 cm or more) is acceptable. The difference between readings at consecutive intervals (in cm) divided by the time interval (in seconds) equals the rate of fall of water in the reservoir, R (in cm/s).

If the granular material being investigated is densely graded or contains many fine particles, the rate of fall of water is so slight that the selected time interval may not be long enough to detect a measurable change in the water level in the reservoir. In this case, a longer

time interval must be selected in order to measure the rate of fall in the reservoir. On the other hand, open graded or coarse materials may allow water to flow very fast through them. A time interval as short as 15 or 20 seconds may be appropriate to make the measurements. Be sure to make the calculation for R based on the actual time interval selected.

Continue monitoring the rate of fall of water in the reservoir until it does not significantly change in three consecutive time intervals. This may take anywhere from roughly 3 to 30 minutes, depending on the type of material. The rate is called R_1 and is defined as the "steady state rate of fall" of water in the reservoir at H_1. H_1 is always the first well height established.

After completing the outflow measurements, DO NOT DISTURB the permeameter in any manner and proceed immediately to Step 3.

Step 3 – Establish 10 cm Well Head Height (H_2)

Slowly raise the air inlet tip by pulling the air tube to establish a second well head height of 10 cm (4 in). Again, use the tape measure seated on the reservoir cap to determine a height of 10 cm.

Step 4 – Measure Permeameter Outflow, Second Ponded Height

As in Step 2, monitor the rate of fall of water in the reservoir until a stable value of R is measured. This rate is called R_2 and is defined as the "steady state rate of fall" of water in the reservoir at H_2. H_2 is the second well height established.

Comments

It is recommended that several measurements be taken in different boreholes to assure the accuracy of the test. Auger another hole about 2 m (6.5 ft) away from the first well hole and repeat the above procedure. A minimum of three tests is suggested until more information on variability is available. The water inside the reservoir may need to be refilled in between tests.

As was mentioned earlier, the time intervals need not be one minute. Any interval that makes it possible to accurately measure the drop in water level inside the reservoir is acceptable. Likewise, the two ponded heights need not be 5 cm (2 in) and 10 cm (4 in). These values are recommended, but any two heads that produce significantly different flow rates may be used.

Calculations

The field-saturated hydraulic conductivity, k_{fs} (cm/s), can now be calculated using the equations below. These equations use the steady state rates of fall along with the geometry of the well hole. In the following calculations, Q is the steady-state flow rate (cm^3/s), H is the head of water in the well (cm), and a is the well radius (cm).

C Factor

The C factor is a numerically derived shape factor that is dependent on the well radius, a, and the head, H, of water in the well. Calculate the H/a ratio for the conditions measured in the field. From this value, determine the C factor from Equation A.1:

$$C = 0.02\left(\frac{H}{a}\right)^{2/3} \tag{A.1}$$

Hydraulic Conductivity

Hydraulic conductivity, k, is the measure of the ability of a material to conduct water under a unit hydraulic potential gradient. Field-saturated hydraulic conductivity, k_{fs}, refers to the conductivity of a material containing entrapped air. This k_{fs} value is usually more appropriate than the truly saturated hydraulic conductivity because materials under typical field conditions almost always contain some amount of entrapped air.

Reynolds and Elrick [26] suggest using the GP-L Equation to calculate the field-saturated hydraulic conductivity. This was described as Equation 2.22 in the report and is reproduced here:

$$k_{fs} = \frac{CQ}{2\pi H^2 \left[1 + \dfrac{C}{2}\left(\dfrac{a}{H}\right)^2\right]} \qquad (A.2)$$

In Equation A.2, the flow rate Q is calculated as the annular area of the permeameter multiplied by the steady-state flow rate R. The C factor is determined from Equation A.1.

The hydraulic conductivity should be calculated from Equation A.2 for each test at a particular site. The value reported should be taken as the average of all the tests.

Theory of Operation

The Mn/DOT permeameter designed for this research project was closely modeled after the Guelph Permeameter developed in the mid-1980's at the University of Guelph, Ontario, Canada. The permeameter is an in-hole constant-head permeameter that employs the Mariotte Principle [18]. The method includes determining the steady-state rate of flow into unsaturated material from a cylindrical well hole where a constant head of water is maintained.

Mariotte Principle

A constant head level in the auger hole is established and maintained by regulating the level of the air tube in the center of the permeameter. As the water level in the permeameter falls, a vacuum is created in the air space above the water. The vacuum is relieved when air, which enters at the top of the air tube, bubbles out of the air inlet tip and rises to the surface of the reservoir. When the water level in the well drops below the elevation of the air inlet tip, air bubbles emerge from the tip and rise into the reservoir air space. The vacuum is then partially

relieved and water from the permeameter refills the water in the well. The size and geometry of the openings in the air inlet tip are designed to control the size of air bubbles in order to prevent the well water level from fluctuating.

An equilibrium is established when the permeameter is operating properly. This operation is based on the Mariotte Principle (Figure A.5). The partial vacuum in the air space above the water in the permeameter along with the pressure of the water column extending from the surface of the well to the surface of the water in the reservoir is equal to the atmospheric pressure.
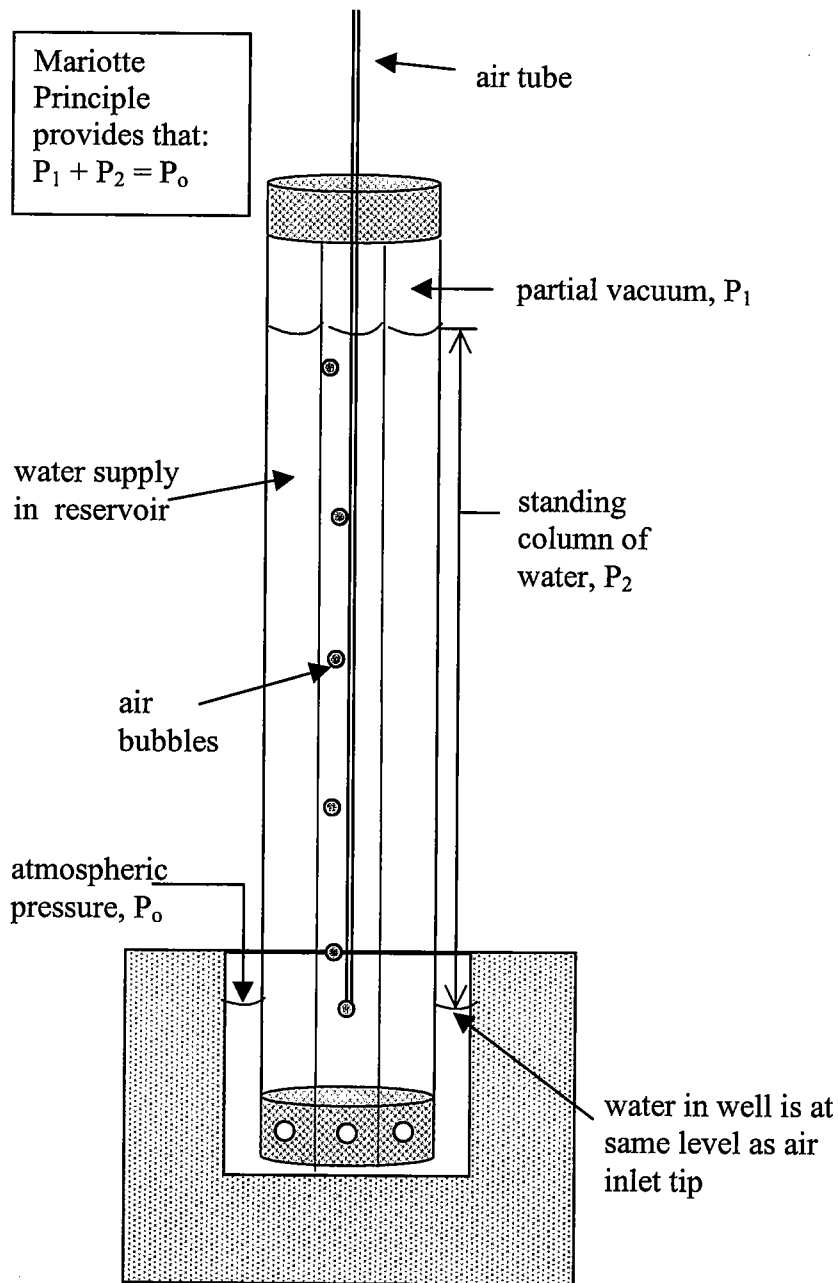
Figure A.5 Mariotte Principle

When a constant ponded height of water is established in a well hole in the material, a "bulb" of saturated soil with specific dimensions is established (Figure A.6). This bulb is relatively stable and its shape depends on the type of soil, the radius of the well, and the head of water in the well. The shape of the bulb is numerically described by the C factor used in the

calculations. Once this bulb is established, the flow of water out from the well reaches a measurable steady state. This constant rate of outflow of water, together with the radius of the well and head of water in the well, is used to determine the field-saturated hydraulic conductivity of the material.
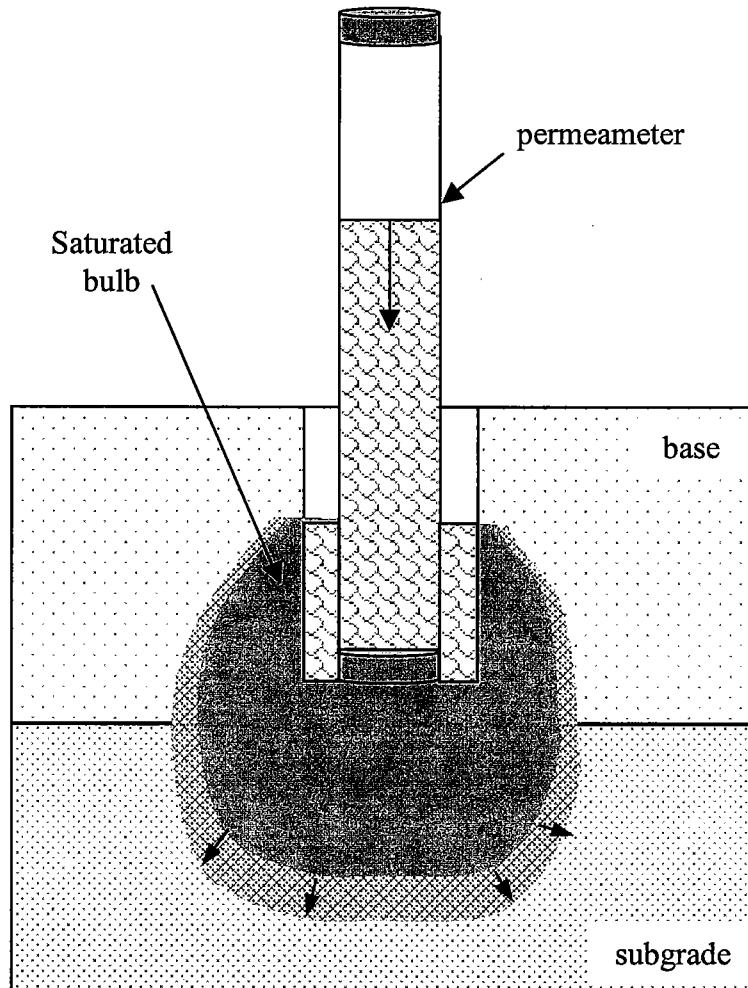
Figure A.6 Saturated Bulb

Sample Data Collection Sheet

FIELD PERMEABILITY TEST

name: positive drainage system:
date and time: (permeable base layer, longitudinal
site: edge drain, filter-separator layer)
precise location: last precipitation event and intensity:
offset from centerline: current weather conditions:
apparent pavement slope: (temperature, humidity, cloud cover, precipitation)
water table depth: visual soil description:
height of embankment: (grain size, color, relative wetness/dryness, etc.)
sample size: geologic description of soil:
borehole depth: (i.e., crushed granite, basalt, limestone, etc.)
device used: COMMENTS:

---

head:
well radius:

time (min)	height, h (cm)	Δh (cm)

head:
well radius:

time (min)	height, h (cm)	Δh (cm)

CALCULATIONS

R_i, the steady state rate of flow, is achieved when R is the same in three consecutive time intervals

For the 1st set of readings: $R_1 =$ _____ cm/s

For the 2nd set of readings: $R_2 =$ _____ cm/s

$$k_{fs-1} = \frac{C_1 Q_1}{2\pi H_1^2 \left[1 + \frac{C_1}{2}\left(\frac{a}{H_1}\right)^2\right]}$$

$$k_{fs-2} = \frac{C_2 Q_2}{2\pi H_2^2 \left[1 + \frac{C_2}{2}\left(\frac{a}{H_2}\right)^2\right]}$$

permeameter	area, cm^2
Mn/DOT 2.5"	22.4060
Mn/DOT 3.0"	35.0737
Guelph	35.39 or 2.14

APPENDIX B

RAW DATA FROM FIELD PERMEABILTY TESTS

NOTE: All tests run with permeameter of annular area A = 22.406 cm^2

Blue Earth Co. Rd. 90
Class 3   7/27/99

Run 1

a	4.7625
H_1	5.08
H_2	10.16
s	12.7
b_1	12.7
b_2	7.62

Run 2

a	4.7625
H_1	5.08
H_2	11.43
s	12.7
b_1	12.7
b_2	6.35

Time, min	R_1, cm/min	Time, min	R_2, cm/min	Time, min	R_1, cm/min	Time, min	R_2, cm/min
1	0.2	1	0.4	1	0.0	1	0.4
2	0.3	2	0.3	2	0.3	2	0.0
3	0.2	3	0.2	3	0.2	3	0.6
4	0.2	4	0.3	4	0.2	4	0.7
5	0.2	5	0.3	5	0.1	5	0.5
		6	0.1	6	0.3	6	0.5
		7	0.4	7	0.2	7	0.5
		8	0.2			8	0.5
		9	0.2				
		10	0.3				
		11	0.2				
		12	0.3				
		13	0.2				
		14	0.3				

Run 3

a	4.7625
H_1	5.08
H_2	11.43
s	12.7
b_1	12.7
b_2	6.35

Run 4

a	4.7625
H_1	5.08
H_2	11.43
s	12.7
b_1	12.7
b_2	6.35

Time, min	R_1, cm/min	Time, min	R_2, cm/min	Time, min	R_1, cm/min	Time, min	R_2, cm/min
1	0.7	1	0.8	1	0.6	1	0.3
2	0.3	2	1.1	2	0.4	2	1.3
3	0.3	3	1.2	3	0.4	3	1.1
4	0.2	4	1.1	4	0.2	4	1.1
5	0.2	5	1.1	5	0.2	5	1.1
6	0.2	6	1.0	6	0.2	6	1.1
7	0.3	7	1.1	7	0.0		
8	0.2			8	0.4		

Run 5

a	4.7625
H_1	5.08
H_2	11.43
s	12.7
b_1	12.7
b_2	6.35

Time, min	R_1, cm/min	Time, min	R_2, cm/min
1	0.4	1	1.0
2	0.2	2	0.5
3	0.1	3	0.0
4	0.1	4	0.7
5	0.3	5	0.6
6	0.1	6	0.6
7	0.1	7	0.5
8	0.0	8	0.5
9	0.2	9	0.5
		10	0.5

Blue Earth Co. Rd. 90
Class 5   7/27/99

	Run 1		Run 2
a	4.7625	a	4.7625
H_1	5.08	H_1	5.08
H_2	10.16	H_2	10.16
s	10.16	s	12.7
b_1	15.24	b_1	12.7
b_2	10.16	b_2	7.62

Time, min	R_1, cm/min	Time, min	R_2, cm/min	Time, min	R_1, cm/min	Time, min	R_2, cm/min
1.0	15.0	0.5	10.2	0.5	16.6	0.33	7.2
1.5	10.4	1.0	12.4	1.0	11.8	0.67	13.2
2.0	9.6	1.5	11.8	1.5	11.6	1.00	11.7
2.5	7.6			2.0	9.6	1.33	12.6
3.0	7.6			2.5	8.4	1.67	10.5
3.5	6.8			3.0	7.8	2.00	10.5
4.0	6.8			3.5	7.0	2.20	10.5
4.5	7.2			4.0	8.0		
5.0	7.0						

	Run 3		Run 4
a	4.7625	a	4.7625
H_1	5.08	H_1	5.08
H_2	10.16	H_2	10.16
s	10.16	s	12.7
b_1	15.24	b_1	12.7
b_2	10.16	b_2	7.62

Time, min	R_1, cm/min	Time, min	R_2, cm/min	Time, min	R_1, cm/min	Time, min	R_2, cm/min
0.33	4.5	0.33	9.9	0.33	19.5	0.33	9.9
0.67	11.1	0.67	8.4	0.67	14.7	0.67	14.1
1.00	10.5	1.00	10.2	1.00	12.3	1.00	13.5
1.33	6.3	1.33	9.9	1.33	12.9	1.33	12.9
1.67	8.4	1.67	9.0	1.67	11.1	1.67	13.2
2.00	6.9	2.00	9.0	2.00	9.3		
2.33	6.9	2.33	9.0	2.33	10.2		
2.67	6.9	2.67	9.0	2.67	8.1		
				3.00	9.0		
				3.33	9.0		

Dakota Co. Rd. 26
Class 5   7/16/99

	Run 1
a	5.08
H_1	5.08
H_2	10.16
s	7.62
b_1	17.78
b_2	12.7

	Run 2
a	5.08
H_1	5.08
H_2	10.16
s	7.62
b_1	17.78
b_2	12.7

Time, min	R_1, cm/min	Time, min	R_2, cm/min	Time, min	R_1, cm/min	Time, min	R_2, cm/min
1	3.6	1	2.5	1	3.7	1	1.5
2	2.8	2	1.9	2	2.2	2	1.7
3	2.3	3	1.9	3	1.9	3	1.5
4	2.0	4	1.9	4	1.9	4	1.8
5	1.9	5	1.8	5	1.7	5	1.7
6	1.6			6	1.5	6	1.7
7	1.8			7	1.6		
8	1.4			8	1.2		
9	1.8			9	1.5		
10	1.4			10	1.4		
11	1.5			11	1.1		
12	1.5			12	1.4		
13	1.5			13	1.1		
				14	1.3		
				15	1.3		
				16	1.1		
				17	1.3		

	Run 3
a	5.08
H_1	5.08
H_2	10.16
s	7.62
b_1	17.78
b_2	12.7

Time, min	R_1, cm/min	Time, min	R_2, cm/min
1	2.1	1	1.2
2	1.8	2	0.9
3	1.1	3	0.7
4	0.9	4	0.7
5	1.0	5	0.5
6	0.7	6	0.7
7	0.8	7	0.7
8	0.6		
9	0.5		
10	0.8		
11	0.6		
12	0.5		
13	0.6		
14	0.6		
15	0.5		

I 35 W Richfield
Class 5   9/1/99

Run 1

a	5.08
H_1	5.08
H_2	10.16
s	0
b_1	7.62
b_2	2.54

Run 2

a	5.08
H_1	2.54
H_2	5.08
s	0
b_1	10.16
b_2	7.62

Time, min	R_1, cm/min	Time, min	R_2, cm/min	Time, min	R_1, cm/min	Time, min	R_2, cm/min
0.33	25.5	0.33	41.1	0.33	12.9	0.33	11.4
0.67	12.6	0.67	27.9	0.67	10.8	0.67	11.1
1.00	14.1	0.97	21.0	1.00	9.3	1.00	8.1
1.33	15.0			1.33	8.4	1.33	9.9
1.67	13.5			1.67	7.5	1.67	8.1
2.00	14.4			2.00	7.5	2.00	9.3
2.33	10.8			2.33	6.6	2.33	7.2
				2.67	6.6	2.67	8.4
				3.00	6.9		

Run 3

a	5.08
H_1	2.54
H_2	5.08
s	0
b_1	10.16
b_2	7.62

Time, min	R_1, cm/min	Time, min	R_2, cm/min
0.33	11.4	0.33	6.0
0.67	6.6	0.67	6.6
1.00	7.2	1.00	7.2
1.33	5.4	1.33	6.0
1.67	5.7	1.67	6.0
2.00	5.4	2.00	5.4
2.33	5.1	2.33	5.1
2.67	4.8	2.67	5.4

TH 25 Monticello
Class 6   8/12/99

	Run 1				Run 2	
	a	4.7625			a	4.7625
	H_1	5.08			H_1	5.08
	H_2	10.16			H_2	10.16
	s	12.7			s	15.24
	b_1	12.7			b_1	10.16
	b_2	7.62			b_2	5.08

Time, min	R_1, cm/min	Time, min	R_2, cm/min	Time, min	R_1, cm/min	Time, min	R_2, cm/min
1	3.0	1	0.1	1	1.5	1	0.0
2	2.2	2	0.9	2	0.7	2	0.0
3	1.9	3	1.2	3	0.6	3	0.4
4	1.3	4	1.1	4	0.5	4	0.8
5	1.1	5	1.3	5	0.3	5	0.5
6	1.2	6	1.0	6	0.4	6	0.5
7	1.1	7	1.1	7	0.3	7	0.4
8	1.0	8	1.0	8	0.2	8	0.5
9	0.9	9	1.0	9	0.2	9	0.5
10	0.9	10	0.7	10	0.2		
11	0.7	11	1.0				
12	0.9	12	0.9				

	Run 3				Run 4	
	a	4.7625			a	4.7625
	H_1	5.08			H_1	5.08
	H_2	10.16			H_2	10.16
	s	11.43			s	10.16
	b_1	13.97			b_1	15.24
	b_2	8.89			b_2	10.16

Time, min	R_1, cm/min	Time, min	R_2, cm/min	Time, min	R_1, cm/min	Time, min	R_2, cm/min
1	1.8	1	0.0	1	2.2	1	0.0
2	1.2	2	0.0	2	1.8	2	1.1
3	0.7	3	0.0	3	1.1	3	1.2
4	0.7	4	0.5	4	1.1	4	1.1
5	0.6	5	0.5	5	0.9	5	1.1
6	0.5	6	0.5	6	0.8	6	1.1
7	0.5	7	0.4	7	1.1	7	0.8
8	0.3	8	0.5	8	0.8	8	1.0
9	0.4			9	0.6	9	0.9
10	0.3			10	0.5	10	0.9
11	0.4			11	0.6	11	0.9
12	0.3			12	0.6		
13	0.2			13	0.7		
14	0.3			14	0.7		
				15	0.7		

TH 371 Brainerd
Class 6   10/8/99

Run 1

a	5.08
H_1	5.08
H_2	10.16
s	0
b_1	10.16
b_2	5.08

Run 2

a	5.08
H_1	5.08
H_2	10.16
s	0
b_1	7.62
b_2	2.54

Time, min	R_1, cm/min	Time, min	R_2, cm/min	Time, min	R_1, cm/min	Time, min	R_2, cm/min
1	0.3	1	0.5	1	0.0	1	0.7
2	0.0	2	0.5	2	0.0	2	1.5
3	0.3	3	0.5	3	0.0	3	1.4
4	0.0	4	0.5	4	0.4	4	1.1
5	0.1			5	0.0	5	0.9
6	0.2			6	0.0	6	1.3
7	0.1			7	0.2	7	1.1
8	0.2			8	0.0	8	1.0
9	0.2			9	0.1	9	1.2
10	0.4			10	0.2	10	1.0
11	0.2			11	0.0	11	1.3
12	0.2			12	0.2	12	0.9
13	0.2			13	0.1	13	1.0
				14	0.2	14	1.0
				15	0.1	15	1.0
				16	0.1		
				17	0.2		
				18	0.1		

Run 3

a	5.08
H_1	5.08
H_2	10.16
s	0
b_1	10.16
b_2	5.08

Run 4

a	4.7625
H_1	5.08
H_2	10.16
s	0
b_1	10.16
b_2	5.08

Time, min	R_1, cm/min	Time, min	R_2, cm/min	Time, min	R_1, cm/min	Time, min	R_2, cm/min
1	0.0	1	0.0	1	0.0	1	0.5
2	0.0	2	0.3	2	0.0	2	1.3
3	0.3	3	0.9	3	0.4	3	1.0
4	0.2	4	0.8	4	0.3	4	1.1
5	0.4	5	0.8	5	0.4	5	1.0
6	0.1	6	0.7	6	0.2	6	1.2
7	0.3	7	0.7	7	0.5	7	1.5
8	0.2	8	0.8	8	0.3	8	1.0
9	0.4	9	0.7	9	0.4	9	1.0
10	0.1	10	0.7	10	0.5	10	1.0
11	0.3	11	0.8	11	0.2		
12	0.2	12	0.7	12	0.4		
13	0.2			13	0.5		
14	0.3			14	0.3		
15	0.2			15	0.2		
16	0.3			16	0.5		
17	0.2			17	0.5		
				18	0.5		

TH 371 Brainerd
Select Granular   10/8/99

	Run 1				Run 2	
a	4.7625			a	4.7625	
H_1	5.08			H_1	3.81	
H_2	10.16			H_2	10.16	
s	12.7			s	12.7	
b_1	12.7			b_1	13.97	
b_2	7.62			b_2	7.62	

Time, min	R_1, cm/min	Time, min	R_2, cm/min	Time, min	R_1, cm/min	Time, min	R_2, cm/min
1	0.6	1	0.3	1	0.7	1	0.5
2	0.7	2	0.5	2	0.6	2	0.9
3	0.6	3	0.4	3	0.7	3	0.6
4	0.4	4	0.5	4	0.4	4	0.7
5	0.4	5	0.4	5	0.6	5	0.7
6	0.4	6	0.4	6	0.5	6	0.5
7	0.3	7	0.5	7	0.4	7	0.7
8	0.4			8	0.4		
				9	0.5		
				10	0.4		

TH 7 Silver Lake
Class 5   10/1/99

Run 1	
a	4.7625
H_1	5.08
H_2	10.16
s	0
b_1	12.7
b_2	7.62

Run 2	
a	5.08
H_1	5.08
H_2	10.16
s	0
b_1	10.16
b_2	5.08

Time, min	R_1, cm/min	Time, min	R_2, cm/min	Time, min	R_1, cm/min	Time, min	R_2, cm/min
1	7.9	1	6.3	1	4.7	1	5.4
2	6.3	2	5.8	2	3.4	2	5.4
3	5.7	3	5.3	3	3.3	3	4.8
4	5.0	4	5.0	4	3.2	4	4.6
5	4.8	5	5.2	5	3.1	5	4.1
6	4.3	5.23	4.29	6	2.9	6	4.5
7	4.3			7	2.9	7	4.4
8	3.9			8	2.8	8	4.4
9	4.0					9	3.9

Run 3	
a	5.08
H_1	5.08
H_2	10.16
s	0
b_1	10.16
b_2	5.08

Time, min	R_1, cm/min	Time, min	R_2, cm/min
1	7.3	1	6.3
2	5.9	2	5.8
3	5.1	3	5.8
4	4.9	4	5.5
5	4.5	4.92	5.13
6	4.1		
7	4.2		
8	4.1		

TH 73 Kettle River
Class 6   **8/18/99**

	Run 1
a	5.08
H_1	5.08
H_2	10.16
s	0
b_1	12.7
b_2	7.62

	Run 2
a	5.08
H_1	5.08
H_2	10.16
s	0
b_1	11.43
b_2	6.35

Time, min	R_1, cm/min	Time, min	R_2, cm/min	Time, min	R_1, cm/min	Time, min	R_2, cm/min
1	2.6	1	2.4	1	1.3	1	0.7
2	1.7	2	1.9	2	0.6	2	0.5
3	1.7	3	1.3	3	0.7	3	0.4
4	1.4	4	1.5	4	0.6	4	0.2
5	1.3	5	1.4	5	0.4	5	0.5
6	1.3	6	1.2	6	0.5	6	0.2
7	1.1	7	0.8	7	0.3	7	0.5
8	1.1	8	1.2	8	0.5	8	0.5
9	1.3	9	1.4	9	0.3	9	0.2
10	1.1	10	1.1	10	0.4	10	0.5
		11	1.3	11	0.4		
		12	1.4	12	0.1		
		13	1.1	13	0.4		
		14	1.3				
		15	1.1				

US 12 Cokato
Class 5   7/22/99

	Run 1					Run 2	
a	4.7625				a	4.7625	
H_1	5.08				H_1	5.08	
H_2	10.16				H_2	10.16	
s	12.7				s	12.7	
b_1	12.7				b_1	12.7	
b_2	7.62				b_2	7.62	

Time, min	R_1, cm/min	Time, min	R_2, cm/min	Time, min	R_1, cm/min	Time, min	R_2, cm/min
1	7.5	0.5	8.4	0.5	9.8	0.5	9.6
2	5.9	1.0	7.8	1.0	6.6	1.0	7.4
3	5.2	1.5	7.2	1.5	6.0	1.5	7.8
4	4.9	2.0	7.0	2.0	5.4	2.0	7.0
5	4.4	2.5	7.2	2.5	5.4	2.5	7.0
6	4.2	3.0	6.2	3.0	4.6	3.0	6.8
7	4.4	3.5	7.0	3.5	5.2		
		4.0	6.6	4.0	4.2		
				4.5	4.6		
				5.0	4.4		

US 169 Mille Lacs
Class 6   7/21/99

Run 1

a	5.08
H_1	5.08
H_2	10.16
s	10.16
b_1	15.24
b_2	10.16

Run 2

a	5.08
H_1	5.08
H_2	10.16
s	10.16
b_1	15.24
b_2	10.16

Time, min	R_1, cm/min	Time, min	R_2, cm/min	Time, min	R_1, cm/min	Time, min	R_2, cm/min
1	0.5	1	0.2	1	1.6	1	0.0
2	0.2	2	0.4	2	0.4	2	0.0
3	0.4	3	0.6	3	0.3	3	0.0
4	0.2	4	0.5	4	0.3	4	0.0
5	0.1	5	0.5	5	0.0	5	0.0
6	0.2	6	0.5	6	0.0	6	0.2
7	0.1			7	0.0	7	0.0
8	0.1			8	0.0	8	0.4
9	0.0			9	0.3	9	0.0
10	0.1			10	0.0	10	0.4
11	0.2			11	0.0	11	0.0
12	0.0			12	0.3	12	0.4
13	0.0			13	0.0	13	0.0
14	0.2			14	0.0	14	0.1
15	0.0			15	0.0	15	0.3
16	0.1			16	0.0		
17	0.1			17	0.4		
18	0.0						

Run 3

a	5.08
H_1	5.08
H_2	10.16
s	10.16
b_1	15.24
b_2	10.16

Time, min	R_1, cm/min	Time, min	R_2, cm/min
1	0.7	1	0.3
2	0.4	2	0.6
3	0.8	3	0.4
4	0.2	4	0.7
5	0.3	5	0.3
6	0.2	6	0.4
7	0.4	7	0.3
8	0.0	8	0.3
9	0.3		
10	0.3		
11	0.1		
12	0.3		
13	0.0		
14	0.0		
15	0.3		

US 169 Onamia
Class 6   8/11/99

Run 1	
a	4.7625
H_1	5.08
H_2	10.16
s	12.7
b_1	12.7
b_2	7.62

Run 2	
a	4.445
H_1	5.08
H_2	11.43
s	11.43
b_1	13.97
b_2	7.62

Time, min	R_1, cm/min	Time, min	R_2, cm/min	Time, min	R_1, cm/min	Time, min	R_2, cm/min
1	0.2	1	1.7	1	0.4	1	1.2
2	0.7	2	1.4	2	0.3	2	2.1
3	0.3	3	0.1	3	0.0	3	1.7
4	0.3	4	0.7	4	0.1	4	1.6
5	0.3	5	0.7	5	0.0	5	1.1
6	0.3	6	0.7	6	0.1	6	0.8
7	0.3	7	0.7	7	0.0	7	0.9
				8	0.1	8	0.9
				9	0.2	9	0.9
				10	0.2	10	0.8
				11	0.1		
				12	0.2		
				13	0.1		
				14	0.1		
				15	0.1		

Run 3	
a	4.7625
H_1	5.08
H_2	11.43
s	13.97
b_1	11.43
b_2	5.08

Run 4	
a	4.7625
H_1	5.08
H_2	11.43
s	11.43
b_1	13.97
b_2	7.62

Time, min	R_1, cm/min	Time, min	R_2, cm/min	Time, min	R_1, cm/min	Time, min	R_2, cm/min
1	1.2	1	1.3	1	0.0	1	3.0
2	1.3	2	1.1	2	0.1	2	2.6
3	1.1	3	1.8	3	0.4	3	2.1
4	0.7	4	1.4	4	0.4	4	1.3
5	0.3	5	1.4	5	0.0	5	1.5
6	0.6	6	1.3	6	0.3	6	1.5
7	0.6	7	1.4	7	0.3	7	1.2
8	0.4			8	0.3	8	0.9
9	0.6			9	0.1	9	1.1
10	0.3			10	0.3	10	1.1
11	0.3			11	0.3	11	0.3
12	0.7					12	0.8
13	0.2					13	0.8
14	0.4					14	0.8
15	0.3						
16	0.3						
17	0.2						
18	0.3						

Run 5	
a	4.7625
H_1	5.08
H_2	11.43
s	12.7
b_1	12.7
b_2	6.35

Run 6	
a	4.7625
H_1	5.08
H_2	11.43
s	12.7
b_1	12.7
b_2	6.35

Time, min	R_1, cm/min	Time, min	R_2, cm/min	Time, min	R_1, cm/min	Time, min	R_2, cm/min
1	0.5	1	0.8	1	0.9	1	0.4
2	0.5	2	1.7	2	0.7	2	1.9
3	0.5	3	1.3	3	0.6	3	1.6
4	0.5	4	0.8	4	0.5	4	1.5
5	0.4	5	0.8	5	0.5	5	1.4
6	0.3	6	0.9	6	0.5	6	1.3
7	0.3	7	0.7	7	0.3	7	1.2
8	0.3	8	0.7	8	0.5	8	1.0
9	0.3	9	0.7			9	1.1
						10	1.0
						11	1.0
						12	1.0

B-12

I 35W Richfield
Class 5   9/13/00

	Run 1				Run 2	
	a	5.3975			a	5.3975
	H_1	2.54			H_1	2.54
	H_2	5.08			H_2	5.08
	s	2.54			s	2.54
	b_1	5.08			b_1	5.08
	b_2	2.54			b_2	2.54

Time, min	R_1, cm/min	Time, min	R_2, cm/min	Time, min	R_1, cm/min	Time, min	R_2, cm/min
1	1.2	1	1.1	1	1.5	1	2.0
2	1.1	2	1.2	2	1.4	2	1.5
3	1.0	3	1.1	3	0.8	3	2.3
4	1.0	4	0.7	4	1.0	4	1.8
5	0.9	5	0.4	5	1.0	5	1.7
6	0.6	6	0.8	6	0.7	6	2.2
7	0.9	7	1	7	1.2	7	1.5
8	0.6	8	1.1	8	0.6	8	2.0
9	0.7	9	0.7	9	0.9	9	2.5
10	0.7	10	1.2	10	1.0	10	2.5
11	0.8	11	1.2	11	0.6	11	2.1
12	0.7	12	0.7	12	0.9	12	2.6
13	0.5	13	0.8	13	0.7	13	2.3
14	0.6	14	1.1	14	0.8	14	2.6
15	0.5	15	1.2	15	0.8	15	2.5
16	0.9					16	3.0
17	0.6						

I 94 Minneapolis
Sand   7/7/00

	Run 1		Run 2
a	4.7625	a	4.7625
H_1	5.08	H_1	5.08
H_2	10.16	H_2	10.16
s	91.44	s	91.44
b_1	12.7	b_1	12.7
b_2	7.62	b_2	7.62

Time, min	R_1, cm/min	Time, min	R_2, cm/min	Time, min	R_1, cm/min	Time, min	R_2, cm/min
1	1.7	1	0.7	1	3.0	1	1.3
2	1.0	2	0.6	2	1.5	2	1.1
3	0.4	3	0.5	3	1.4	3	0.9
4	0.5	4	0.5	4	1.0	4	1
5	0.5	5	0.4	5	0.9	5	1.0
6	0.3	6	0.4	6	0.9	6	0.7
7	0.5	7	0.5	7	0.8	7	1
8	0.2	8	0.4	8	0.8	8	0.8
9	0.4	9	0.3	9	0.8	9	0.8
10	0.2	10	0.4	10	0.6	10	0.7
11	0.3	11	0.4	11	0.8	11	0.8
12	0.3	12	0.3	12	0.6	12	0.9
13	0.2	13	0.2	13	0.8	13	0.7
14	0.4	14	0.5	14	0.7	14	0.8
15	0.2	15	0.2	15	0.6	15	0.8
16	0.2	16	0.3	16	0.6		
17	0.3	17	0.3	17	0.6		
18	0.2						

MnROAD Cell 32
Class 1c   **6/21/00**

Run 1

a	5.3975
H_1	5.08
H_2	10.16
s	5.08
b_1	7.62
b_2	2.54

Time, min	R_1, cm/min	Time, min	R_2, cm/min
1	0.6	1	1.1
2	0.3	2	1.3
3	0.1	3	1.0
4	0.3	4	0.7
5	0.1	5	0.7
6	0.1	6	0.2
7	0.1	7	0.7
8	0.1	8	0.4
9	0.0	9	0.3
10	0.2	10	0.5
11	0.1	11	0.7
12	0.0	12	0.0
13	0.1	13	0.6
14	0.1	14	0.3
		15	0.5
		16	0.0
		17	0.5
		18	0.5
		19	0.2
		20	0.5

MnROAD Cell 52
Class 4   6/21/00

	Run 1	
a	4.7625
H_1	5.08
H_2	7.62
s	1.27
b_1	6.35
b_2	3.81

Time, min	R_1, cm/min	Time, min	R_2, cm/min
1	1.3	1	0.3
2	0.3	2	0.6
3	0.0	3	0.7
4	0.1	4	0.9
5	0.3	5	0.2
6	0.4	6	0.9
7	0.0	7	0.5
8	0.1	8	0.4
9	0.3	9	0.7
10	0.3	10	0.5
11	0.2	11	0.5
12	0.2	12	0.7
13	0.3	13	0.6
14	0.3	14	0.3
15	0.2	15	0.7

Olmsted Co. Rd. 104
Class 5 Modified   10/4/00

	Run 1				Run 2
a	6.35			a	6.35
H_1	5.08			H_1	5.08
H_2				H_2	
s	5.08			s	5.08
b_1	5.08			b_1	5.08
b_2				b_2	

Time, min	R_1, cm/min	Time, min	R_2, cm/min	Time, min	R_1, cm/min	Time, min	R_2, cm/min
1	1.9	*One head only*		1	0.2	*One head only*	
2	0.9			2	0.2		
3	0.3			3	0.2		
4	0.8			4	0.3		
5	0.4			5	0.2		
6	0.4			6	0.3		
7	0.0			7	0.2		
8	0.4			8	0.3		
9	0.6			9	0.2		
10	0.2			10	0.3		
11	0.0			11	0.3		
12	0.4			12	0.2		
13	0.0			13	0.3		
14	0.4			14	0.2		
15	0.0			15	0.3		
16	0.5			16	0.3		
17	0.0			17	0.2		
18	0.4			18	0.2		
19	0.0			19	0.3		
20	0.0			20	0.2		
21	0.6						

	Run 3
a	5.715
H_1	5.08
H_2	
s	5.08
b_1	5.08
b_2	

Time, min	R_1, cm/min	Time, min	R_2, cm/min
1	1.4	*One head only*	
2	0.9		
3	1.0		
4	0.6		
5	0.5		
6	0.6		
7	0.6		
8	0.6		
9	0.6		
10	0.6		
11	0.6		
12	0.6		
13	0.5		
14	0.6		
15	0.6		
16	0.5		
17	0.6		
18	0.5		

B-17

Olmsted Co. Rd. 117
Class 5   10/4/00

Run 1			Run 2	
a	5.715		a	5.715
H_1	5.08		H_1	5.08
H_2			H_2	
s	7.62		s	5.08
b_1	2.54		b_1	5.08
b_2			b_2	

Time, min	R_1, cm/min	Time, min	R_2, cm/min	Time, min	R_1, cm/min	Time, min	R_2, cm/min
1	1.4	*One head only*		1	2.5	*One head only*	
2	1.5			2	1.5		
3	0.8			3	1.2		
4	1.1			4	1.3		
5	0.7			5	0.5		
6	0.7			6	1.1		
7	0.7			7	1.1		
8	0.6			8	1.0		
9	0.7			9	1.0		
10	0.7			10	1.0		
11	0.6			11	1.2		
12	0.7			12	0.9		
13	0.3			13	0.7		
14	0.2			14	1.3		
15	0.2			15	0.9		
16	0.3			16	1.1		
17	0.8			17	1.0		
18	0.5			18	0.7		
19	0.3			19	0.9		
20	0.5			20	0.9		
21	0.6						

TH 14 Mankato
Class 7   7/14/00

	Run 1			Run 2	
a	5.08		a	5.08	
H_1	5.08		H_1	2.54	
H_2			H_2	5.08	
s	31.75		s	31.75	
b_1	3.81		b_1	6.35	
b_2			b_2	3.81	

Time, min	R_1, cm/min	Time, min	R_2, cm/min	Time, min	R_1, cm/min	Time, min	R_2, cm/min
1	6.7	*One head only*		1	4.1	1	1.9
2	4.5			2	2.8	2	1.9
3	2.9			3	2.1	3	1.7
4	2.9			4	1.7	4	1.6
5	2.4			5	1.8	5	1.5
6	2.1			6	1.5	6	1.3
7	2.2			7	1.5	7	1.5
8	1.8			8	1.3	8	1.4
9	1.9			9	1.3	9	1.5
10	1.7			10	1.3	10	1.1
11	1.6			11	1.2	11	1.6
12	1.6			12	1.1	12	1.2
13	1.6			13	1.0	13	1.1
14	1.3			14	1.1	14	1.3
15	1.5			15	1.0	15	1.3
16	1.4			16	1.0	16	1.2
17	1.5			17	1.0	17	1.0
18	1.3						

TH 14 Mankato
Select Granular   **7/14/00**

<center>Run 1</center>

a	4.7625
H_1	5.08
H_2	10.16
s	12.7
b_1	12.7
b_2	7.62

Time, min	R_1, cm/min	Time, min	R_2, cm/min
1	1.5	1	3.1
2	1.5	2	3.2
3	1.2	3	2.9
4	1.3	4	2.6
5	1.1	5	2.7
6	1.1	6	2.5
7	1.0	7	2.4
8	1.1	8	2.3
9	1.1	9	2.4
10	1.1	10	2.3
11	0.9	11	2.3
12	1.0	12	2.1
13	1.0	13	2.3
		14	2.2
		15	2.1
		16	2.1
		17	2.1

TH 22 St. Peter
Class 7   5/17/00

Run 1					Run 2	
a	5.715				a	5.08
H_1	5.08				H_1	5.08
H_2	10.16				H_2	10.16
s	12.7				s	15.24
b_1	12.7				b_1	10.16
b_2	7.62				b_2	5.08

Time, min	R_1, cm/min	Time, min	R_2, cm/min	Time, min	R_1, cm/min	Time, min	R_2, cm/min
1	0.7	1	2.2	1	0.5	1	1.3
2	0.5	2	2.0	2	0.3	2	1.3
3	0.4	3	1.6	3	0.3	3	0.6
4	0.4	4	1.5	4	0.0	4	0.6
5	0.1	5	2.1	5	0.1	5	0.5
6	0.3	6	1.2	6	0.3	6	0.4
7	0.3	7	1.6	7	0.2	7	0.5
8	0.0	8	1.3	8	0.0	8	0.7
9	0.4	9	2.1	9	0.3	9	0.5
10	0.3	10	1.3	10	0.1	10	0.5
11	0.1	11	1.6	11	0.1	11	0.4
12	0.1	12	1.6	12	0.1	13	0.5
13	0.2	13	1.5	13	0.2	14	0.3
14	0.2	14	1.5	14	0.2		
15	0.1	15	1.7	15	0.0		
16	0.1	16	1.6	16	0.0		
17	0.3			17	0.1		
18	0.0						
19	0.3						
20	0.0						

TH 22 St. Peter
Select Granular   **6/26/00**

	Run 1			Run 2
a	5.08		a	5.08
H_1	5.08		H_1	5.08
H_2	10.16		H_2	10.16
s	22.86		s	22.86
b_1	10.16		b_1	10.16
b_2	5.08		b_2	5.08

Time, min	R_1, cm/min	Time, min	R_2, cm/min	Time, min	R_1, cm/min	Time, min	R_2, cm/min
1	2.1	1	1.9	1	1.9	1	1.5
2	1.2	2	1.5	2	1.1	2	1.3
3	1.1	3	1.8	3	1.2	3	1.3
4	1.0	4	1.2	4	1.0	4	0.9
5	0.8	5	1.5	5	0.9	5	1.0
6	0.9	6	1.3	6	1.1	6	1.1
7	0.7	7	1.3	7	0.7	7	1.1
8	0.8	8	1.2	8	0.8	8	1.0
9	0.9	9	1.1	9	0.9	9	1.1
10	0.3	10	1.3	10	0.8	10	1.1
11	1.0	11	1.0	11	0.4	11	0.8
12	0.5	12	1.3	12	1.1	13	0.8
13	0.9	13	0.8	13	0.6	14	1.0
14	0.7	14	1.0	14	0.9	15	1.1
15	0.7	15	1.1	15	0.8	16	1.0
16	0.6	16	1.2	16	0.5		
17	0.5	17	1.1	17	0.8		
18	0.7	18	1.1	18	0.7		
19	0.7						

TH 371 Brainerd
Class 5   5/16/00

Run 1

a	5.08
H_1	5.08
H_2	10.16
s	15.24
b_1	10.16
b_2	5.08

Run 2

a	5.08
H_1	5.08
H_2	10.16
s	12.7
b_1	12.7
b_2	7.62

Time, min	R_1, cm/min	Time, min	R_2, cm/min	Time, min	R_1, cm/min	Time, min	R_2, cm/min
1	4.7	1	0.5	1	3.7	1	0.0
2	3.0	2	2.3	2	2.8	2	1.0
3	2.1	3	1.9	3	2.1	3	1.9
4	1.6	4	1.8	4	1.7	4	1.6
5	1.8	5	1.5	5	1.6	5	1.6
6	1.6	6	1.7	6	1.4	6	1.4
7	1.4	7	1.4	7	1.5	7	1.4
8	1.5	8	1.4	8	1.2	8	1.4
9	1.3	9	1.3	9	1.5	9	1.3
10	1.3	10	1.2	10	1.3	10	1.2
11	1.4	11	1.2	11	1.0	11	1.3
				12	1.0	12	1.2
				13	1.3	13	1.2
				14	1.1	14	1.1
				15	1.0	15	1.1
				16	1.0	16	1.2
				17	0.9	17	1.0
				18	1.3	18	1.1
				19	0.8		
				20	1.0		

Run 3

a	5.08
H_1	5.08
H_2	10.16
s	12.7
b_1	12.7
b_2	7.62

Time, min	R_1, cm/min	Time, min	R_2, cm/min
1	3.6	1	0.0
2	2.1	2	0.3
3	1.9	3	1.0
4	1.6	4	1.1
5	1.3	5	1.0
6	1.2	6	1.2
7	1.3	7	1.0
8	1.2	8	1.0
9	1.2	9	1.0
10	1.0	10	0.9
11	0.8	11	1.0
12	1.1	12	0.8
13	0.9	13	1.0
14	1.1	14	0.9
15	0.8	15	0.9
16	0.8	16	0.8
17	0.9	17	0.9
18	0.8	18	0.8
19	0.9		

TH 371 Brainerd
Sand 2   5/18/00

	Run 1					Run 2	
	a	4.445				a	4.445
	H_1	5.08				H_1	2.54
	H_2	7.62				H_2	5.08
	s	101.6				s	101.6
	b_1	15.24				b_1	15.24
	b_2	12.7				b_2	12.7

Time, min	R_1, cm/min	Time, min	R_2, cm/min	Time, min	R_1, cm/min	Time, min	R_2, cm/min
1.00	19.0	0.33	17.4	0.33	12.6	0.33	10.8
1.33	16.2	0.67	16.8	0.67	11.4	0.67	11.1
1.67	16.5	1.00	16.5	1.00	10.5	1.00	11.4
2.00	15.3	1.33	15.9	1.33	11.1	1.33	9.9
		1.67	15.6	1.67	9.9	1.67	11.7
		2.00	15.3	2.00	10.2	2.00	10.2
		2.33	15.0	2.33	9.3	2.33	11.1
				2.67	9.6	2.67	10.5
				3.00	9.9	3.00	10.2
				3.33	10.8	3.33	11.1
						3.67	10.5
						4.00	9.9
						4.33	10.8
						4.67	10.2

	Run 3					Run 4	
	a	4.445				a	4.445
	H_1	2.54				H_1	2.54
	H_2	5.08				H_2	5.08
	s	101.6				s	101.6
	b_1	15.24				b_1	15.24
	b_2	12.7				b_2	12.7

Time, min	R_1, cm/min	Time, min	R_2, cm/min	Time, min	R_1, cm/min	Time, min	R_2, cm/min
0.33	13.2	0.33	10.5	0.33	9.3	0.33	9.3
0.67	8.7	0.67	9.6	0.67	10.2	0.67	9.9
1.00	10.2	1.00	10.5	1.00	8.4	1.00	9.3
1.33	9.0			1.33	9.6	1.33	9.6
1.67	12.0			1.67	9.3	1.67	8.7
2.00	6.9			2.00	8.1	2.00	9.6
2.33	8.7			2.33	9.0	2.33	9.6
2.67	9.6			2.67	9.0	2.67	8.7
3.00	9.6			3.00	8.1	3.00	9.6
3.33	8.1			3.33	7.5	3.33	9.6
3.67	8.7			3.67	9.0	3.67	9.3
4.00	8.7			4.00	7.8	4.00	8.4
4.33	9.6			4.33	9.3	4.33	9.6
4.67	8.4			4.67	8.7		
5.00	9.0			5.00	8.1		

TH 5 Eden Prairie
Class 5   5/22/00

	Run 1			Run 2	
a	5.08		a	5.08	
H_1	5.08		H_1	5.08	
H_2	10.16		H_2	10.16	
s	15.24		s	15.24	
b_1	10.16		b_1	10.16	
b_2	5.08		b_2	5.08	

Time, min	R_1, cm/min	Time, min	R_2, cm/min	Time, min	R_1, cm/min	Time, min	R_2, cm/min
1	2.8	1	0.4	1	2.3	1	0.0
2	0.9	2	0.8	2	1.4	2	0.8
3	0.8	3	0.6	3	1.2	3	1.3
4	0.4	4	0.8	4	1.2	4	1.3
5	0.6	5	0.6	5	0.9	5	1.2
6	0.5	6	0.6	6	0.9	6	1.3
7	0.5	7	0.5	7	0.9	7	0.8
8	0.3	8	0.6	8	0.6	8	1.0
9	0.5	9	0.6	9	0.8	9	1.1
10	0.5	10	0.4	10	0.9	10	1.0
11	0.3	11	0.5	11	0.7	11	1.0
12	0.3	12	0.2	12	0.6	12	0.8
13	0.3	13	0.3	13	0.5	13	1.0
14	0.3	14	0.6	14	0.8	14	0.6
15	0.3	15	0.1	15	0.5	15	0.9
		16	0.5	16	0.5	16	0.8
		17	0.3	17	0.5	17	0.9
		18	0.4	18	0.7		

TH 610 Brooklyn Center
Select Granular   5/23/00

Run 1	
a	4.7625
H_1	5.08
H_2	12.7
s	12.7
b_1	12.7
b_2	5.08

Run 2	
a	4.7625
H_1	5.08
H_2	12.7
s	12.7
b_1	12.7
b_2	5.08

Time, min	R_1, cm/min	Time, min	R_2, cm/min	Time, min	R_1, cm/min	Time, min	R_2, cm/min
1	0.8	1	0.7	1	0.6	1	0.2
2	0.6	2	0.6	2	0.6	2	0.4
3	0.3	3	0.6	3	0.3	3	0.3
4	0.4	4	0.5	4	0.4	4	0.4
5	0.3	5	0.6	5	0.3	5	0.1
6	0.3	6	0.4	6	0.3	6	0.4
7	0.3	7	0.6	7	0.2	7	0.5
8	0.3	8	0.5	8	0.3	8	0.2
9	0.3	9	0.4	9	0.3	9	0.4
10	0.2	10	0.4	10	0.1	10	0.3
11	0.3	11	0.5	11	0.3	11	0.3
12	0.2	12	0.5	12	0.1	12	0.3
13	0.2	13	0.3	13	0.2	13	0.3
14	0.2	14	0.5	14	0.3	14	0.3
15	0.3	15	0.4	15	0.2	15	0.3
		16	0.4	16	0.2		
				17	0.2		

Run 3	
a	4.7625
H_1	5.08
H_2	12.7
s	12.7
b_1	12.7
b_2	5.08

Time, min	R_1, cm/min	Time, min	R_2, cm/min
1	0.7	1	0.6
2	0.6	2	0.5
3	0.3	3	0.1
4	0.4	4	0.5
5	0.3	5	0.3
6	0.2	6	0.4
7	0.3	7	0.2
8	0.4	8	0.3
9	0.2	9	0.4
10	0.2	10	0.2
11	0.1	11	0.4
12	0.3	12	0.1
13	0.3	13	0.4
14	0.0	14	0.4
15	0.2	15	0.2
16	0.3	16	0.3
17	0.2		
18	0.3		

US 10 Hastings
Class 5   9/19/00

	Run 1				Run 2	
	a	5.3975			a	5.3975
	H_1	5.08			H_1	2.54
	H_2				H_2	5.08
	s	25.4			s	25.4
	b_1	10.16			b_1	12.7
	b_2				b_2	10.16

Time, min	R_1, cm/min	Time, min	R_2, cm/min	Time, min	R_1, cm/min	Time, min	R_2, cm/min
0.50	19.6	*One head only*		0.33	9.3	0.33	13.5
1.00	21.0			0.67	8.1	0.67	12.9
1.33	19.2			1.00	8.4	1.00	12.0
1.67	18.3			1.33	8.4	1.33	11.7
2.00	19.8			1.67	8.7	1.67	12.6
2.33	18.6			2.00	8.1	2.00	11.7
2.67	17.4			2.33	8.4	2.33	12.3
3.00	18.6			2.67	7.5	2.67	12.6
3.33	18.0			3.00	8.1	3.00	12.0
3.67	15.6			3.33	8.4	3.33	12.3
4.00	17.1			3.67	8.1		
4.33	15.9			4.00	8.1		

	Run 3	
	a	5.3975
	H_1	2.54
	H_2	5.08
	s	25.4
	b_1	12.7
	b_2	10.16

Time, min	R_1, cm/min	Time, min	R_2, cm/min
0.33	12.3	0.33	14.7
0.67	12.6	0.67	11.1
1.00	11.4	1.00	13.8
1.33	10.8	1.33	13.5
1.67	11.1	1.67	12.3
2.00	9.9	2.00	12.6
2.33	10.8	2.33	10.8
2.67	9.6	2.67	13.8
3.00	9.9	3.00	12.6
3.33	9.6	3.33	12.3
3.67	9.0		

US 10 Hastings
Class 6   9/19/00

	Run 1				Run 2	
	a	5.3975			a	5.3975
	H_1	5.08			H_1	5.08
	H_2	9.525			H_2	10.16
	s	12.7			s	12.7
	b_1	7.62			b_1	7.62
	b_2	3.175			b_2	2.54

Time, min	R_1, cm/min	Time, min	R_2, cm/min	Time, min	R_1, cm/min	Time, min	R_2, cm/min
1	2.9	1	0.3	1	2.6	1	2.1
2	1.9	2	1.3	2	1.8	2	2.3
3	1.5	3	1.4	3	1.7	3	2.0
4	1.2	4	1.6	4	1.6	4	1.3
5	1.3	5	1.3	5	1.4	5	2.0
6	1.4	6	1.7	6	1.3	6	1.7
7	1.0	7	1.3	7	1.3	7	1.2
8	1.0	8	1.2	8	1.3	8	1.3
9	1.1	9	0.7	9	0.9	9	1.9
10	1.1	10	1.6	10	1.3	10	1.1
11	0.9	11	1.1	11	1.0	11	1.3
12	0.9	12	1	12	1.3	12	1.7
13	0.9	13	1.4	13	0.9	13	0.8
14	0.9	14	1.4	14	0.9	14	1.5
15	1.1	15	0.6	15	1.2	15	1.4
16	0.7	16	1.1	16	0.9		
		17	1.3				

US 12 Cokato
Select Granular   8/3/00

Run 1

a	5.08
H_1	5.08
H_2	10.16
s	99.06
b_1	17.78
b_2	12.7

Run 2

a	5.08
H_1	5.08
H_2	10.16
s	99.06
b_1	17.78
b_2	12.7

Time, min	R_1, cm/min	Time, min	R_2, cm/min	Time, min	R_1, cm/min	Time, min	R_2, cm/min
0.5	14.6	0.33	13.2	0.33	5.7	0.33	8.4
1.0	10.6	0.67	11.7	0.67	5.7	0.67	8.1
1.5	10.4	1.00	12.9	1.00	5.7	1.00	7.5
2.0	9.4	1.33	11.1	1.33	4.8	1.33	8.7
2.5	8.8	1.67	11.4	1.67	5.4	1.67	7.5
3.0	9.0	2.00	12.3	2.00	5.1	2.00	8.1
3.5	8.8	2.25	11.2	2.33	4.5	2.33	7.5
4.0	8.2			2.67	5.7	2.67	7.8
4.5	8.6			3.00	4.5	3.00	8.1
				3.33	5.4	3.67	7.7
				3.67	4.2	4.00	8.4
				4.00	5.7	4.33	8.1
				4.33	4.2	4.67	7.8
				4.67	5.4	5.00	7.5
				5.00	4.8	5.33	7.8
				5.33	5.1	5.67	8.1
				5.67	5.4		
				6.00	4.5		
				6.33	5.1		
				6.67	5.1		

Run 3

a	5.08
H_1	5.08
H_2	10.16
s	99.06
b_1	17.78
b_2	12.7

Time, min	R_1, cm/min	Time, min	R_2, cm/min
0.5	5.0	0.5	7.8
1.0	4.0	1.0	6.6
1.5	3.6	1.5	7.0
2.0	4.2	2.0	6.2
2.5	2.6	2.5	6.6
3.0	5.4	3.0	6.4
3.5	3.8	3.5	7.0
4.0	4.0	4.0	6.4
4.5	4.0	4.5	6.8
5.0	4.2	5.0	6.4
5.5	3.6	5.5	6.8
6.0	4.0	6.0	6.0
6.5	4.0	6.5	7.2
7.0	4.0	7.0	6.6
		7.5	6.4
		8.0	6.4

US 169 Jordan
Class 5   8/4/00

	Run 1
a	5.08
H_1	5.08
H_2	7.62
s	30.48
b_1	7.62
b_2	5.08

	Run 2
a	5.08
H_1	2.54
H_2	5.08
s	30.48
b_1	10.16
b_2	7.62

Time, min	R_1, cm/min	Time, min	R_2, cm/min	Time, min	R_1, cm/min	Time, min	R_2, cm/min
0.5	12.6	0.5	12.2	0.5	2.8	0.5	4.2
1.0	9.2	1.0	10.2	1.0	2.6	1.0	3.4
1.5	8.4	1.5	9.6	1.5	2.6	1.5	3.6
2.0	7.2	2.0	9.6	2.0	2.4	2.0	3.2
2.5	6.8	2.5	8.6	2.5	2.0	2.5	3.4
3.0	6.2	3.0	8.2	3.0	2.6	3.0	3.4
3.5	5.8	3.5	8.6	3.5	2.4	3.5	3.4
4.0	5.8	4.0	8.8	4.0	2.2	4.0	3.2
4.5	5.4			4.5	2.0	4.5	3.2
				5.0	2.2	5.0	3.2
				5.5	2.4	5.5	3.4
				6.0	2.4	6.0	3.2
				6.5	2.0	6.5	3.0
				7.0	2.4	7.0	3.4
				7.5	2.0	7.5	3.0
				8.0	2.0	8.0	2.0
						8.5	4.2
						9.0	3.2
						9.5	3.2
						10.0	2.8

B-30

US 212 Eden Prairie
Select Granular   5/22/00

Run 1

a	4.445
H_1	5.08
H_2	10.16
s	13.97
b_1	13.97
b_2	8.89

Time, min	R_1, cm/min	Time, min	R_2, cm/min
0.33	14.7	0.33	10.8
0.67	12.3	0.67	8.7
1.00	9.0	1.00	9.3
1.33	9.6	1.33	9.3
1.67	9.0	1.67	8.1
2.00	8.1	2.00	8.1
2.33	8.1	2.33	8.4
2.67	8.1	2.67	8.1
3.00	7.2	3.00	8.1
3.33	7.5	3.33	8.1
		3.67	7.8
		4.00	8.4
		4.33	7.2
		4.67	7.8
		5.00	7.5

Run 2

a	4.445
H_1	2.54
H_2	5.08
s	13.97
b_1	13.97
b_2	8.89

Time, min	R_1, cm/min	Time, min	R_2, cm/min
0.33	6.0	0.33	5.4
0.67	5.4	0.67	5.4
1.00	4.5	1.00	5.4
1.33	5.1	1.33	5.7
1.67	4.8	1.67	5.1
2.00	5.1	2.00	5.4
2.33	5.1	2.33	5.4
2.67	4.2	2.67	5.7
3.00	5.1	3.00	4.8
3.33	4.8	3.33	5.7
3.67	5.1	3.67	4.8
4.00	4.5	4.00	5.1
4.33	4.8	4.33	5.7
4.67	4.5	4.67	5.4
5.00	5.1	5.00	4.8
5.33	4.5	5.33	5.4
5.67	4.8	5.67	5.7
6.00	5.1	6.00	5.1
6.33	4.8		
6.67	4.5		

Run 3

a	4.445
H_1	2.54
H_2	5.08
s	13.97
b_1	13.97
b_2	8.89

Time, min	R_1, cm/min	Time, min	R_2, cm/min
0.33	5.7	0.33	5.1
0.67	4.8	0.67	5.1
1.00	4.5	1.00	5.1
1.33	4.8	1.33	4.8
1.67	4.5	1.67	5.4
2.00	4.8	2.00	5.1
2.33	4.8	2.33	4.8
2.67	4.5	2.67	5.1
3.00	4.5	3.00	4.8
3.33	4.5	3.33	4.8
3.67	4.5	3.67	5.1
4.00	4.2	4.00	4.8
4.33	4.8	4.33	4.8
4.67	4.5	4.67	5.1
5.00	4.2	5.00	5.1
5.33	4.8	5.33	5.1
5.67	4.5	5.67	4.8
		6.00	5.1
		6.33	4.8
		6.67	5.1

B-31

APPENDIX C

SIEVE ANALYSIS DATA

Sieve Size		I 35W Richfield Class 5	I 94 Minneapolis Sand	MnROAD Cell 32 Class 1c
English	Metric (mm)	% Passing	% Passing	% Passing
1 1/4"	31.5	100%	100%	100%
1"	25.0	100%	99%	100%
3/4"	19.0	95%	94%	97%
1/2"	12.5	86%	90%	90%
3/8"	9.5	80%	88%	82%
#4	4.75	65%	83%	60%
#8	2.36	52%	77%	43%
#16	1.18	40%	70%	33%
#30	0.600	29%	57%	24%
#50	0.300	15%	25%	14%
#100	0.150	7.5%	11%	9.0%
#200	0.075	5.0%	8.0%	7.0%

(2000)

Sieve Size		MnROAD Cell 52 Class 4	Olmsted Co. Rd. 104 Class 5	Olmsted Co. Rd. 117 Class 5 Modified
English	Metric (mm)	% Passing	% Passing	% Passing
1 1/4"	31.5	100%	99%	100%
1"	25.0	100%	93%	100%
3/4"	19.0	98%	83%	100%
1/2"	12.5	91%	61%	90%
3/8"	9.5	85%	52%	78%
#4	4.75	71%	37%	53%
#8	2.36	58%	27%	35%
#16	1.18	45%	20%	24%
#30	0.600	32%	16%	20%
#50	0.300	18%	14%	17%
#100	0.150	11%	12%	15%
#200	0.075	9.2%	10.0%	13.1%

(2000)

Sieve Size		TH 14 Mankato Class 7	TH 14 Mankato Select Granular	TH 22 St. Peter Class 7
English	Metric (mm)	% Passing	% Passing	% Passing
1 1/4"	31.5	100%	100%	100%
1"	25.0	100%	100%	100%
3/4"	19.0	94%	100%	93%
1/2"	12.5	81%	99%	73%
3/8"	9.5	72%	98%	65%
#4	4.75	56%	95%	48%
#8	2.36	45%	90%	35%
#16	1.18	37%	86%	26%
#30	0.600	29%	81%	19%
#50	0.300	20%	26%	11%
#100	0.150	14%	14%	7.4%
#200	0.075	9.1%	10.2%	5.6%

(2000)

Sieve Size		TH 22 St. Peter Select Granular % Passing	TH 371 Brainerd Class 5 % Passing	TH 371 Brainerd Sand 2 % Passing
English	Metric (mm)			
1 1/4"	31.5	100%	100%	100%
1"	25.0	100%	100%	100%
3/4"	19.0	97%	97%	97%
1/2"	12.5	92%	80%	96%
3/8"	9.5	90%	72%	95%
#4	4.75	76%	60%	91%
#8	2.36	61%	50%	86%
#16	1.18	47%	40%	78%
#30	0.600	34%	29%	66%
#50	0.300	20%	16%	32%
#100	0.150	14%	8.4%	12%
#200	0.075	11.9%	6.2%	8.4%

(2000)

Sieve Size		TH 5 Eden Prairie Class 5 % Passing	TH 610 Brooklyn Center Select Granular % Passing	US 10 Hastings Class 5 % Passing
English	Metric (mm)			
1 1/4"	31.5	100%	100%	100%
1"	25.0	100%	100%	100%
3/4"	19.0	90%	97%	93%
1/2"	12.5	74%	95%	76%
3/8"	9.5	64%	92%	65%
#4	4.75	49%	89%	47%
#8	2.36	37%	83%	37%
#16	1.18	27%	75%	31%
#30	0.600	19%	55%	27%
#50	0.300	11%	18%	21%
#100	0.150	5.2%	6.7%	15%
#200	0.075	3.4%	4.8%	10.8%

(2000)

Sieve Size		US 10 Hastings Class 6 % Passing	US 12 Cokato Select Granular % Passing	US 169 Jordan Class 5 % Passing
English	Metric (mm)			
1 1/4"	31.5	100%	100%	100%
1"	25.0	100%	100%	100%
3/4"	19.0	95%	100%	94%
1/2"	12.5	76%	97%	88%
3/8"	9.5	66%	96%	85%
#4	4.75	50%	90%	78%
#8	2.36	39%	80%	70%
#16	1.18	33%	69%	60%
#30	0.600	28%	55%	46%
#50	0.300	21%	30%	24%
#100	0.150	14%	10.0%	10.2%
#200	0.075	10.4%	7.0%	7.2%

(2000)

	Sieve Size		US 212 Eden Prairie Select Granular % Passing
	English	Metric (mm)	
2000	1 1/4"	31.5	100%
	1"	25.0	100%
	3/4"	19.0	99%
	1/2"	12.5	99%
	3/8"	9.5	98%
	#4	4.75	94%
	#8	2.36	90%
	#16	1.18	84%
	#30	0.600	76%
	#50	0.300	54%
	#100	0.150	19%
	#200	0.075	8.0%

	Sieve Size		Blue Earth Co. Rd. 90 Class 3 % passing	Blue Earth Co. Rd. 90 Class 5 % passing	Dakota Co. Rd. 26 Class 5 % passing
	English	Metric (mm)			
1999	2"	50.0	100%	100%	100%
	1 1/2"	37.5	100%	100%	97%
	1"	25.0	100%	100%	92%
	3/4"	19.0	100%	96%	87%
	3/8"	9.5	96%	85%	67%
	#4	4.75	91%	77%	52%
	#10	2.0	81%	64%	42%
	#20	0.85	65%	51%	34%
	#40	0.425	42%	30%	22%
	#100	0.150	14%	9.5%	9.5%
	#200	0.075	10.3%	6.9%	7.4%

	Sieve Size		I 35W Richfield Class 5 % passing	TH 25 Monticello Class 6 % passing	TH 371 Brainerd Class 6 % passing
	English	Metric (mm)			
1999	2"	50.0	100%	100%	100%
	1 1/2"	37.5	100%	100%	100%
	1"	25.0	100%	100%	100%
	3/4"	19.0	97%	93%	96%
	3/8"	9.5	75%	81%	77%
	#4	4.75	58%	71%	64%
	#10	2.0	47%	57%	50%
	#20	0.85	33%	40%	38%
	#40	0.425	21%	24%	26%
	#100	0.150	9.2%	9.6%	11%
	#200	0.075	7.1%	7.7%	7.7%

	Sieve Size		TH 371 Brainerd Select Granular % passing	TH 7 Silver Lake Class 5 % passing	TH 73 Kettle River Class 6 % passing
	English	Metric (mm)			
1999	2"	50.0	100%	100%	100%
	1 1/2"	37.5	100%	100%	100%
	1"	25.0	100%	100%	100%
	3/4"	19.0	99%	96%	100%
	3/8"	9.5	97%	84%	88%
	#4	4.75	95%	71%	73%
	#10	2.0	93%	51%	58%
	#20	0.85	91%	38%	44%
	#40	0.425	83%	24%	32%
	#100	0.150	18%	12%	16%
	#200	0.075	7.4%	10.2%	11.7%

	Sieve Size		US 12 Cokato Class 5 % passing	US 169 Mille Lacs Class 6 % passing	US 169 Onamia Class 6 % passing
	English	Metric (mm)			
1999	2"	50.0	100%	100%	100%
	1 1/2"	37.5	100%	100%	100%
	1"	25.0	100%	100%	100%
	3/4"	19.0	94%	96%	94%
	3/8"	9.5	80%	72%	76%
	#4	4.75	68%	62%	65%
	#10	2.0	54%	53%	55%
	#20	0.85	39%	43%	45%
	#40	0.425	27%	30%	31%
	#100	0.150	12%	12%	9.5%
	#200	0.075	8.9%	9.4%	6.3%